

## Chapter 3

### POREWATER AND WATER COLUMN CHEMISTRY IN THE SEDIMENTS OF THREE SUBALPINE SIERRAN LAKES

#### 3.1. Introduction

In order to calculate the flux of chemical constituents from sediments to lake water using a diffusion model, the concentration of chemical constituents in the pore water of the sediments must be measured in small depth increments. These depth variations, i.e. the chemical gradients, are the driving forces that cause diffusive flux between the sediments and the lake. These diffusive fluxes of chemical constituents, most notably bicarbonate, are the processes that determine the importance of sediments as buffers against acid deposition in subalpine watersheds.

Many measurements of chemical gradients are ideally needed to determine both the spatial and temporal variability in a given lake. However, these measurements are both time consuming and labor intensive, placing limits on the number of replicates possible. Nonetheless, the number of measurements of chemical gradients made in this study make it one of the most intensive examinations of pore water chemistry ever reported for lakes. These chemical data provide an opportunity to determine possible mechanisms which control the composition of the pore water and are the raw data on which our calculations of flux are based.

Lake sediments have long been recognized as an important

conditions. He attributed this result to the elimination of an adsorptive "oxidized microzone" at the sediment-water interface.

The purpose of this section of the report is to present data on the porewater chemistry of the three lakes examined in the study, to consider the reactions controlling the composition of the waters, and discuss the probable direction that the constituents are being transported.

### 3.2. Methods and Equipment

Lake and pore waters were sampled at various times from June, 1985 to October, 1986. Water column samples were taken using a variety of Niskin, van Dorn, and Kemmerer depth samplers, at 1 m intervals measured from the lake surface. Clean, water-washed polyethylene bottles were used for samples which were later analyzed for their alkalinity, anions and monovalent cations (by ion chromatography), and silica. Acidified polyethylene bottles were used for cations to be analyzed by atomic absorption. Water samples were injected by syringe into evacuated glass serum bottles for CO<sub>2</sub> and CH<sub>4</sub> analyses. Temperature and dissolved O<sub>2</sub> were taken using a YSI probe. Table 1 provides more information on the frequency and dates of lake and pore water sampling. The standard deviations for the water analyses are summarized in Table 2. They were generally obtained from repeated standards or samples done throughout an analytical procedure. Both overall (pooled) standard deviations and standard deviations for blanks are given. More detail is given below with

Table 2. Water analyses: Summary table of pooled standard deviations and standard deviations of blanks

Species	Pooled Standard deviation	Degrees of freedom for pooled std. dev.	Std. dev. of blanks	Degrees of freedom for blank std. dev.	Method
Alk ( $\mu\text{eq L}^{-1}$ , 50ml samples)	4.1	103	2.4	31	Titration
Alk ( $\mu\text{eq L}^{-1}$ , 1ml samples)	19.	252	10.	49	Titration
Ca ( $\mu\text{M}$ )	1.1	41	0.81	9	AA
Mg ( $\mu\text{M}$ )	0.54	50	0.17	14	AA
Na ( $\mu\text{M}$ )	3.3	68	3.2	19	AA
K ( $\mu\text{M}$ )	2.7	30	2.6	8	AA
Fe ( $\mu\text{M}$ )	3.8	92	3.0	20	AA
Mn ( $\mu\text{M}$ )	0.70	68	0.44	16	AA
Cl <sup>-</sup> ( $\mu\text{M}$ )	0.42	190	0.58	33	IC
NO <sub>3</sub> <sup>-</sup> ( $\mu\text{M}$ )	0.39	187	0.35	31	IC
SO <sub>4</sub> <sup>2-</sup> ( $\mu\text{M}$ )	0.52	185	0.24	32	IC
NO <sub>2</sub> <sup>-</sup> ( $\mu\text{M}$ )	0.17	69	0.081	13	IC
Br <sup>-</sup> ( $\mu\text{M}$ )	0.30	62	0.11	13	IC
Na <sup>+</sup> ( $\mu\text{M}$ )	1.8	228	0.67	41	IC
NH <sub>4</sub> <sup>+</sup> ( $\mu\text{M}$ )	5.0	235	0.64	44	IC
K <sup>+</sup> ( $\mu\text{M}$ )	1.9	230	0.61	42	IC
SiO <sub>2</sub> (ppm) <sup>a</sup>	8.7%	174	0.0052ppm	5	colorimetric
CH <sub>4</sub> (mM)	0.10	65	0.013	50	GC
CO <sub>2</sub> (mM)	0.13	65	0.047	50	GC
Temperature <sup>b</sup> (°C)	0.41	10	-	-	thermocouple
Dissolved O <sub>2</sub> <sup>b</sup> (ppm)	0.55	13	-	-	electrode

AA = atomic absorption spectrophotometry

IC = ion chromatography

GC = gas chromatography

a. A coefficient of variation is used because it remained constant over the concentration range.

b. Field measurements

source of alkalinity inputs into lakewater. Examples are Hutchinson (1941), Mortimer (1941, 1942) and Yoshimura (1931). Specific sources of alkalinity contained in or mediated by sediments include: nitrate and sulfate reduction; ammonium and base cation production from the decomposition of organic matter; alkaline earth element release by cation exchange; and proton consumption and cation release by mineral weathering. The relative importance of these processes varies depending on lake and watershed properties.

Redox reactions mediated by micro-organisms play an important role. Biological activity reduces oxygen concentrations to zero and, as a result, most of the organic matter decomposition occurs via anaerobic pathways. Under these conditions, alkalinity is produced via the reduction of sulfate and nitrate contained in the overlying lake waters, the reduction of iron and manganese from oxides, and from the production of ammonium a base cations during the mineralization of organic matter. The oxidation of  $\text{Fe}^{2+}$ ,  $\text{Mn}^{2+}$ , and  $\text{NH}_4^+$  after transport into the oxygenated lakewater results in an accompanying loss of alkalinity. Therefore, many of the redox driven alkalinity producing reactions do not greatly alter the alkalinity of the lake except in anoxic bottom waters during stratification.

Seasonal stratification caused by temperature gradients often produces an anoxic layer of water extending some distance above the sediments. The shifting position of this oxic-anoxic boundary may play an important role in alkalinity flux. Mortimer (1941,1942), using oxic and anoxic microcosms, found greatly increased fluxes, including alkalinity flux, under anoxic

length in the overlying water varied from time to time. At each date, one or two peepers were deployed and were allowed to equilibrate a minimum of three weeks before sampling.

### 3.2.1. Short Peepers

Samples were removed from the chambers, immediately after removing the peeper from the sediments and washing the mud off the chambers with lakewater followed by DI, by extraction with a 10 ml syringe fitted with an 18 or 20 gage needle. Short peepers had three columns of chambers, each with a volume of approximately 8 ml. For all but the first sampling, every third chamber was designated for the analysis of either (1) gases, (2) acidified cations, or (3) unacidified cations, anions, silica, pH, and alkalinity. The first peeper for each lake was sampled by placing the contents of each chamber into a 9 ml Wheaton serum bottle, covered with rubber septum. Vertical resolution between samples was 1 1/8 in (2.8575 cm). Samples for gas analysis were collected in Vacutainer blood serum bottles until 5/86; after this date evacuated Wheaton bottles with butyl rubber septa were used. Samples for alkalinity, pH, silica, and ions (determined by ion chromatography) were collected in water-washed polyethylene bottles. Acid soaked (first HCL and later HNO<sub>3</sub>) bottles, with an additional aliquot of acid, were used to preserve samples for metal analyses. Once collected, the samples were stored in ice chests, transported to the laboratory, and stored in a 5 °C coldroom until analyses were performed.

Table 1. The frequency of lake and pore water sampling.

Water column sampling dates for each lake.					
Eastern Brook		Emerald		Mosquito	
Date	Code	Date	Code	Date	Code
6-11-85	WC1	7-9-85	WC1	4-3-85	WC1
7-2-85	WC2	7-29-85	WC2	6-4-85	WC2
7-22-85	WC3	9-15-85	WC3	6-25-85	WC3
8-13-85	WC4	10-2-85	WC4	7-16-85	WC4
9-26-85	WC5	3-4-86	WC5	8-6-85	WC5
2-27-86	WC6	4-9-86	WC6	9-17-85	WC6
3-20-86	WC7	5-1-86	WC7	3-26-86	WC7
7-8-86	WC8	7-31-86	WC8	4-17-86	WC8
7-29-86	WC9	8-19-86	WC9	8-25-86	WC9
				9-23-86	WC10

Peeper sampling dates and codes								
Emerald			Eastern Brook			Mosquito		
Date	Code <sup>a</sup>	No.& type <sup>b</sup>	Date	Code <sup>a</sup>	No.& type <sup>b</sup>	Date	Code <sup>a</sup>	No.& type <sup>b</sup>
7-9-85	P1	1S	7-2-85	P1	1S	6-25-85	P1	1S
7-30-85	P2	2S	7-22-85	P2	2S	7-16-85	P2	2S
9-5-85	P3	2S	8-14-85	P3	2S	8-8-85	P3	2S
10-2-85	P4	2S	9-26-85	P4	2S	9-17-85	P4	2S
5-1-86	WP	2S	3-20-86	WP	1S	4-17-86	WP	1S
8-19-86	LP	2L	7-29-86	LP	2L	9-27-86	LP	2L

- a. Codes are used in the data file names.  
 b. S = short peepers, L = long peepers

bias. Table 3 provides statistics for the regression of nominal against measured values.

Table 3. Regression of nominal against measured alkalinities					
Sample volume (ml)	Intercept	Std. error Intercept	Slope	Std. error slope	R <sup>2</sup>
1	-2.82	1.68	0.998	0.004	0.995
50	1.32	0.47	1.03	0.0051	0.998

For the 1 ml samples, neither the intercept nor the slope show statistically significant bias at the  $p < 0.05$  level. For the 50 ml samples, both the intercept and the slope show statistically significant bias at the  $p > 0.05$  level, but it is small: the intercept is  $1.3 \text{ ueq L}^{-1}$  and the slope indicates that the titrations underestimated the alkalinity by about 3 %.

After alkalinity was measured, the remaining sample was filtered through Millipore HA 0.45  $\mu\text{m}$  filters that had been soaked and rinsed in de-ionized water. Red, precipitated iron was removed from peeper samples by this process.

The unacidified peeper sample remaining after Gran titration was then diluted to provide enough sample for the subsequent analyses. The volume of filtered sample was noted and an equal volume of deionized water was passed through the filter apparatus for a 1:1 dilution or two volumes for a 2:1 dilution. Tests with standards indicated that the 1:1 dilution actually produced a dilution factor of 2.13. Based on these tests, it was assumed that the 2:1 dilutions had a dilution factor of 3.26. Statistical

the description of each analysis.

Pore water samples were obtained using in situ dialysis samplers ("peepers") modified from a design described by Hesslein (1976). From summer 1985 through May 1986, short ( 75 cm long and 25 cm wide) peepers were used and long peepers (200 cm long x 10 cm wide) were used for the remaining sampling dates. Short peeper chambers were spaced 3/8 inch (0.9525 cm) apart center-to-center in the vertical dimension. Because any given species was only sampled from every third chamber, vertical resolution with these peepers was 1 1/8 inches (2.8575 cm).

The long peepers had a more streamlined design to facilitate their insertion deeper into the sediments. Since the center-to-center distance of the chambers was 1.75 inches (4.445 cm) and pairs of chambers were combined for analysis, the vertical resolution of these peepers was 3.5 inches (8.89 cm).

Preceding peeper insertion into the sediments, the following steps were taken by technicians (wearing vinyl gloves to minimize contamination): the chambers were cleaned, and then filled with clean deionized water. A presoaked and rinsed Millipore 0.45 um HA membrane was placed over the chamber to fit the length and width of the peeper. The top plexiglass plate was then screwed on with plastic screws (stainless steel for long peepers). The peepers were driven into the sediments vertically from a raft (on one date, peepers were positioned by scuba divers). Drives from the raft were estimated so that about 10 cm of the peeper would be left in the overlying lakewater. Long peepers were driven in as deeply as possible so that the

bottles) were found to contain approximately 3 times as much CO<sub>2</sub> as they should if they had been filled with air-equilibrated water. The concentration in the headspace of the blanks was close to atmospheric values, suggesting that all CO<sub>2</sub> was not removed during evacuation or that some leakage into the blanks occurred prior to analysis. To account for this CO<sub>2</sub>, the excess CO<sub>2</sub> in the blanks was subtracted from the total calculated for each water sample. In general, the presence of atmospheric concentrations in the blanks made a negligible difference to the high CO<sub>2</sub> levels which were present in pore water samples.

The standard deviations for gases (Table 2) were based on replicate analyses of high concentration standards (~ 2.0 % for methane and ~ 2.5 % for carbon dioxide). The best estimate for gas uncertainties is to use coefficients of variation (3.4 % for methane and 2.9 % for carbon dioxide) or the standard deviations of the blanks (13 uM for methane and 47 uM for carbon dioxide), whichever is larger.

An indicator of the quality of water analyses is charge balance. A number of these are shown in Table 4. The water columns and long peepers show a positive bias in the ratio of cations to anions. This is probably due to the absence of organic anions measurements. The flux planes of the short peepers (see Chapter 4) do not show a statistically significant bias, but there are only 9 samples in the mean, compared with 85 for the water columns and 121 for the long peepers. For the short peepers, a measure of charge balance is provided by showing the sums of anions and cations on the same graphs, which are titled

### 3.2.2. Long Peepers

The long peepers had a more streamlined design in order to facilitate their placement at great depths in the sediments. In sampling the water from these peepers, adjacent pairs of chambers were combined so that all analyses could be performed on a single, homogeneous water sample. Pore water from two adjacent chambers was drawn into a syringe, mixed, and distributed to clean, water-washed bottles; acidified bottles; or evacuated serum bottles depending on the analyses to be performed. Vertical resolution for these peepers was 3.5 inches (8.89 cm) between samples. These peepers were the last to be employed and, as a result of the improvement in our methods of analysis and equipment design, we feel that they provide the best data.

### 3.2.3. Laboratory Methods

Alkalinities were performed by the Gran method (Stumm and Morgan, 1981) on unfiltered samples using Gam-Rad electrodes and an Orion Model 601A pH meter. Water column alkalinities were performed on 50 ml aliquots and peeper alkalinities on 1 ml aliquots. The pooled statistics are shown in Table 2. Alkalinities were always compared with gravimetric sodium carbonate standards. Hence, these standard deviations reflect not just the variance of the standard referred to itself, but referred to its gravimetrically determined value. The considerably higher variance in the small samples is probably due to problems in accurately and rapidly measuring 1 ml volumes. While there is considerable scatter, there is little systematic

"Ion Balance". Direct ratios and sums cannot be simply calculated because all ions were not analyzed in each chamber. The concentrations for the short-peeper flux planes in Table 4 were produced by interpolation, and so charge balance can be directly calculated.

### 3.3. Results

#### 3.3.1. Emerald Lake Water Column

A more complete report on the dynamics of water column properties of Emerald Lake can be found in Melack et al. (1987). Since our efforts were directed more toward porewater chemistry, our analyses of lake water chemistry were not as extensive as those of Melack et al. (1987).

Emerald Lake is dimictic, with stratification occurring in the winter under ice and to a lesser extent in late summer (Stoddard, 1985; Melack et al., 1987). Snowmelt occurs from April to June. Because of low rainfall in the summer, inlets and outlets sometimes cease flowing. Turnover occurs in September through October when cool temperatures cause settling of surface waters. During winter, a layer of ice and slush, which may reach a depth of 4 m, develops on the lake. Conditions of diminished oxygen may persist for a few months under the ice cover in the water layer immediately above the sediments. Measured temperature and dissolved oxygen profiles for May, July, and August of 1986 are illustrated in Fig. 1.

Carbon dioxide and methane were the only constituents

analysis of these tests indicate that the dilution procedure added an error of about 5 % to subsequent ion determinations.

Filtered and diluted samples were run on a Dionex 2000i/sp ion chromatograph. Anions ( $\text{SO}_4^{2-}$ ,  $\text{NO}_3^-$ ,  $\text{NO}_2^-$ ,  $\text{PO}_4^{3-}$ ,  $\text{Br}^-$ , and  $\text{Cl}^-$ ) were determined using a Dionex AS4A column, and monovalent cations ( $\text{Na}^+$ ,  $\text{K}^+$ ,  $\text{NH}_4^+$ ) were determined with a Dionex CS1 Column. Dissolved silica was determined as  $\text{SiO}_2$  on a Lachat autoanalyzer using the heteropoly blue method (QuickChem<sup>R</sup> Method No. 10-114-27-1-B).

Dissolved cations ( $\text{Ca}^{2+}$ ,  $\text{Mg}^{2+}$ ,  $\text{K}^+$ ,  $\text{Na}^{2+}$ , iron, manganese) were determined by atomic absorption spectrophotometry. Prior to analysis, the samples were diluted, digested in  $\text{HNO}_3/\text{HClO}_4$ , 2:1 digesting solution for 4 hrs. Samples were run on a Perkin-Elmer 303 flame AA, using an acetylene-air flame.

Samples for  $\text{CO}_2$  and  $\text{CH}_4$  analysis were shaken on a reciprocal shaker at ambient temperature for 1 hr to ensure equilibration between the water and the gas in the headspace. A 0.25 ml sample of the headspace gas was removed with a gas-tight, locking syringe and was injected onto a Poropak column of a Carle AGC Series 100 gas chromatograph using a thermal conductivity detector. Peak heights were compared to those of a certified, mixed standard of  $\text{CO}_2$  and  $\text{CH}_4$ . After calculating the concentration of these gases in the headspace, the concentration in the water was calculated using a value for Henry's constant of 0.0015 mol/L atm for methane and 0.0339 mol/L atm for carbon dioxide. The dissolved  $\text{CH}_4$  and  $\text{CO}_2$  concentrations were then calculated by assuming that all of the gases were originally in the dissolved phase. Even the best blanks (evacuated Wheaton

monitored in the water column over the entire study in Emerald Lake. In the absence of limestone bedrock, the CO<sub>2</sub> concentrations represent a balance between atmospheric equilibration, uptake by photosynthesis, and production from organic matter decomposition. The large amount of organic matter in the sediments serves as an important source of CO<sub>2</sub>. The standard deviation of our CO<sub>2</sub> measurements was 45 uM except for samples taken on 7/9/85 and 8/19/86, when it was 11 uM. Using two standard deviations as a significance criterion, the CO<sub>2</sub> levels in the summer are not different from what one would expect from atmospheric equilibration (13 uM) (Fig. 2). The mean concentration in winter water columns (91, 92, and 127 uM in March, April, and May) are significantly larger than atmospheric concentrations. Methane was not found in any of the water column samples except for two samples, which was probably the result of contamination or analytical error (data not shown).

Alkalinity in the water column ranged from 10 to 25 ueq L<sup>-1</sup> in summer and from 25 to 50 ueq L<sup>-1</sup> in winter (Fig. 3). Ammonium was generally below 3 uM except near the bottom when conditions became anoxic.

Nitrate concentrations in Emerald Lake ranged from 0 to 3 uM in the summer and from 5 to 15 uM in the winter (Fig. 4). The winter alkalinity and nitrate profiles are opposite to each other, suggesting that the alkalinity profiles resulted from nitrate dynamics. Sulfate concentrations in the summer were about 2 uM and in the winter about 5 uM. The winter profiles show a slight decreasing trend with depth.

Table 4. Charge balance for water analyses					
Sample type	COA	SE of COA	CMA ( $\mu\text{eq L}^{-1}$ )	SE of CMA	<i>n</i>
Water column	1.18	0.045	3.14	3.10	85
Long peepers	1.15	0.025	27.6	7.6	121
Short peepers (flux planes)	0.95	.030	-19.8	9.8	9

COA = cations over anions  
CMA = cations minus anions  
SE = standard error of the mean  
*n* = number of samples in the mean

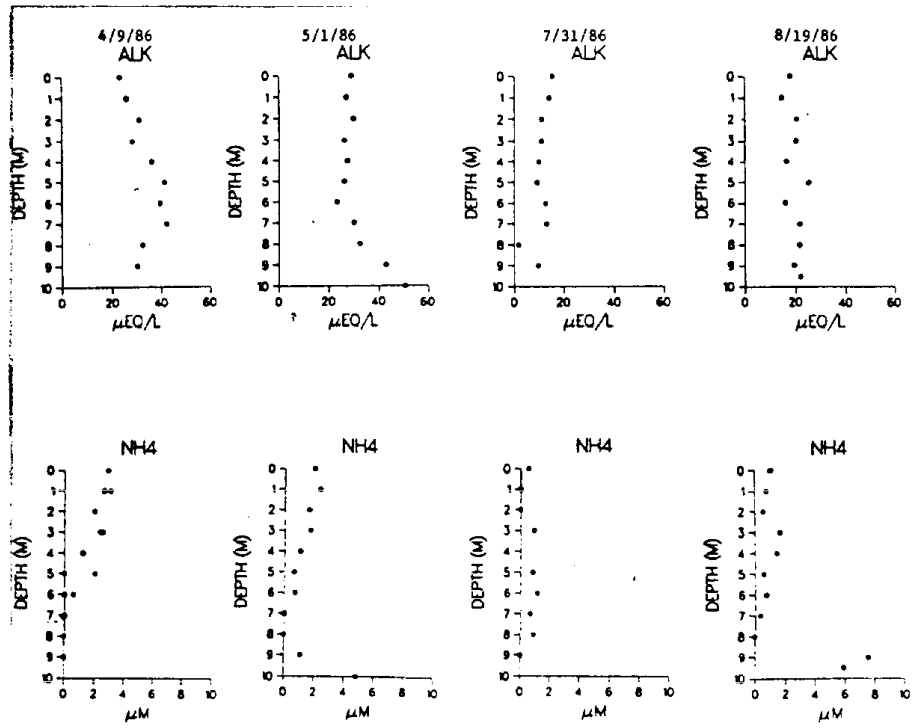


Figure 3 . The concentration of alkalinity (Alk) and ammonium ( $\text{NH}_4$ ) in Emerald Lake water at selected times during the study.

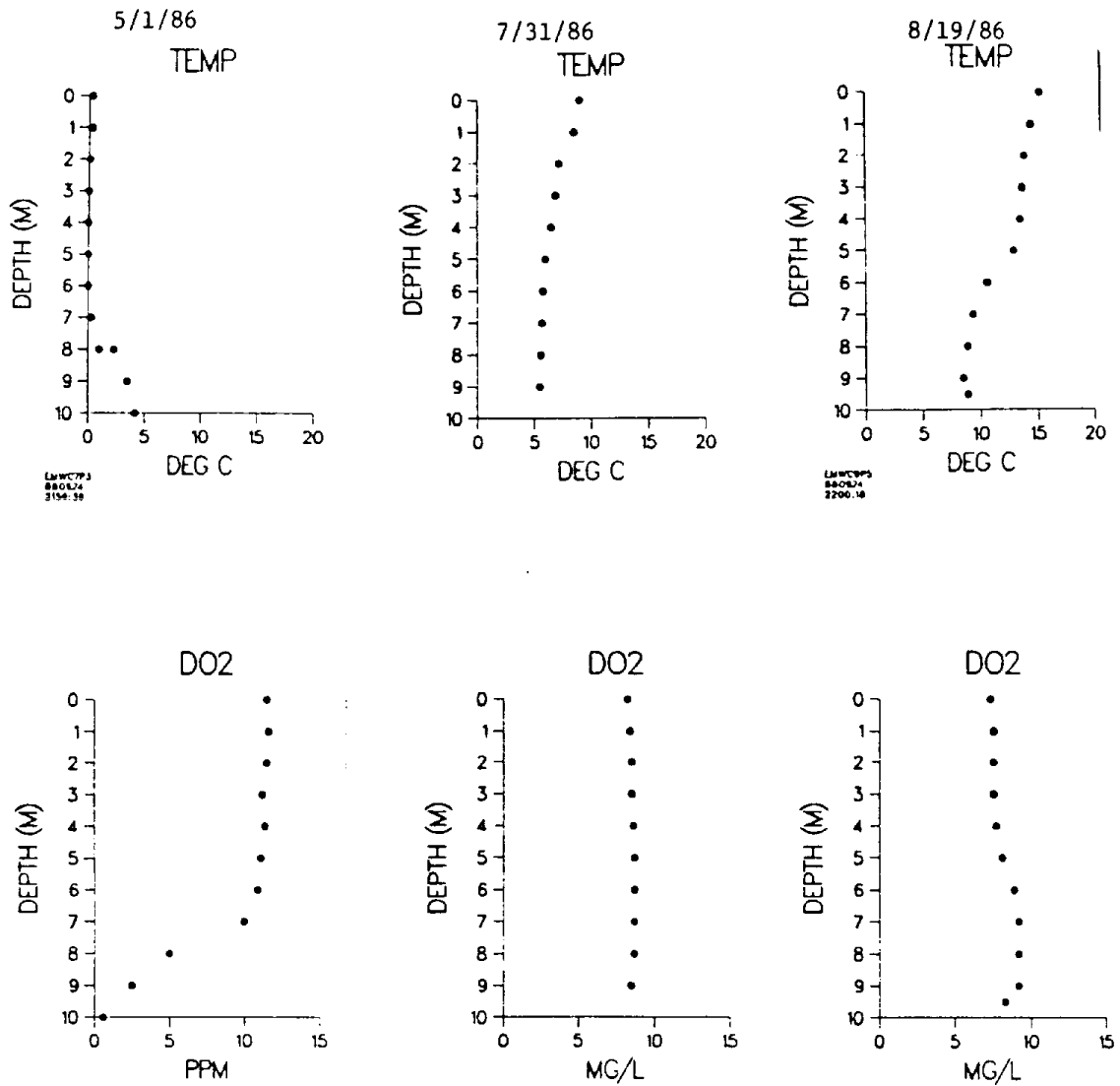


Figure 1 . The temperature (temp.) and dissolved oxygen (DO<sub>2</sub>) content of Emerald Lake water at selected times during the study.

Dissolved silica was measured only in two sets of winter water column samples (Fig. 5). Concentrations were less than 4 ppm and are similar to values reported by Melack et al. (1987). Iron concentrations were less than 2 uM in summer water columns and as high as 10 uM in the one winter water column (Fig. 6). Much of this measured iron was probably suspended particulates since the samples were not filtered and the dissolved O<sub>2</sub> content was too high for measurable dissolved Fe<sup>2+</sup>. The under-ice water samples (April) had higher iron concentrations because of release from the sediments under reduced oxygen conditions. Manganese concentrations were less than 1 uM in summer, but increased with depth in winter also as a result of the reduced oxygen conditions (Fig. 6).

### 3.3.2. Emerald Lake Interstitial Water

The concentration of most constituents in peeper samples increased greatly with increasing depth, indicating diffusion-driven transport from the sediments to the overlying lake water. Variability in concentrations of anions and cations between different peepers may have resulted from horizontal heterogeneity in sediments, heterogeneity in disturbance effects caused by peeper insertion, or different total sediment depth at different points.

One of the most important aspects of interpreting these data was knowing the location of the sediment/water interface (SWI). This could not be determined in the field because we inserted the peepers from a raft on the lake surface. In the summer, because vertical transport in the overlying water is usually at least 100

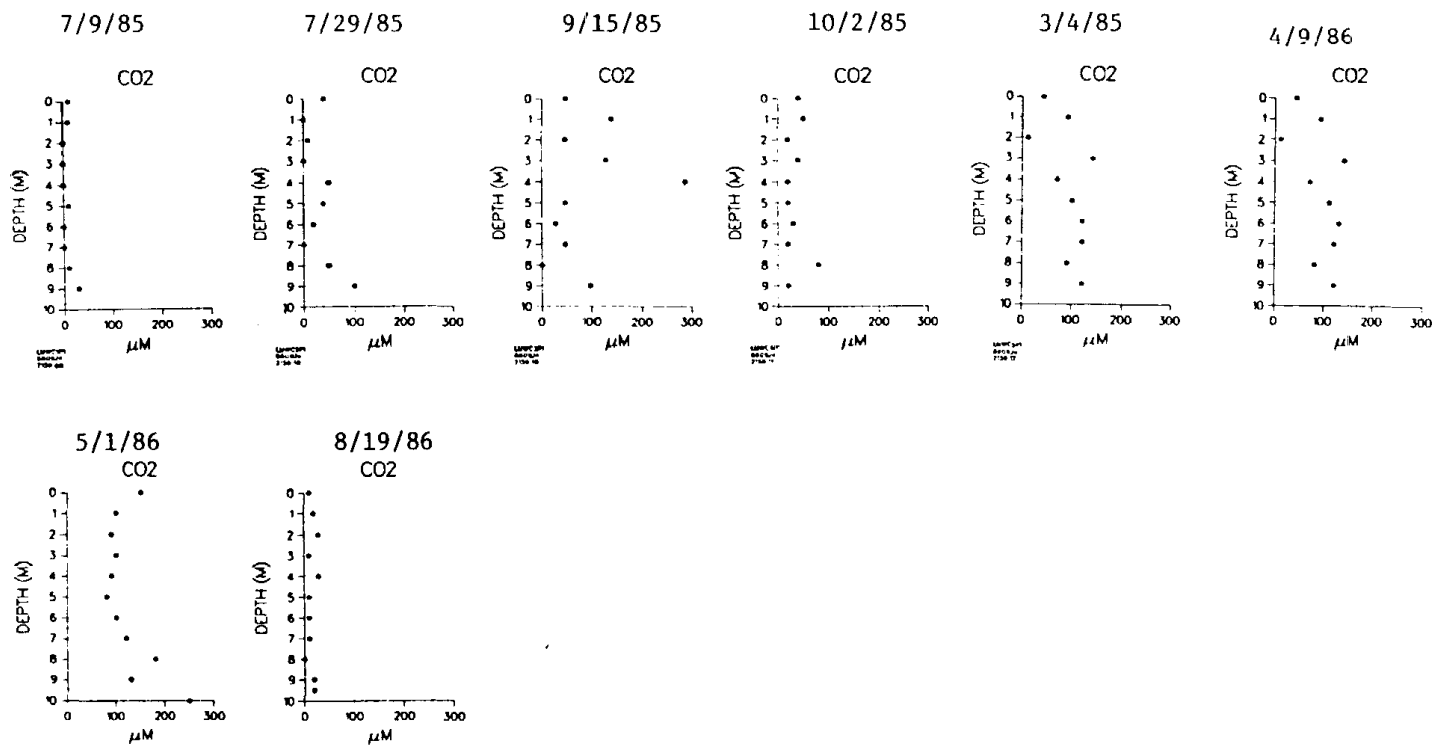


Figure 2 . The carbon dioxide (CO<sub>2</sub>) content of Emerald Lake water during the study.

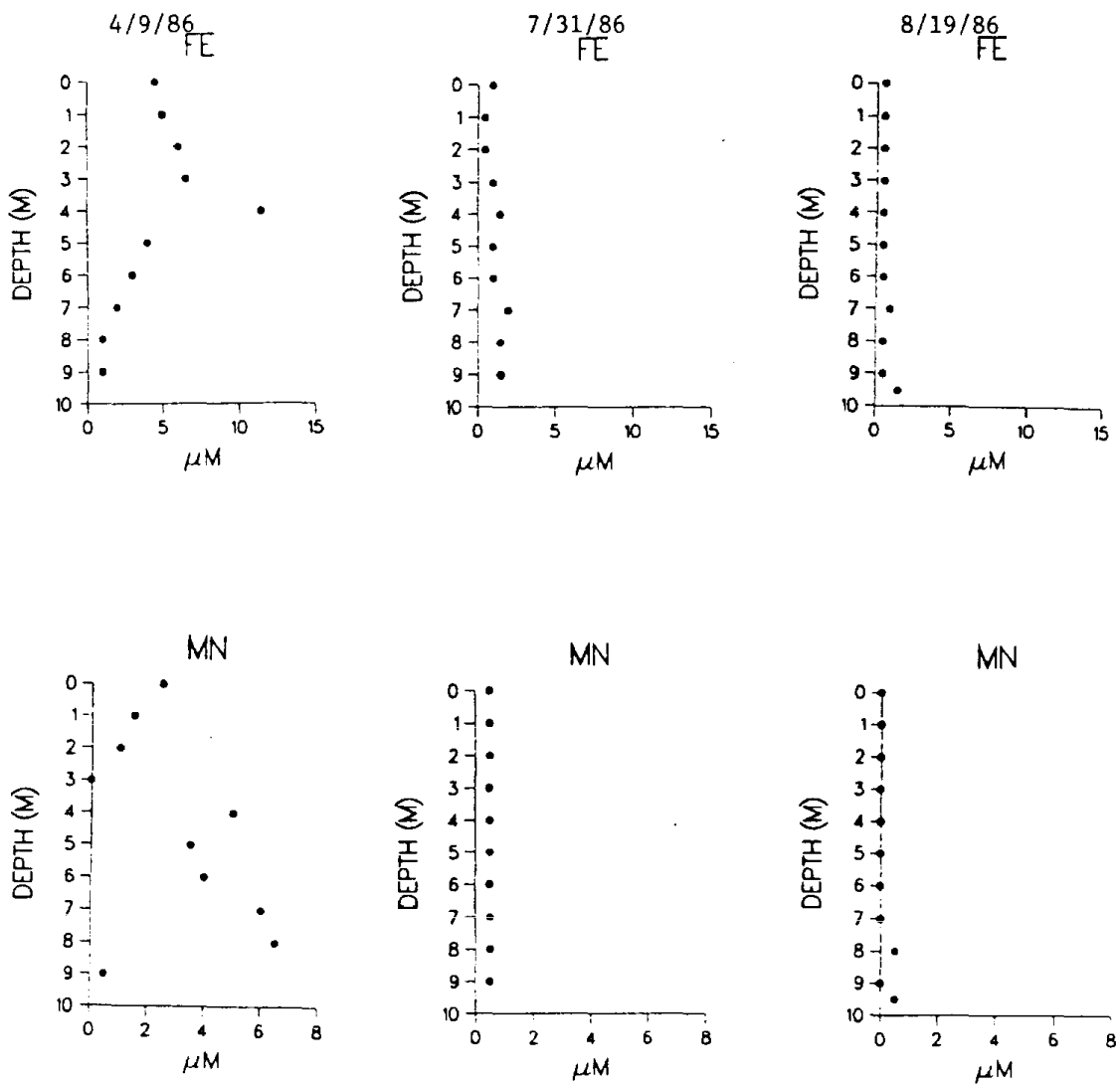


Figure 6 . The concentration of iron (Fe) and manganese (Mn) in Emerald Lake water at selected times during the study.

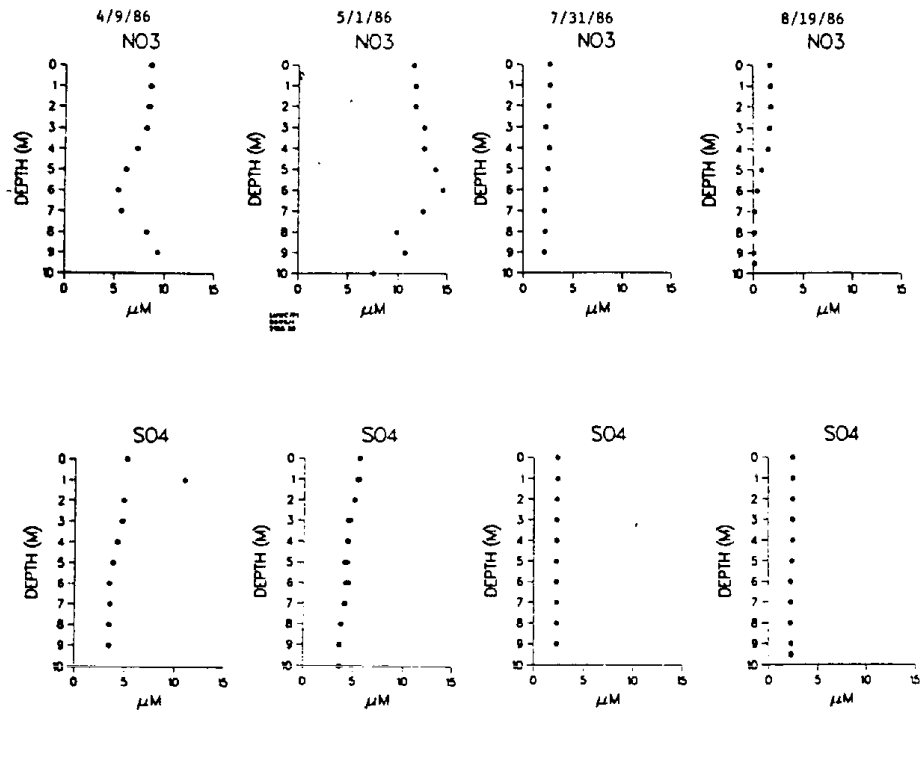


Figure 4 . The concentration of nitrate ( $\text{NO}_3$ ) and sulfate ( $\text{SO}_4$ ) in Emerald Lake water at selected times during the study.

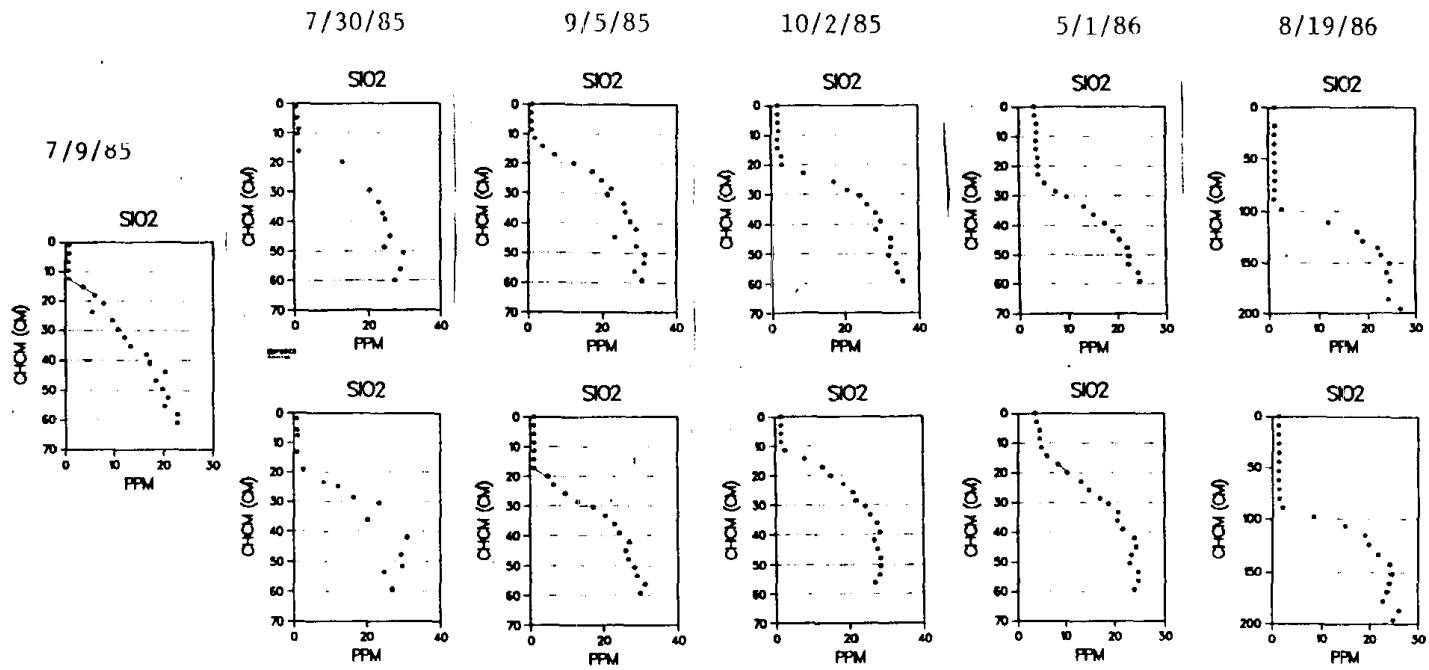


Figure 7 . The concentration of silica in the pore water and overlying lake water of Emerald Lake.

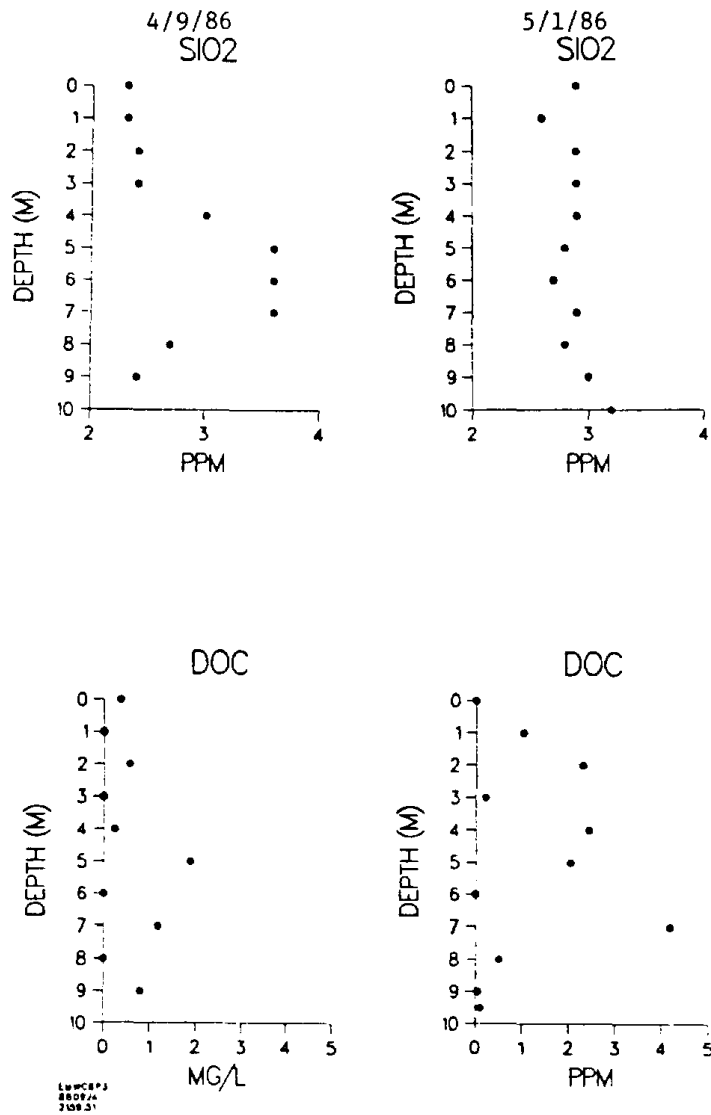


Figure 5. The concentration of silica (SiO<sub>2</sub>) and dissolved organic carbon (DOC) at selected times during the study.

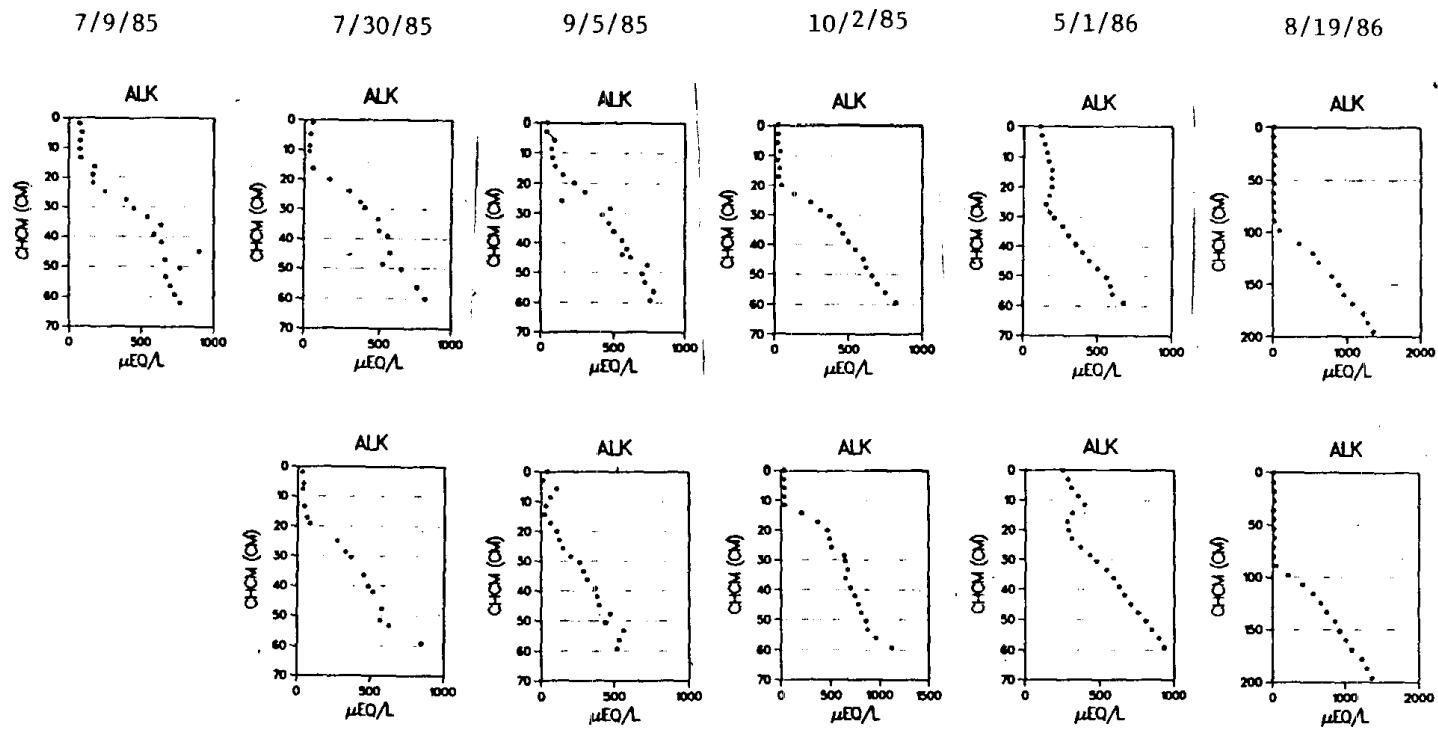


Figure 8 . The alkalinity of the pore water and overlying lake water in Emerald Lake.

time faster than in the porewater, we used a sudden decrease in the gradients of chemical constituents as an indicator of the SWI. Silica is a good indicator because it is not involved significantly in adsorption or precipitation reactions. This technique actually estimates the top of the diffusive boundary layer. Under ice, if the bottom water is very still and the diffusive boundary layer quite thick, this technique will not work. Melack et al. (1987) measured this layer to be ~ 1 mm in the summer. While the precise location, and chemical gradients, at the SWI are important for calculation of fluxes and modeling, these data are not as important in this section, where a general analysis of the porewater chemistry and a less quantitative assessment of the fluxes are being made.

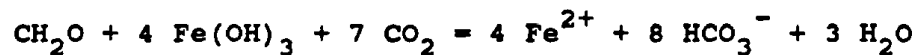
In the winter, the concentration gradients at the SWI are much less than in the summer due in part to the development of an extremely still layer at the bottom of the lake. In some cases, for specific elements, there was even a reversed concentration gradient. These trends will be discussed for individual elements below.

The concentration of silica in the lake water is less than 5 ppm but increased rapidly below the SWI, reaching maximum concentrations of 25 ppm about 50 cm below this boundary (Fig. 7). Below 50 cm, silica concentrations remained approximately constant with depth, possibly as a result of equilibration with some silica-bearing solid. One of the most likely silica sources is diatom frustules, which comprise an important percentage of the sediment solids (Holmes, 1986).

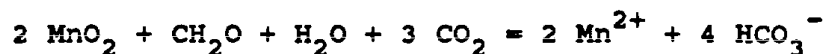
the depths which were measured. In the aerobic water above the sediments in the summer months,  $\text{NH}_4$  was very low despite diffusion out of the sediments, presumably as a result of nitrification followed by denitrification near the SWI (Seitzinger, 1988) and some uptake of N by aquatic plants. Sharp nitrate peaks are often seen at the SWI (Fig. 15), supporting a tightly coupled nitrification-denitrification scenario. In several of the peepers, two distinct segments in the concentration gradient can be seen. The upper gradient extends from the SWI to about 10 or 20 cm in depth. The lower segment of the gradient extends from 20 cm to the bottom of the peeper. This trend was apparent in the long peepers as well, but over a greater distance. The differences in the slope of the gradients is most probably a result of differences in the rate of organic matter decomposition, with the greatest decomposition rates near the surface and lower rates associated with the deeper sediments. In winter peepers, the presence of  $\text{NH}_4$  above the SWI indicates lowered  $\text{O}_2$  and results in a decreased concentration gradient at the SWI.

Methane was absent from the lake water in the summer and early fall but was present in the winter as indicated by its presence in the chambers which lie above the SWI (Fig. 10).  $\text{CO}_2$  levels were also higher in the lake in the winter than in the summer (Fig. 11). The higher methane can be explained by the reduced  $\text{O}_2$  concentration in lakewater during the winter. The  $\text{CO}_2$  buildup is also a result of this stratification which allows constituents diffusing from the sediments to accumulate in the

Of primary interest in this project is the generation of alkalinity by the sediments. On most sampling dates, alkalinity concentrations increase rapidly from 25 to 50 ueq/L in the lakewater to 700 or 800 ueq/L less than a meter below the SWI (Fig. 8). Also, for most peepers, the measured alkalinity does not appear to reach a constant value even at the deepest depths sampled. It is important to note that the measured alkalinities presented in Fig. 8 are the alkalinities measured on unacidified samples which were stored for periods ranging from several days to weeks before the alkalinities were measured. During the storage, the reduced Fe oxidized and precipitated, resulting in a loss of alkalinity. Therefore, in situ porewater alkalinities are higher than those shown in Fig. 8 by an amount equal to the equivalents of  $\text{Fe}^{2+}$ . Good charge balance after making this correction supports its validity. The concentration gradients at the SWI were lower in the winter due to a buildup of alkalinity in the anoxic hypolimnion. For one peeper (5/1/86, Fig. 8), there was a reversed gradient at the SWI, probably due to the rapid oxidation of labile organic matter at the SWI accompanied by the reduction under anoxic conditions of ferric oxyhydroxides and manganese dioxide:



and



where  $\text{CH}_2\text{O}$  is used as a schematic formula for organic matter.

Ammonium reached concentrations of more than 800 uM in the deepest pore water samples (Fig. 9). For  $\text{NH}_4$ , as well as alkalinity, maximum concentrations were apparently not reached at

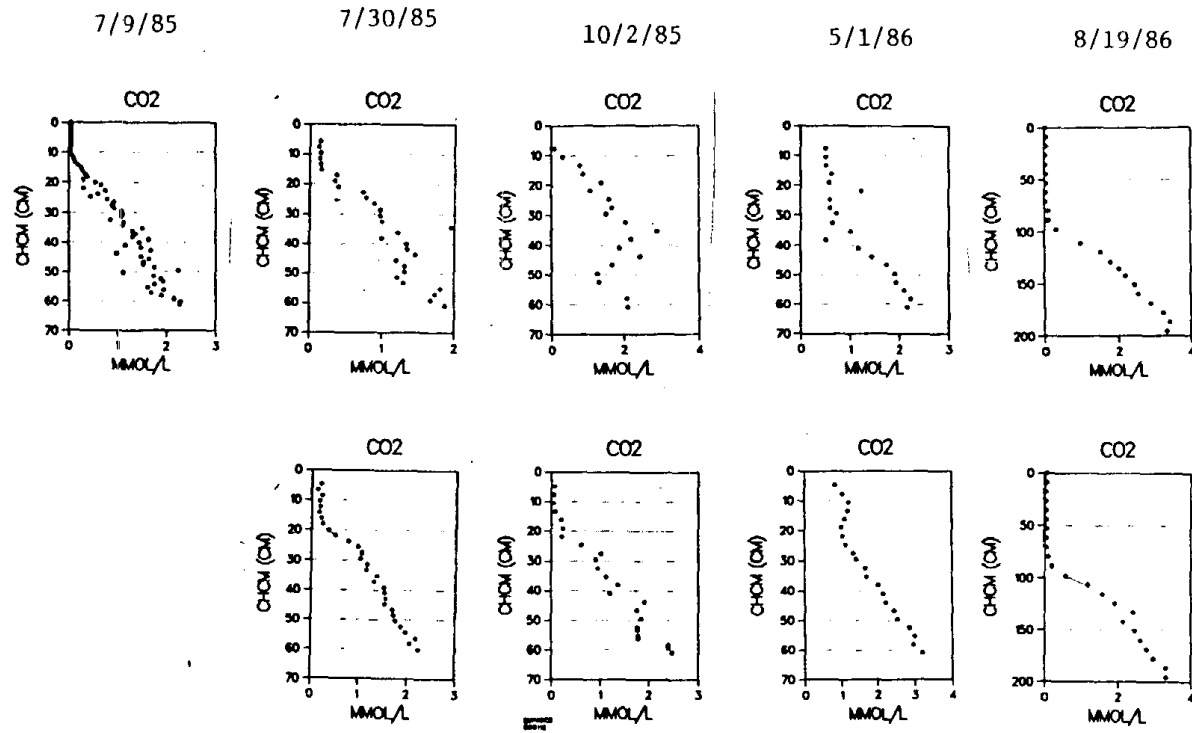


Figure 11. The concentration of carbon dioxide in the pore water and overlying lake water in Emerald Lake.

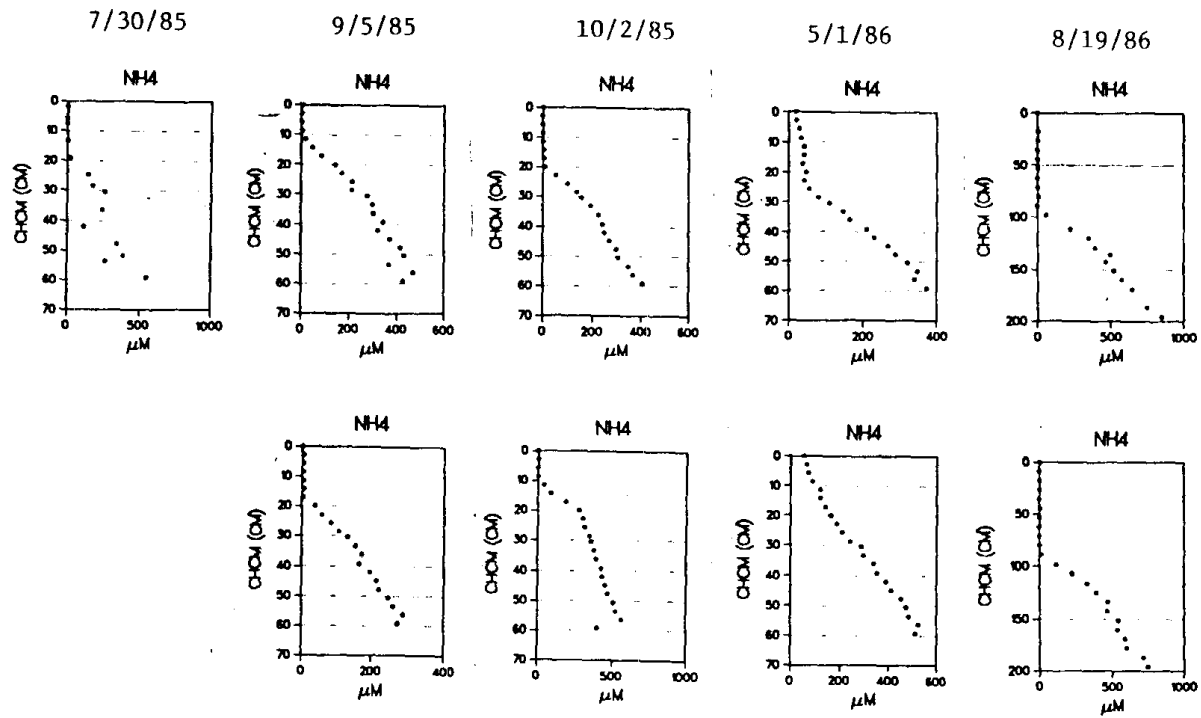


Figure 9 . The ammonium concentration of the pore water and overlying lake water in Emerald Lake.

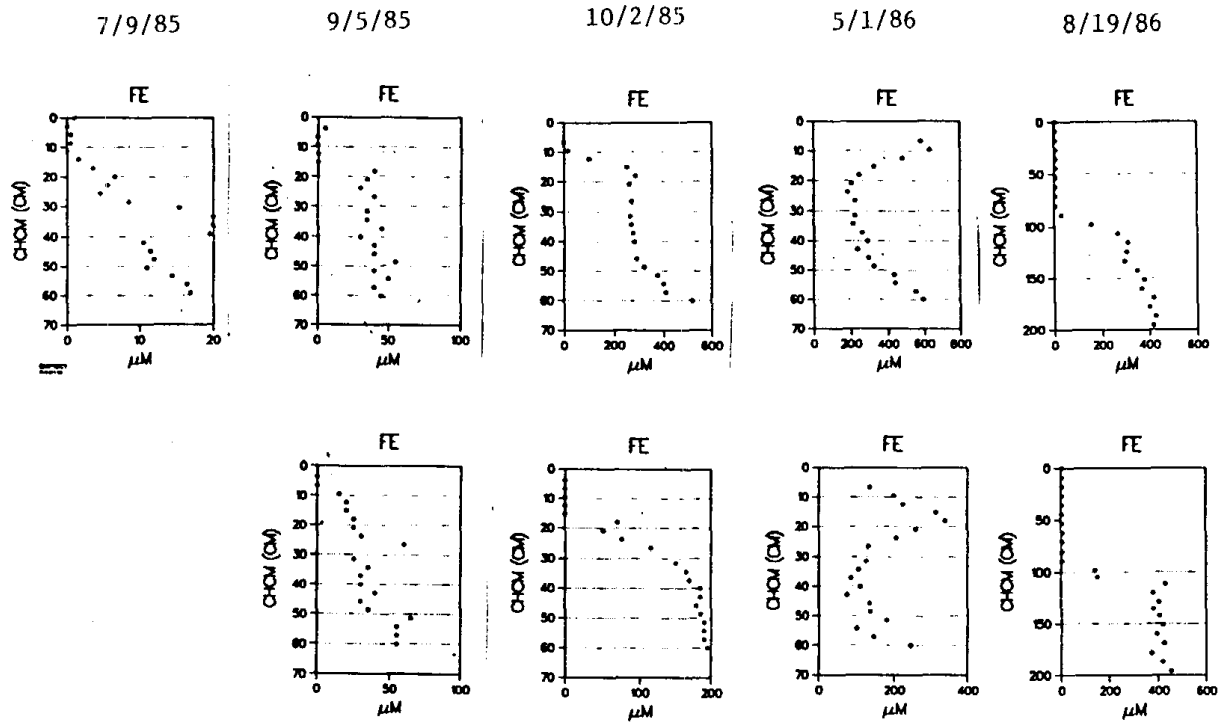


Figure 12. The concentration of iron in the pore water and overlying lake water of Emerald Lake.

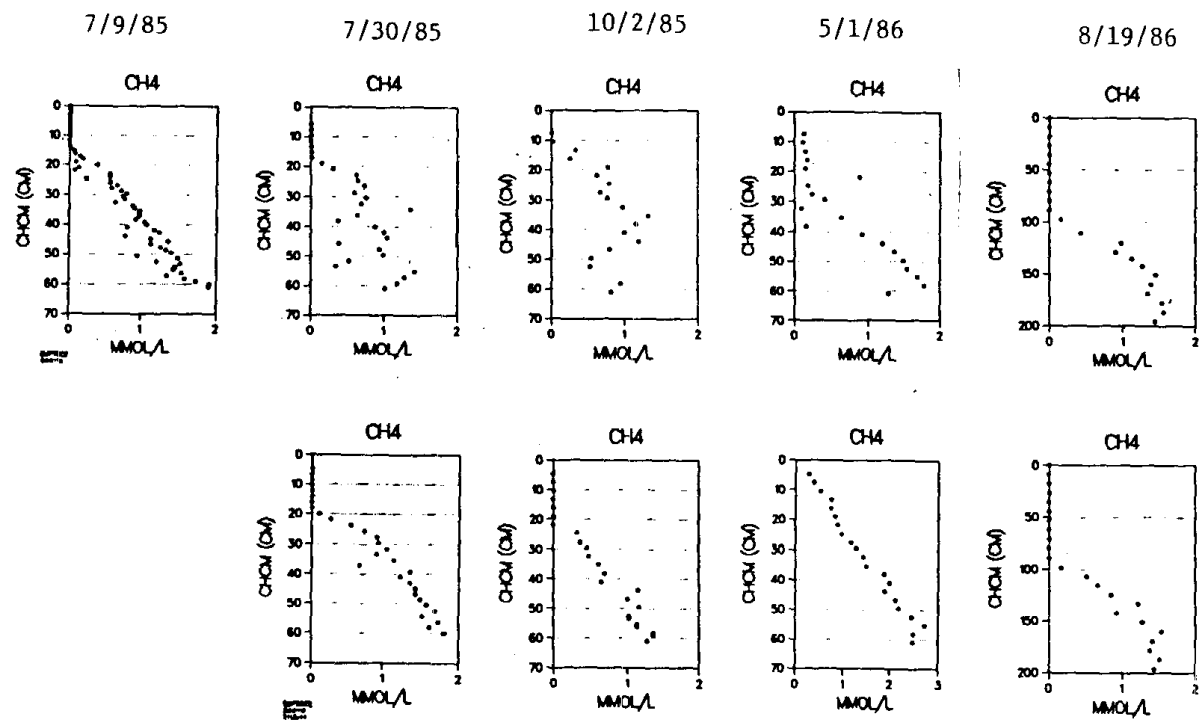


Figure 10. The concentration of methane in the pore water and overlying lake water of Emerald Lake.

mineral dissolution (siderite ??) at these depths.

The sum of base cations ( $\text{Ca}^{2+}$ ,  $\text{Mg}^{2+}$ ,  $\text{Na}^+$ ,  $\text{K}^+$ ) (SBC) is an important parameter of the pore waters because the alkalinity associated with them is not lost as these cations diffuse into oxygenated water. The SBC reached maximum values of approximately 400 ueq/L (Fig. 14). In the winter peepers (5/1/86) the concentrations in the overlying lake water were much greater than during ice-free conditions.

Nitrate and  $\text{SO}_4^{2-}$  were low, but detectable, in most peepers (Figs. 15 and 16). The existence of  $\text{NO}_3^-$  or  $\text{SO}_4^{2-}$ , especially in the deepest chambers where anoxic conditions almost certainly prevailed, is probably an artifact of processes which occurred during sample handling and storage (nitrification of  $\text{NH}_4^+$  and oxidation of reduced S compounds). In most peepers, the concentrations are so low and the scatter is so high that significant trends are not discernable, although one would expect that  $\text{NO}_3^-$  and  $\text{SO}_4^{2-}$  are diffusing into the sediments from the overlying lake (Rudd et al., 1986) and are being lost through biological reduction. As discussed above, the sharp  $\text{NO}_3^-$  peaks at the SWI in some of the peepers with low scatter support a coupled nitrification-denitrification scenario for  $\text{NH}_4^+$ .

The charge balance of anions and cations are presented for a number of peepers in Fig. 17. For most peepers, there was good agreement between the sum of cations and the sum of anions. The discrepancy for the first peeper (7/9/85) is most likely the result of the precipitation of iron and manganese in unacidified samples since anions are much greater than cations. The reason for a

unmixed waters near the bottom of the lake. In one of the winter peepers (5/1/86, Fig. 11), a reversed concentration gradient occurred at the SWI for  $\text{CO}_2$ . This unusual gradient resulted from the rapid decomposition of labile organic matter at the SWI combined with extremely slow vertical transport in the stratified bottom waters. Greater, but spatially and temporally variable, concentration gradients of  $\text{CO}_2$  across the SWI occurred under ice-free conditions.

Iron and manganese are found in their reduced states ( $\text{Fe}^{2+}$  and  $\text{Mn}^{2+}$ ) in the peepers (Figs. 12 and 13). Manganese concentrations were less than 10  $\mu\text{M}$  under ice-free lake conditions, and were variable, but did indicate that a concentration gradient existed from the sediments to the overlying lakewater. The Mn concentration in one winter peeper (5/1/86) reached 40  $\mu\text{M}$  about 30 cm below the SWI. Iron concentrations varied but seemed to reach levels between 200 and 600  $\mu\text{M}$  at 50 cm below the SWI and, in summer, were near zero in the overlying lake water. The low concentrations in the first peeper (7/9/85) are a result of not acidifying the samples upon extraction from the chambers, which resulted in precipitation of much of the iron. In the winter peepers (5/1/86), an unusual iron concentration gradient was present and some of the highest iron concentrations occurred near the SWI. These gradients are probably the result of the microbially-mediated reduction by organic matter of the thin layer of iron hydroxide which lies at the SWI during oxygenated conditions. The iron concentrations in the long peepers reach relatively constant levels below 150 cm. This seems to indicate that its solubility is being controlled by

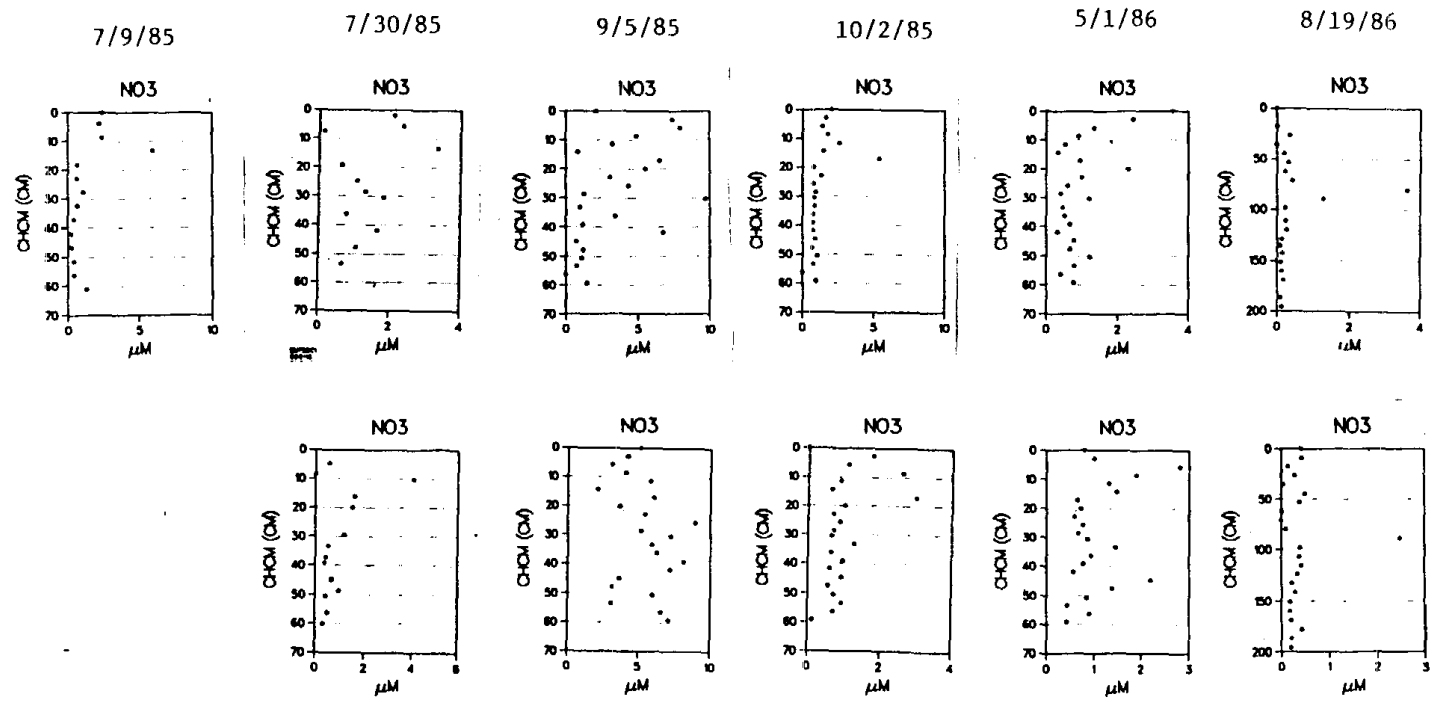


Figure 15. The concentration of nitrate in the pore water and overlying lake water of Emerald Lake.

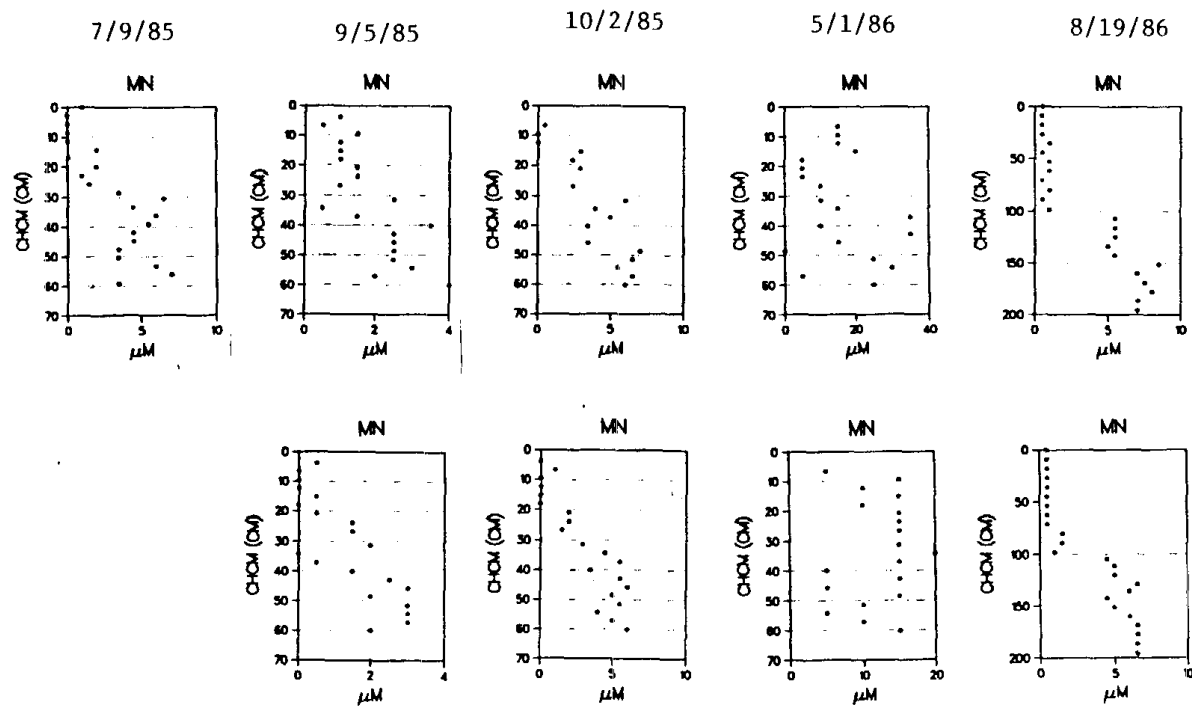


Figure 13. The concentration of manganese in the pore water and overlying lake water in Emerald Lake.

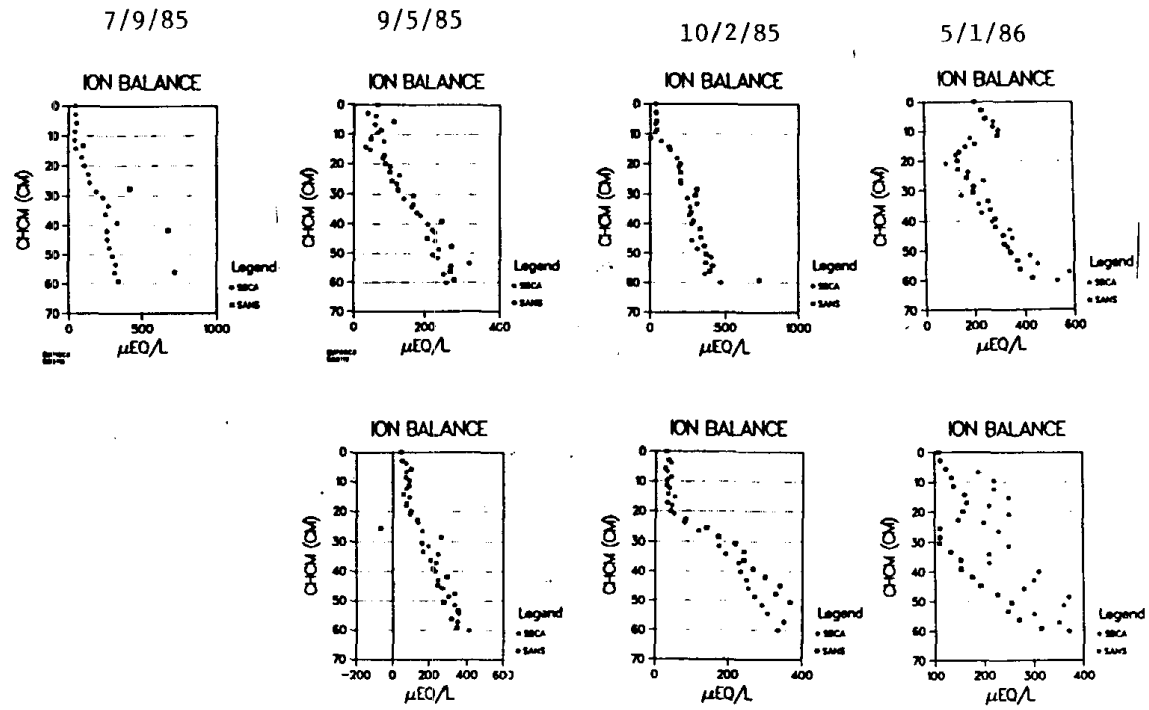


Figure 17. The balance of measured anions and cations in the pore water and overlying lake water in Emerald Lake.

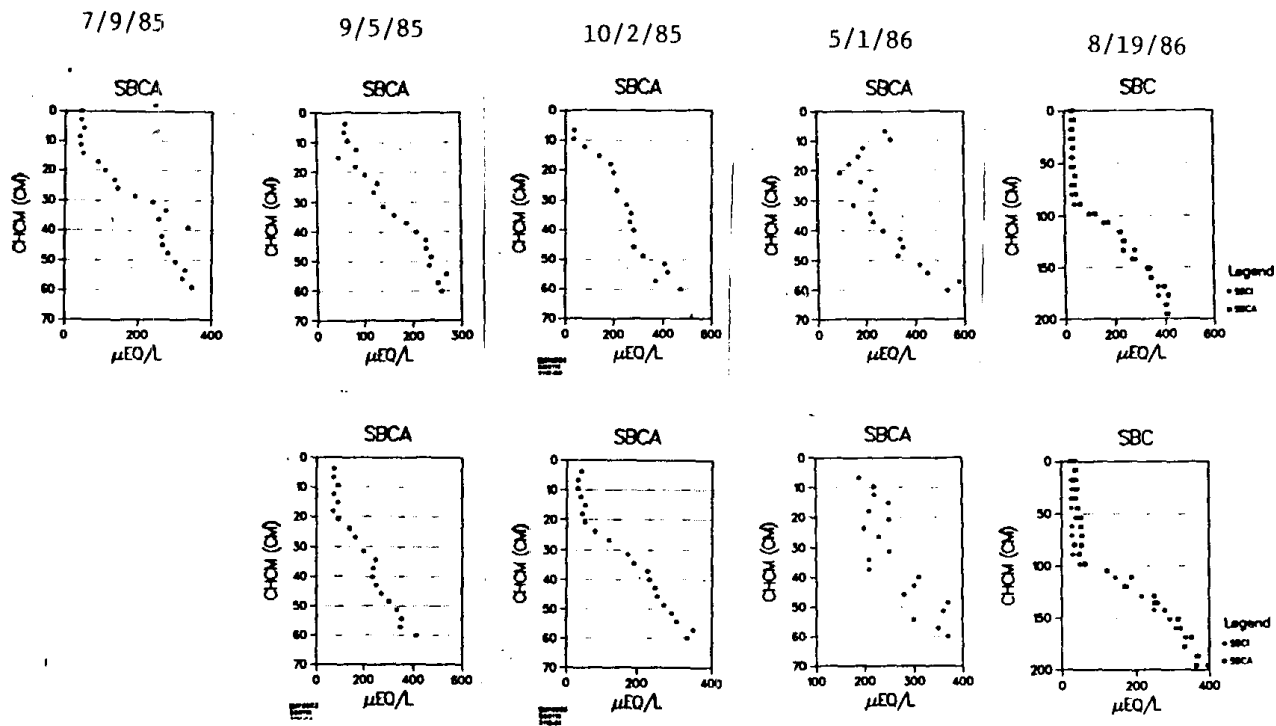


Figure 14. The sum of base cations (Ca, Mg, Na, K) in the pore water and overlying lake water in Emerald Lake.

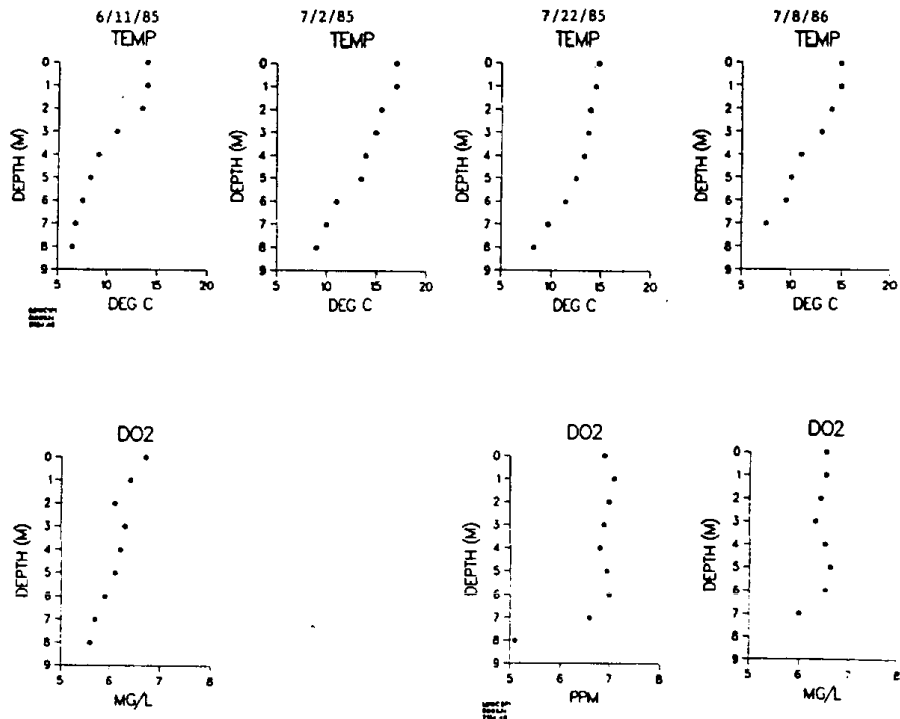


Figure 18 . The temperature (temp) and dissolved oxygen (DO<sub>2</sub>) of Eastern Brook lake water at selected times during the study.

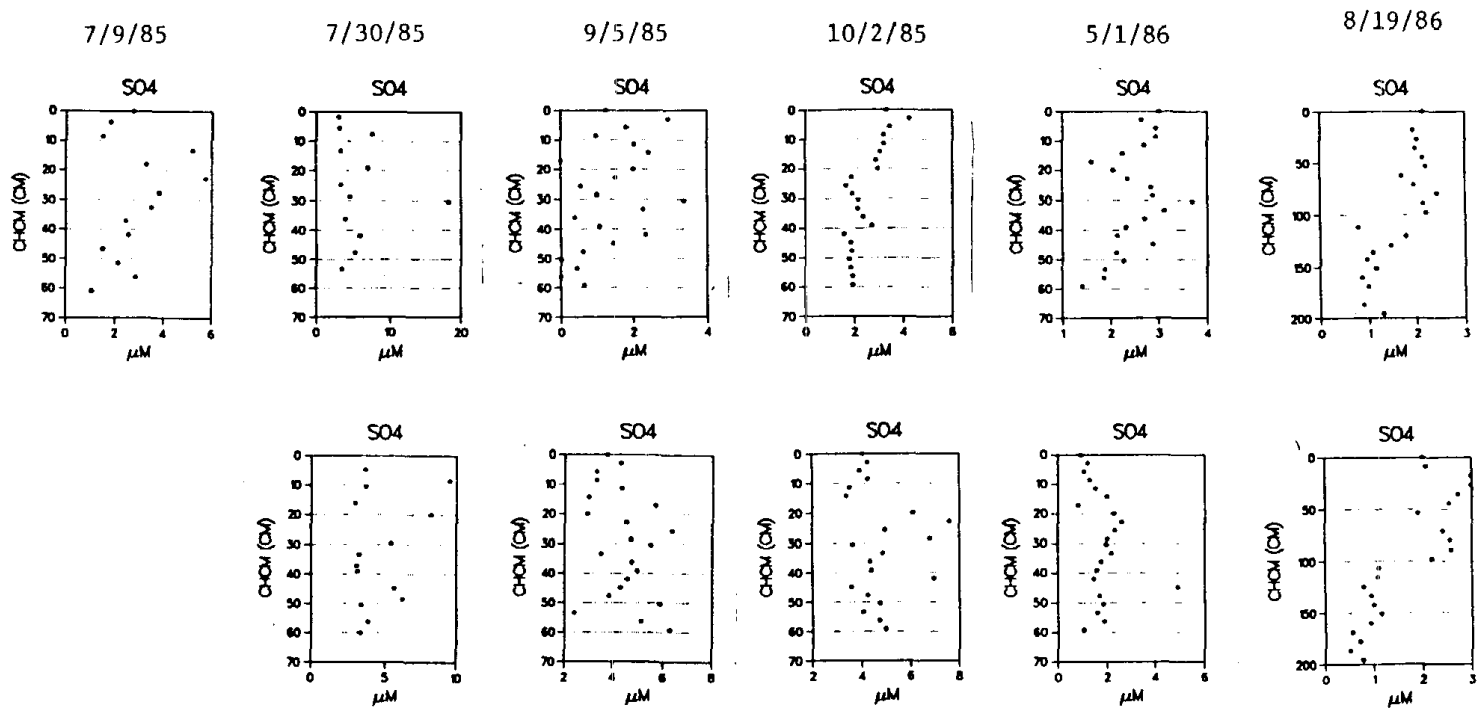


Figure 16 . The concentration of sulfate in the pore water and overlying lake water in Emerald Lake.

our measurements was 45  $\mu\text{M}$ , so some apparent trends may be ruled out as scatter. Lake water near the surface is expected to be in equilibrium with the atmosphere and to contain about 13  $\mu\text{M}$   $\text{CO}_2$ . The presence of methane in the summer water columns is probably the result of analytical error. The higher  $\text{CH}_4$  concentrations at 8 m in winter water columns indicate a zone of lowered oxygen levels.

Alkalinity in the water columns ranged from 100 to 130  $\text{ueq/L}$  during the summer and from 150 to about 350  $\text{ueq/L}$  in the winter (Fig. 20). Alkalinity profiles, which show increasing alkalinities with increasing depth, clearly suggest that the sediments are a prominent source of lakewater alkalinity.

Ammonium in summer water columns ranged from 0 to 10  $\mu\text{M}$  (Fig. 20). Much higher levels ( $\sim 35 \mu\text{M}$ ) were seen in the winter below 6 m due to a lack of mixing, lowered oxygen levels, and a resulting buildup from sediment fluxes during that time. The two summer profiles show little change with depth.

Dissolved Si was measured for only two water columns, both under ice, and ranged from 3 to 6 ppm (Fig. 21). Nitrate levels were  $< 1.5 \mu\text{M}$  (Fig. 22). Sulfate levels were slightly higher and, at four out of five sampling dates, decreased in concentration near the SWI. The Fe and Mn concentrations of the lake water showed great seasonal variability (Fig. 23). For both metals, concentrations were low in summer but became quite high in stratified bottom waters in winter samples.

#### 3.3.4. Eastern Brook Lake Interstitial Water

discrepancy in one of the winter peepers (5/1/86) is not known.

### 3.3.3. Eastern Brook Lake Water Column

Eastern Brook lake, like Emerald, is dimictic. Stratification occurs under ice in winter and under ice-free conditions in the summer. Snowmelt normally occurs from April to June. Eastern Brook is fed by a perennial stream, as well as by secondary inlets, and enough water enters the lake that the outlet flows during most years. During the winter, alternating layers of ice and slush develop on the lake, reaching a depth of up to 3 m. Under ice, conditions of lowered oxygen may exist for periods of up to a few months.

Detailed, long-term study has been done on Eastern Brook lake by researchers at the Sierra Nevada Aquatic Research Lab, although none has been published at this time. Our objective was not to intensively duplicate ongoing measurements made by these other researchers but instead to focus on sediment pore water chemistry. Therefore, our set of lakewater chemistry data provide only a glimpse of the seasonal dynamics of the lakewater chemistry. Some temperature and dissolved oxygen profiles are presented in Fig. 18.

Dissolved  $\text{CO}_2$  and  $\text{CH}_4$  in the water column were monitored periodically during the course of the study (Fig. 19). In general, winter water columns contained much more  $\text{CO}_2$  than summer water columns and usually a gradient from the sediment to the lakewater was observed. However, the standard deviation of

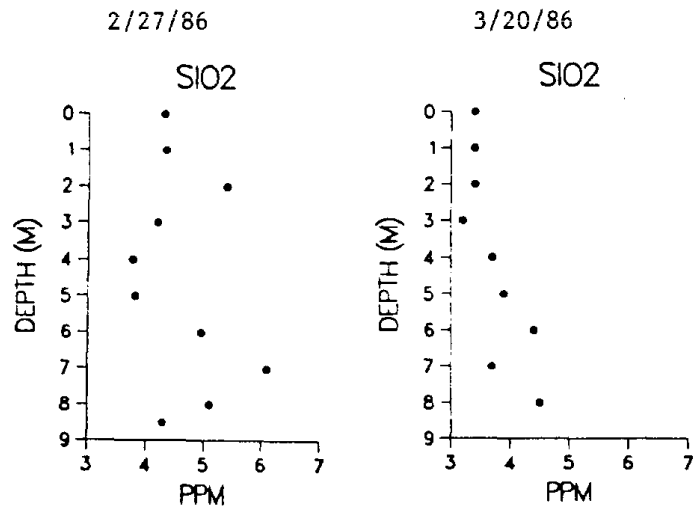


Figure 21. The concentration of silica ( $\text{SiO}_2$ ) in Eastern Brook Lake water at selected times during the study.

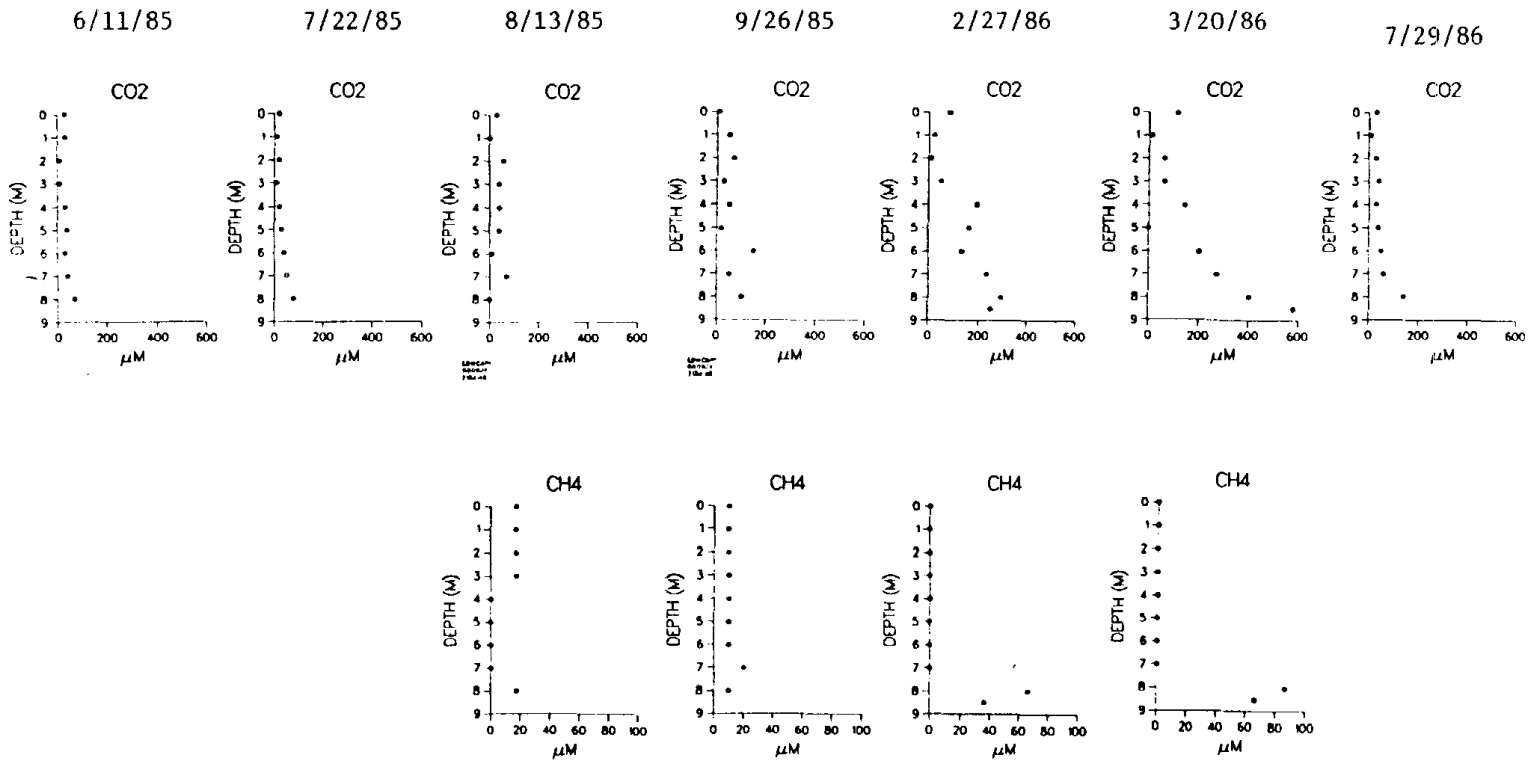


Figure 19. The concentration of carbon dioxide (CO<sub>2</sub>) and methane (CH<sub>4</sub>) in Eastern Brook lake water at selected times during the study.

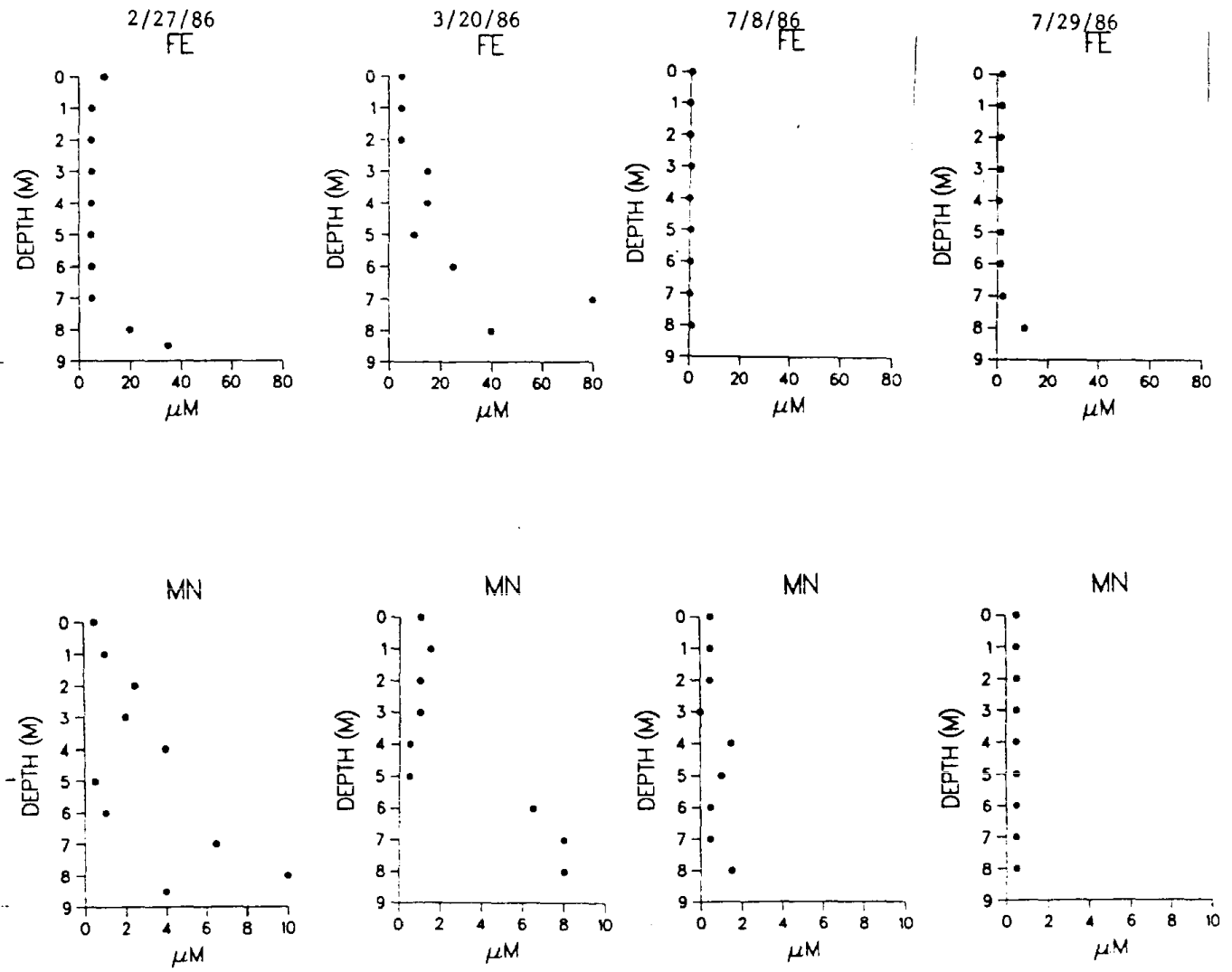


Figure 23 . The concentration of iron (Fe) and manganese (Mn) in Eastern Brook Lake water at selected times during the study.

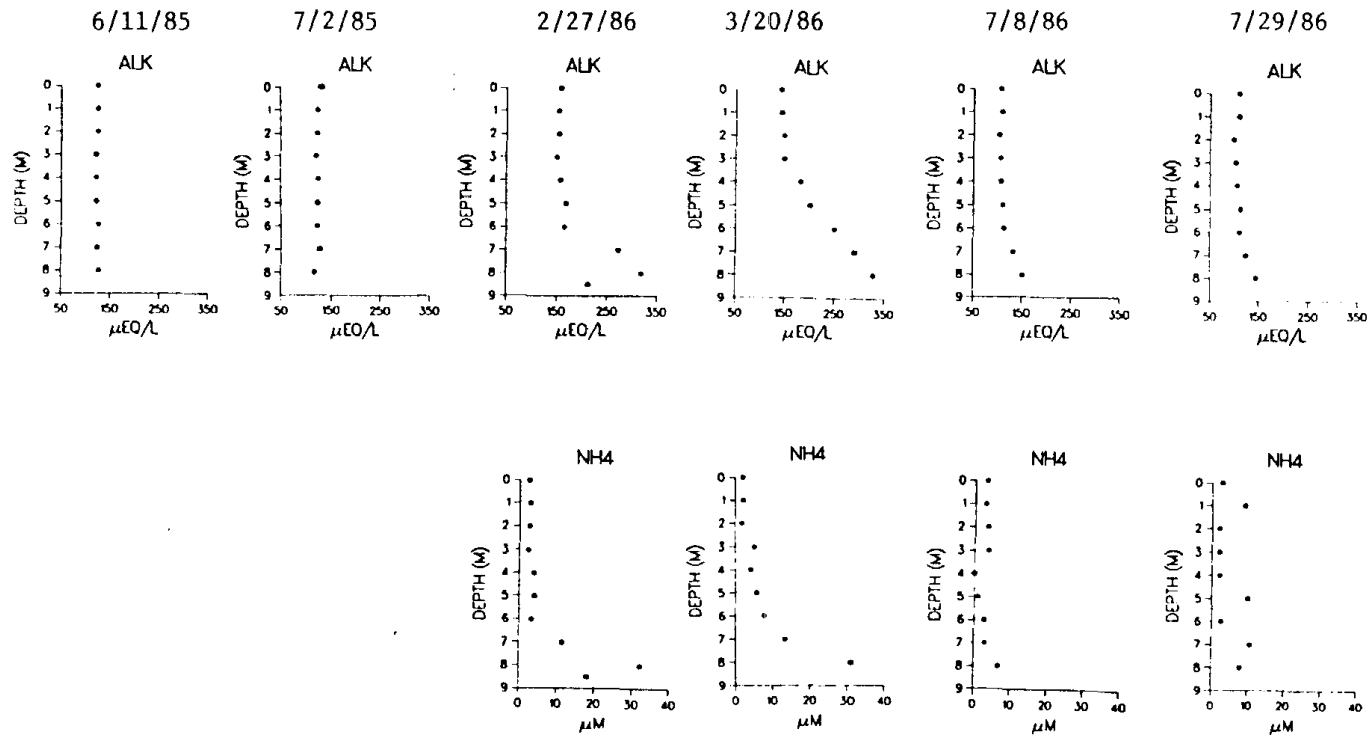


Figure 20. The concentration of alkalinity (Alk) and ammonium ( $\text{NH}_4$ ) in Eastern Brook lake water at selected times during the study.

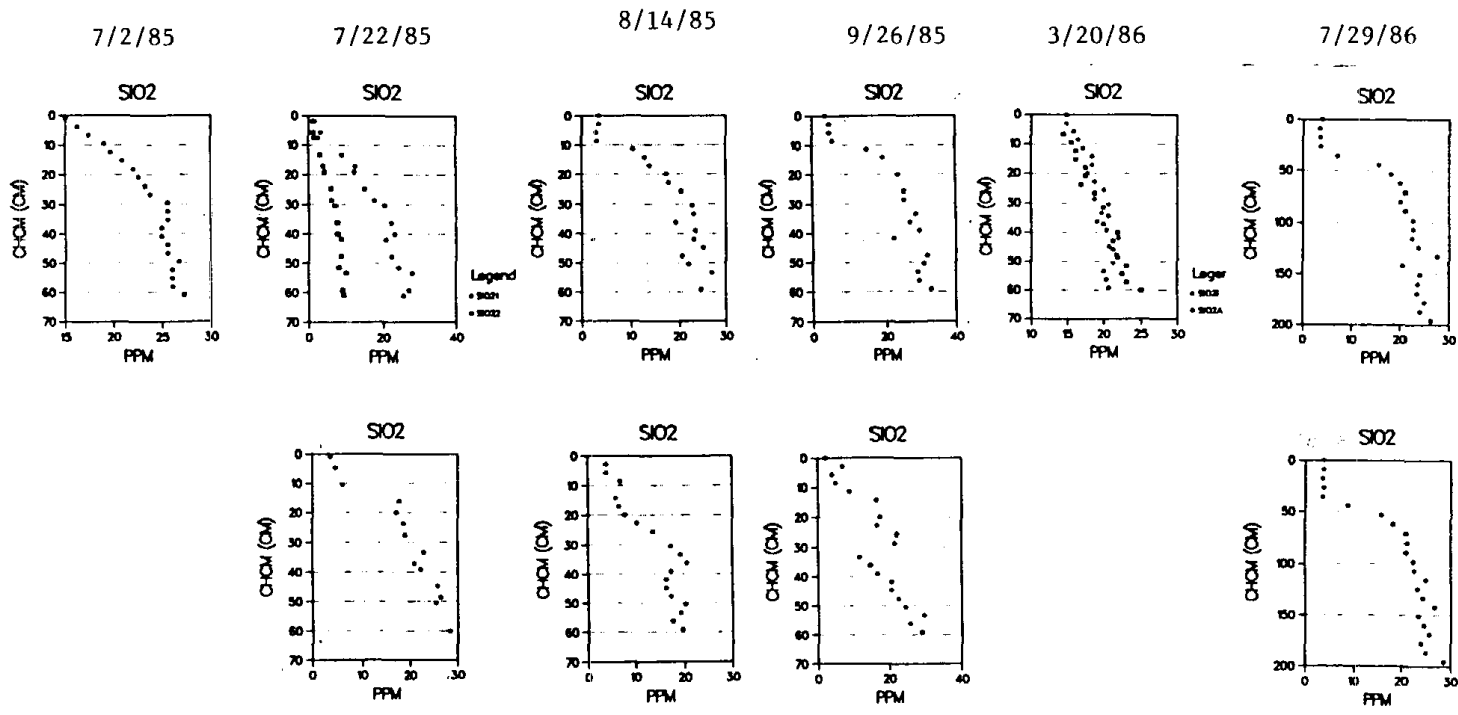


Figure 24. The silica concentration of the pore water and overlying lake water in Eastern Brook Lake.

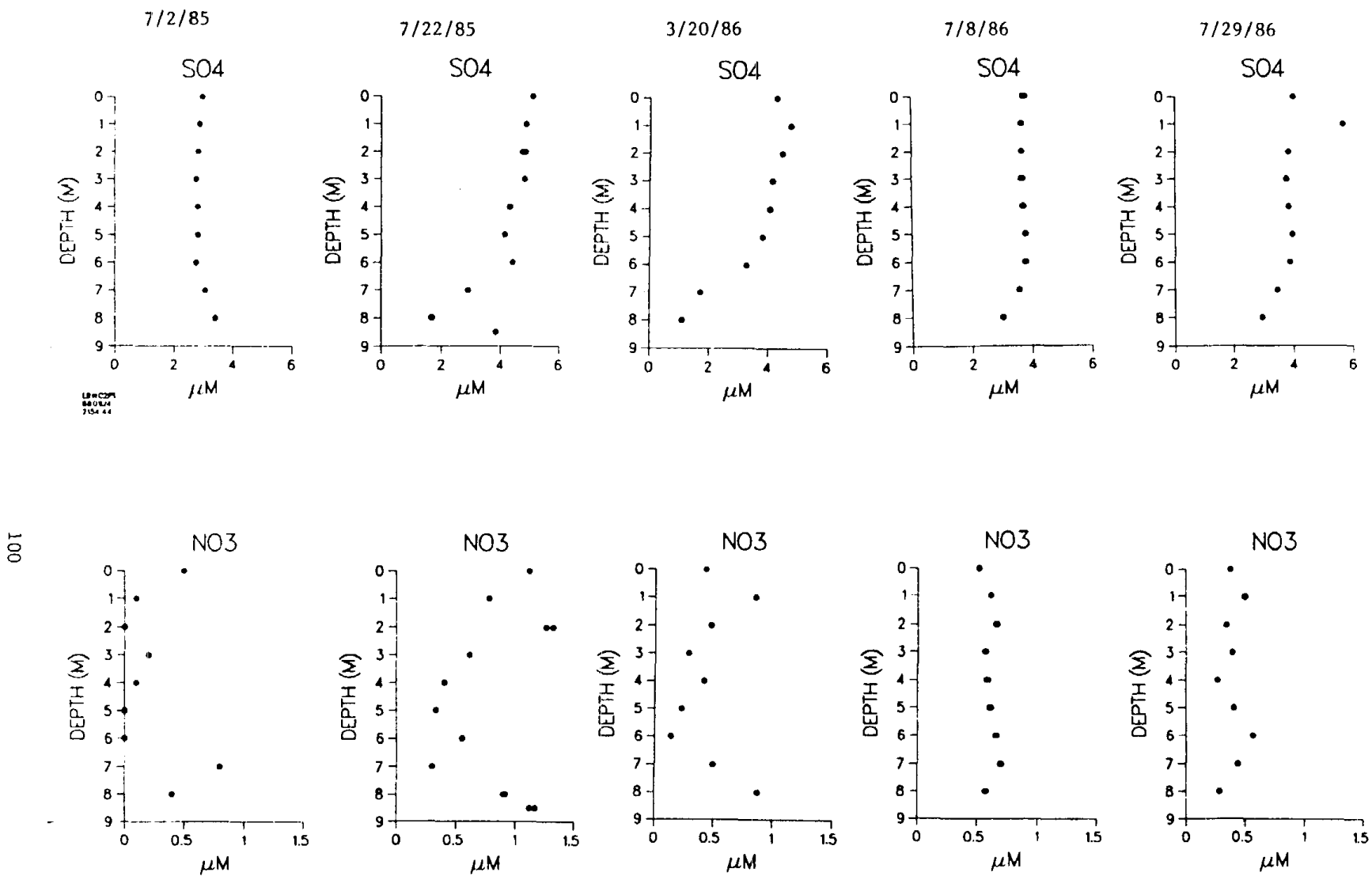


Figure 22. The concentration of sulfate (SO<sub>4</sub>) and nitrate (NO<sub>3</sub>) in Eastern Brook Lake water at selected times during the study.

1200 ueq/l) in the pore water lies below the depths which were sampled.

The  $\text{NH}_4^+$  concentration in most peepers was near zero in the lakewater and increased steadily with depth (Fig. 26). The unusual concentration gradient in one of the 8/14/85 peepers corresponds to the same trend noted for alkalinity and may have been due to restricted diffusion caused by the metal plate at the SWI. In the long peepers (7/29/86), the  $\text{NH}_4^+$  concentration continued to increase with depth indicating that the maximum  $\text{NH}_4^+$  concentration, which must be greater than 500  $\mu\text{M}$ , lies below the depths studied.

The concentration of  $\text{CO}_2$  and  $\text{CH}_4$  increased with depth (Fig. 27 and 28) in a manner similar to Emerald lake. Maximum concentrations of the gases in peepers, however, were approximately half those in Emerald lake, implying a higher rate of organic matter decomposition in the Emerald sediments. Again, the unusual concentration gradient of  $\text{CO}_2$  in one of the 8/14/85 peepers suggests interference by the metal plate on the peeper.

Manganese and iron concentrations were low in the first peeper (7/2/85) because these were not acidified (Fig. 29 and 30). For the other peepers, the manganese concentrations were as high as 15  $\mu\text{M}$ , but show a lot of scatter. Similar to the other chemical constituents, an unusual concentration gradient for manganese was evident in one of the 8/14/85 peepers. In general, the manganese concentration of the pore waters in both Emerald and Eastern Brook lakes were approximately the same. In contrast, the iron concentrations at the lowest point in the long peepers from

The soft nature of the deeper Eastern Brook lake sediments, relative to those in Emerald, allowed us to insert several of the peepers slightly too deep in the sediments. This caused the aluminum plate, designed to prevent the peeper from being completely immersed in the sediment, to lie on top of or below the SWI, possibly interfering with diffusion. This problem was indicated by a buildup of several constituents beneath the SWI at times of the year when such an occurrence would seem unreasonable. This was not a problem for the under-ice peepers or in the summer of 1986 when use of the aluminum plate was discontinued.

As in Emerald lake, we have taken the location where silica gradients decrease suddenly to be the SWI. Silica concentrations in the 7/2/85 peeper suggest that the entire peeper was driven past the SWI since silica levels do not decrease to water column values (Fig. 24). The 3/20/86 peeper also shows no gradient change, but since this is an under-ice peeper, it is possible that transport in the overlying water is by molecular diffusion only and hence a gradient change does not mark the SWI. There is no way of knowing the location of the SWI for these peepers. The maximum silica concentration in any peeper was about 25 ppm, which was similar to that in Emerald lake.

Alkalinity profiles usually showed increasing alkalinity with depth (Fig. 25). Exceptions were peepers on 8/14/85. The apparent buildup of alkalinity beneath the SWI in these peepers may have been due to restricted diffusion caused by the aluminum plates. In the two long peepers (7/29/86), the alkalinity continued to increase with depth suggesting that the maximum alkalinity (>

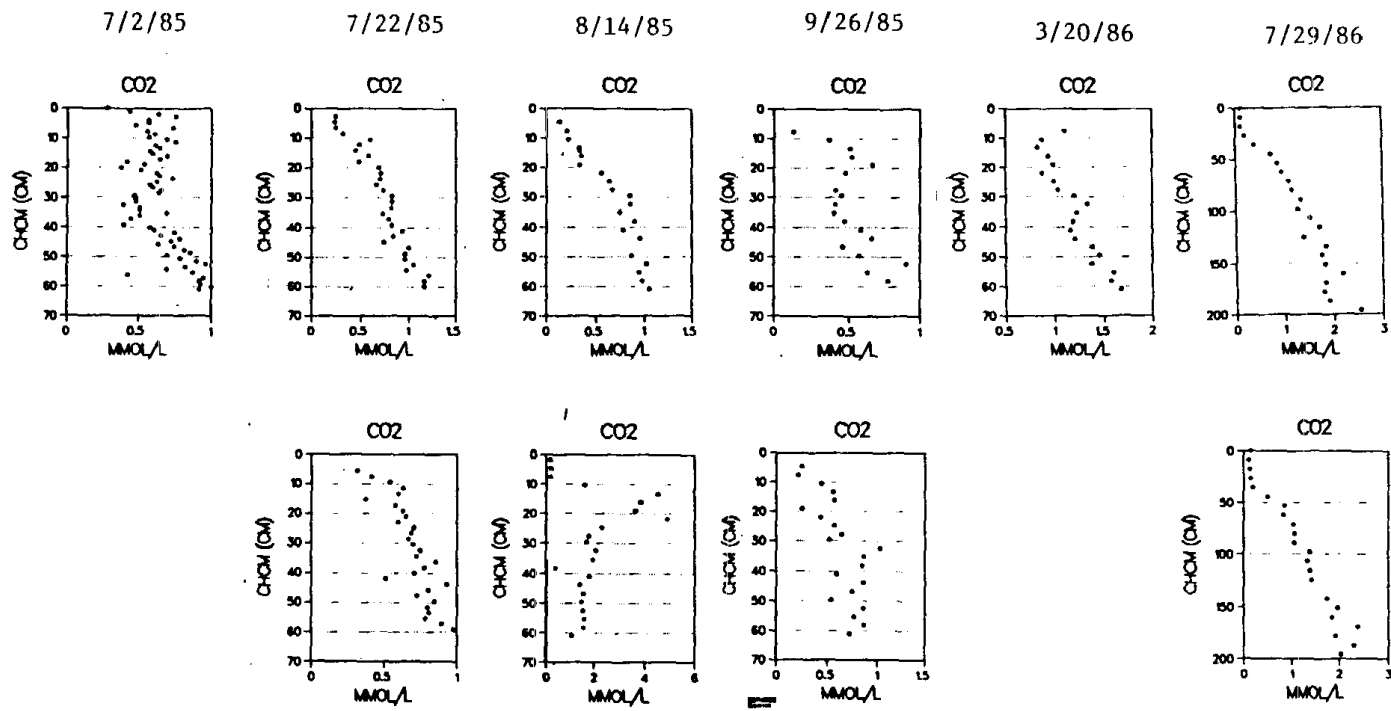


Figure 27. The concentration of carbon dioxide in the pore water and overlying lake water in Eastern Brook Lake.

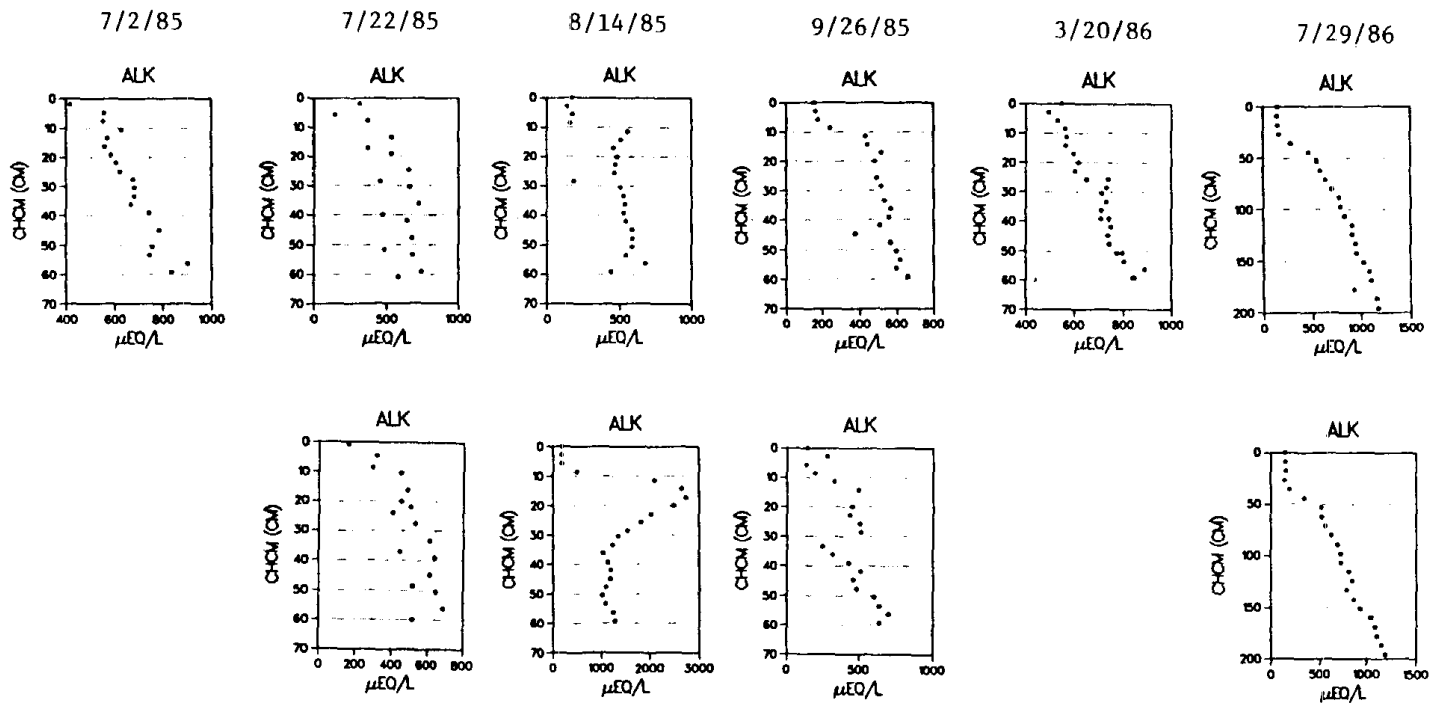


Figure 25. The alkalinity of the pore water and overlying lake water of Eastern Brook Lake.

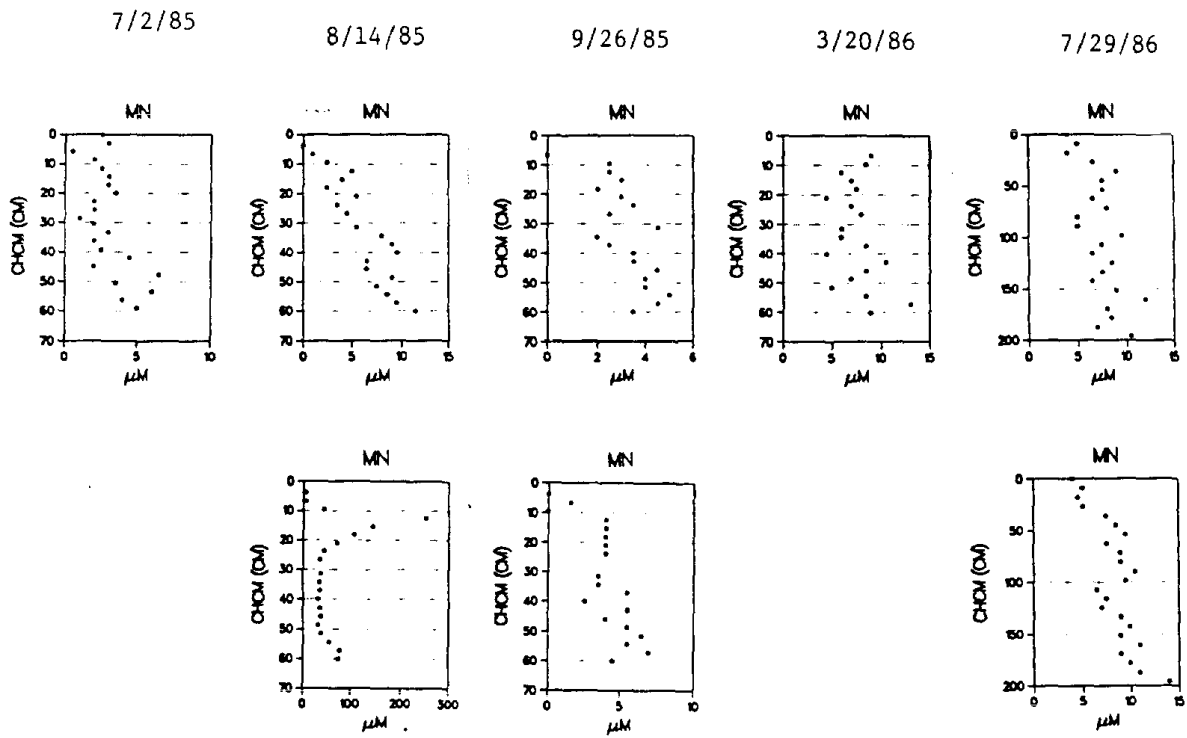


Figure 29. The manganese concentration of the pore water and overlying lake water in Eastern Brook Lake.

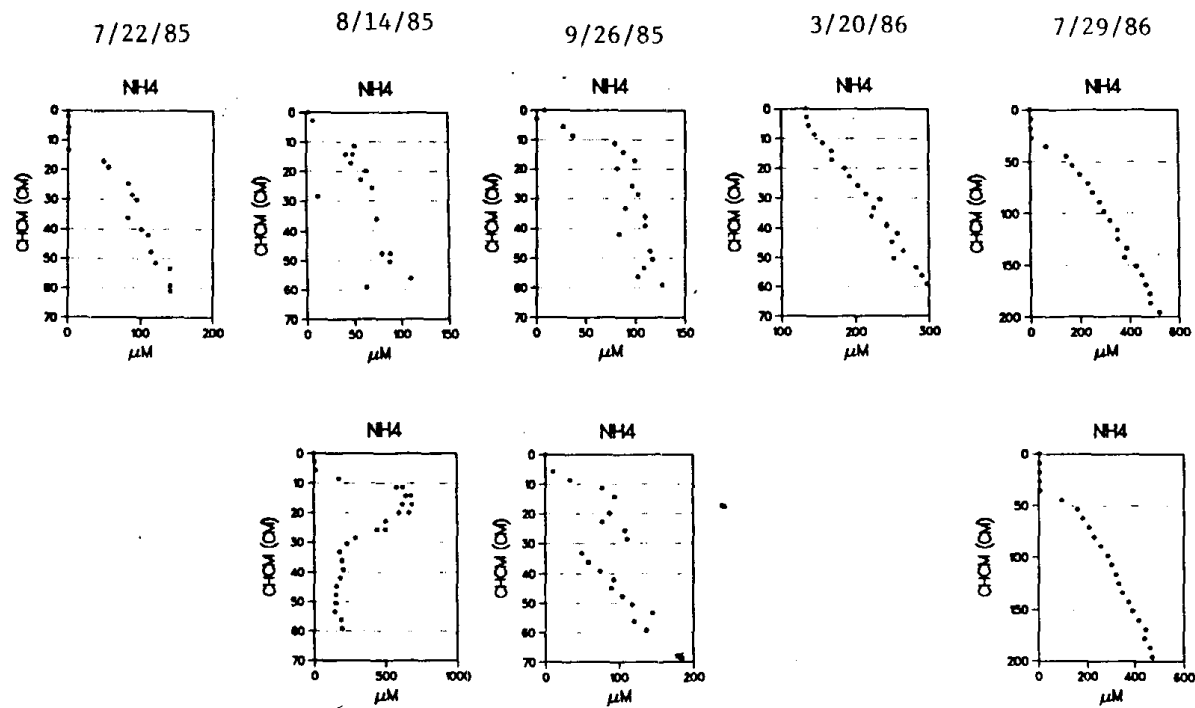


Figure 26 . The ammonium concentration in the pore water and overlying lake water of Eastern Brook Lake.

Eastern Brook are nearly 3 times as great as that in Emerald (1100 vs. 400  $\mu\text{M}$ ). In both lakes, higher pore water concentrations were probable below the maximum depth sampled since there was little indication that a maximum concentration had been reached.

The sum of base cations (SBC) in Eastern Brook lake reached maximum concentrations of approximately 600 to 800  $\mu\text{eq/L}$  except for the anomalous 8/14/85 peeper (Fig. 31). These concentrations were very similar to those found in Emerald Lake.

As mentioned in the discussion of the Emerald lake pore waters, the presence of  $\text{SO}_4^{2-}$  and  $\text{NO}_3^-$  in the pore waters is considered a sampling artifact based on the presumed anaerobic conditions in the sediments. The measured concentrations of  $\text{NO}_3^-$  and  $\text{SO}_4^{2-}$  are similar to those found in Emerald lake and, in some peepers, there was a decrease in concentration with increasing depth which might indicate that diffusion into the sediments is occurring (Fig. 32 and 33). However, based on low concentrations, high scatter, and uncertainties in processes which may have affected the samples prior to analysis, the apparent concentration gradients are somewhat speculative.

In general, the charge balance diagrams (Fig. 34) indicate a reasonable agreement between measured cations and anions. In some peepers anions were consistently in excess while in one other, they were in deficit.

### 3.3.5. Mosquito Lake Water Column

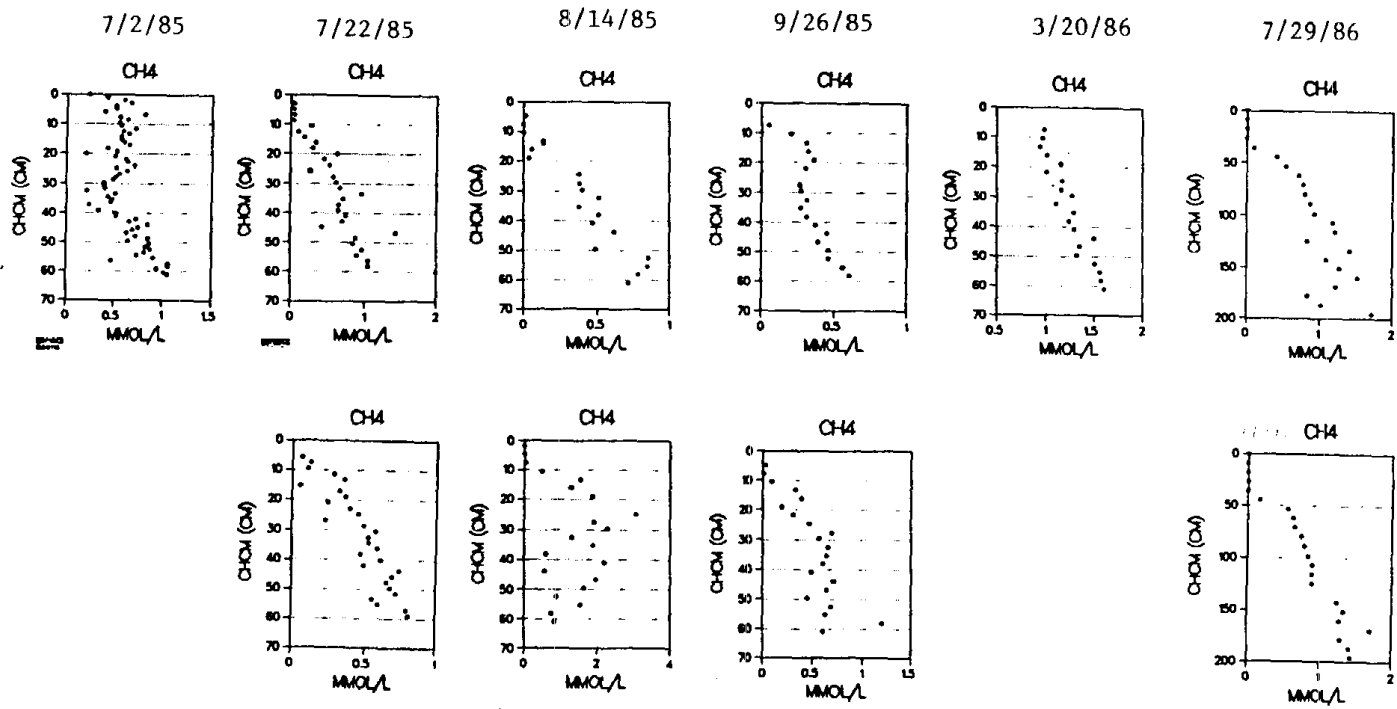


Figure 28. The concentration of methane in the pore water and overlying lake water in Eastern Brook Lake.

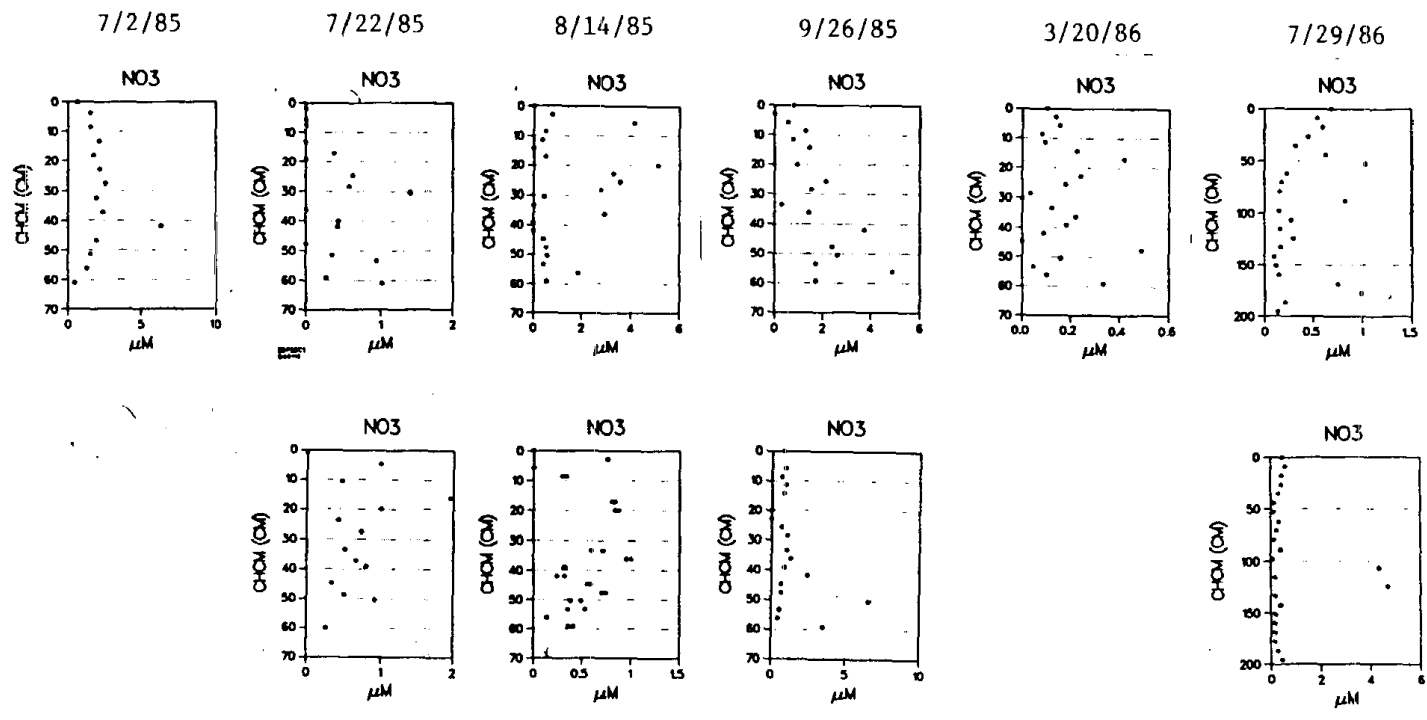


Figure 32 . The concentration of  $\text{NO}_3$  in pore water and overlying lake water in Eastern Brook Lake.

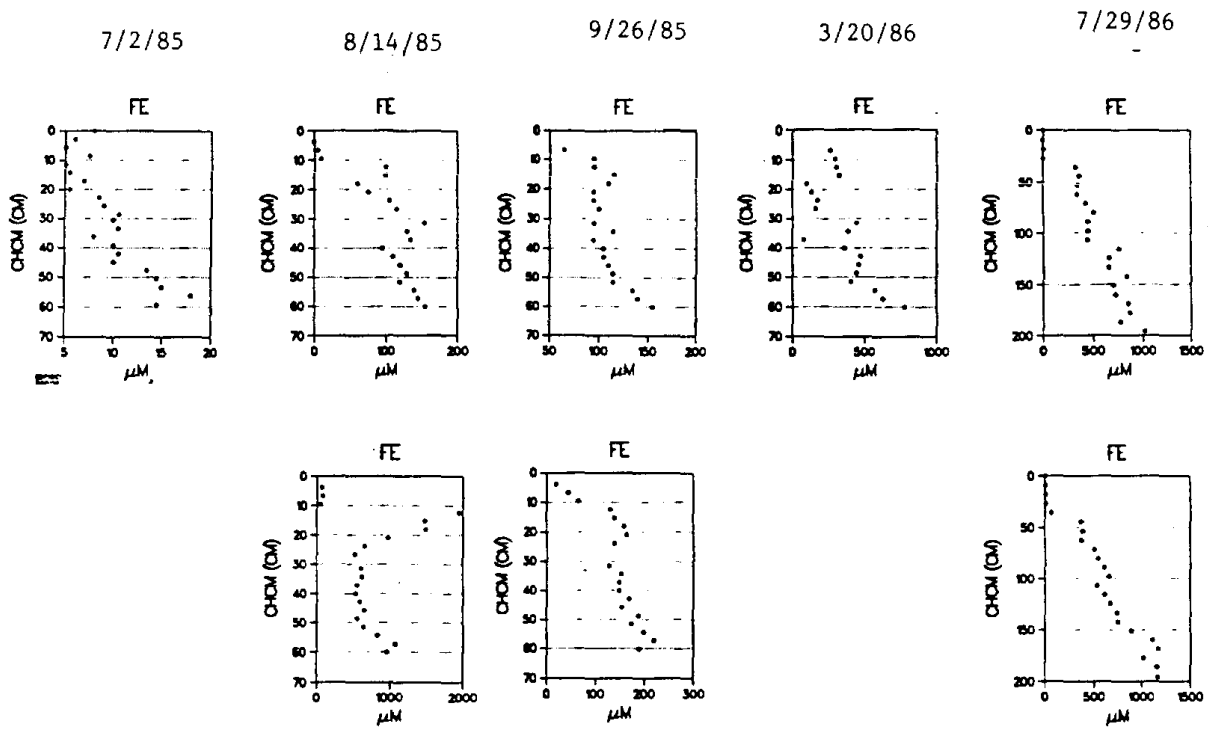


Figure 30. Fe concentration in the pore water and overlying lake water in Eastern Brook Lake.

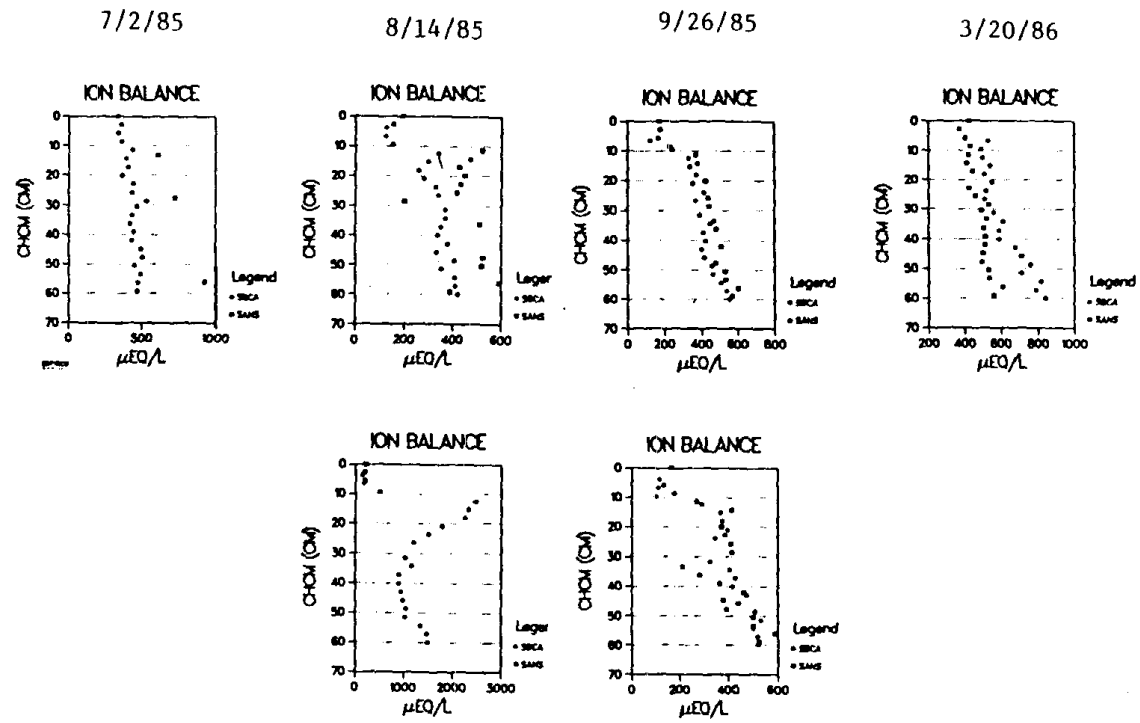


Figure 34. The balance of measured anions and cations in the pore water and overlying lake water in Eastern Brook Lake.

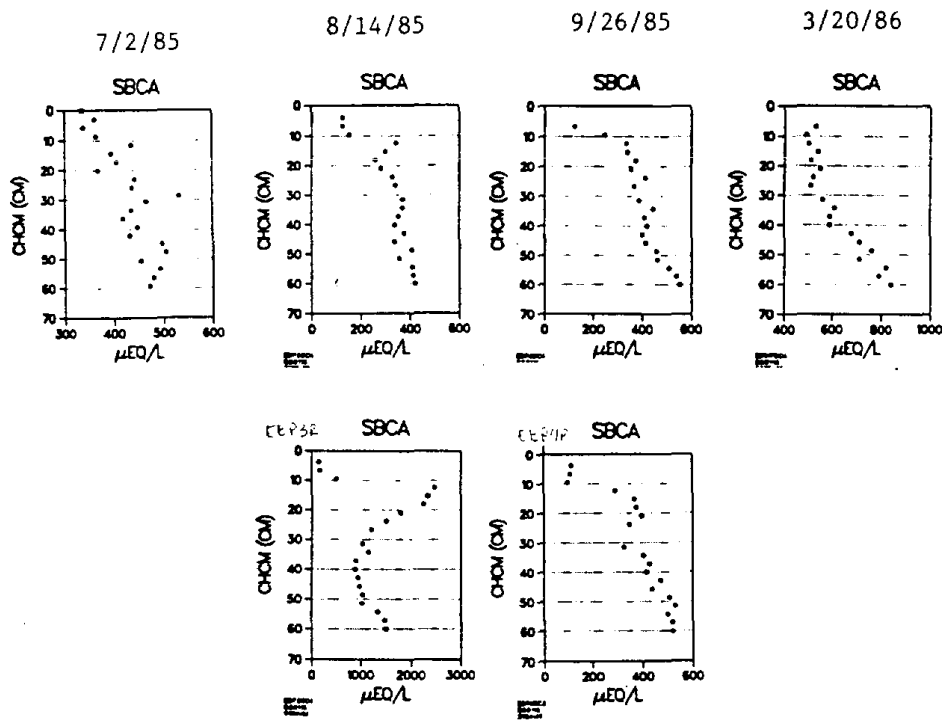


Figure 31. The sum of base cations (Ca, Mg, Na, K) in the pore water and overlying lake water in Eastern Brook Lake.

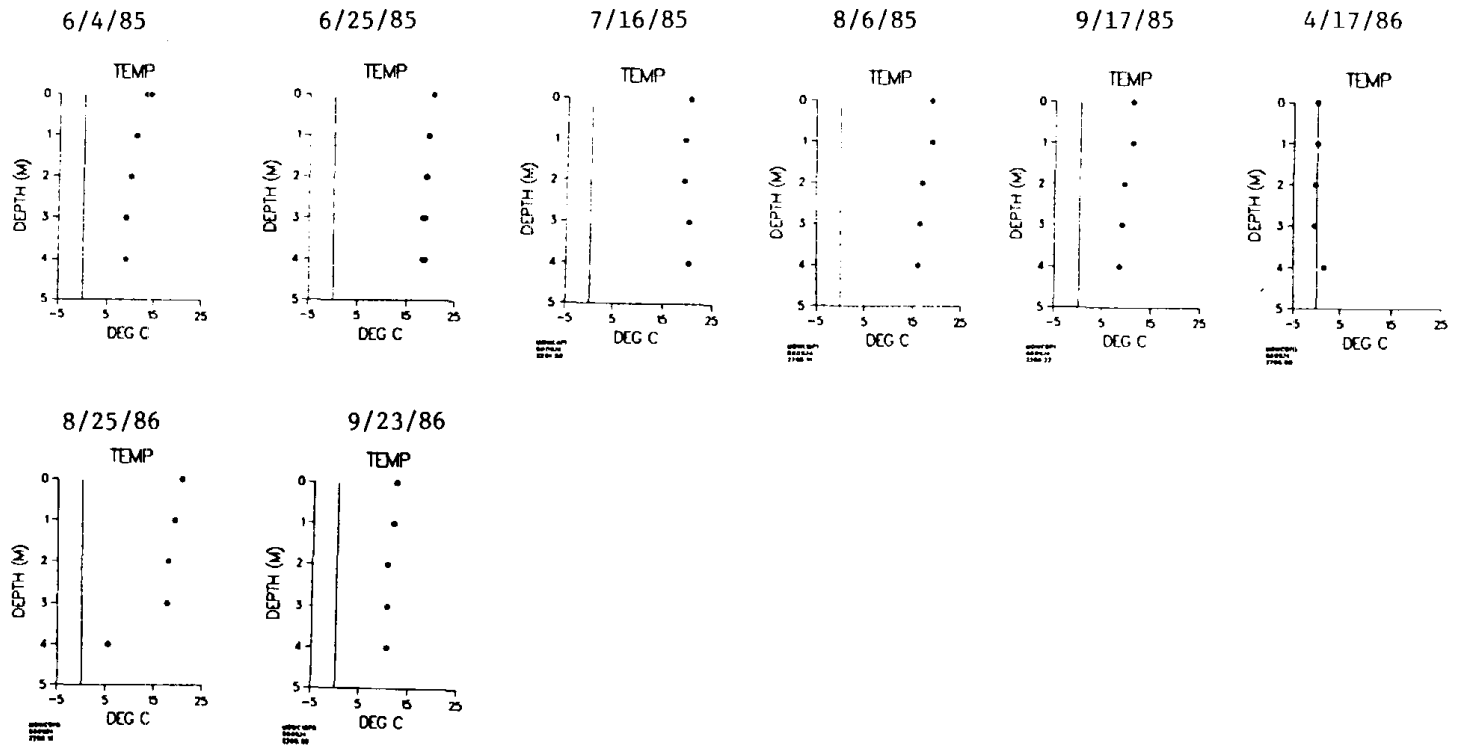


Figure 35 . The temperature of Mosquito lake at various times during the study.

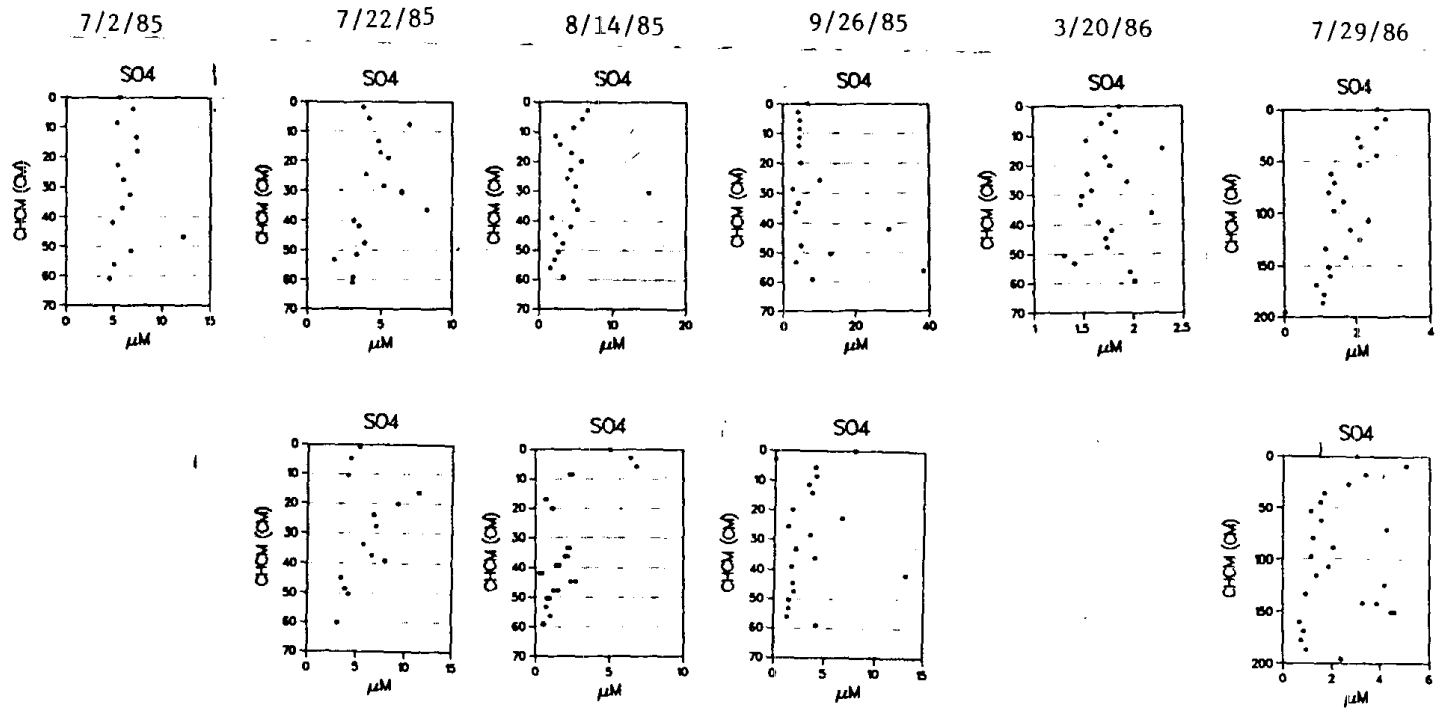


Figure 33. The concentration of  $\text{SO}_4$  in pore water and overlying lake water in Eastern Brook Lake.

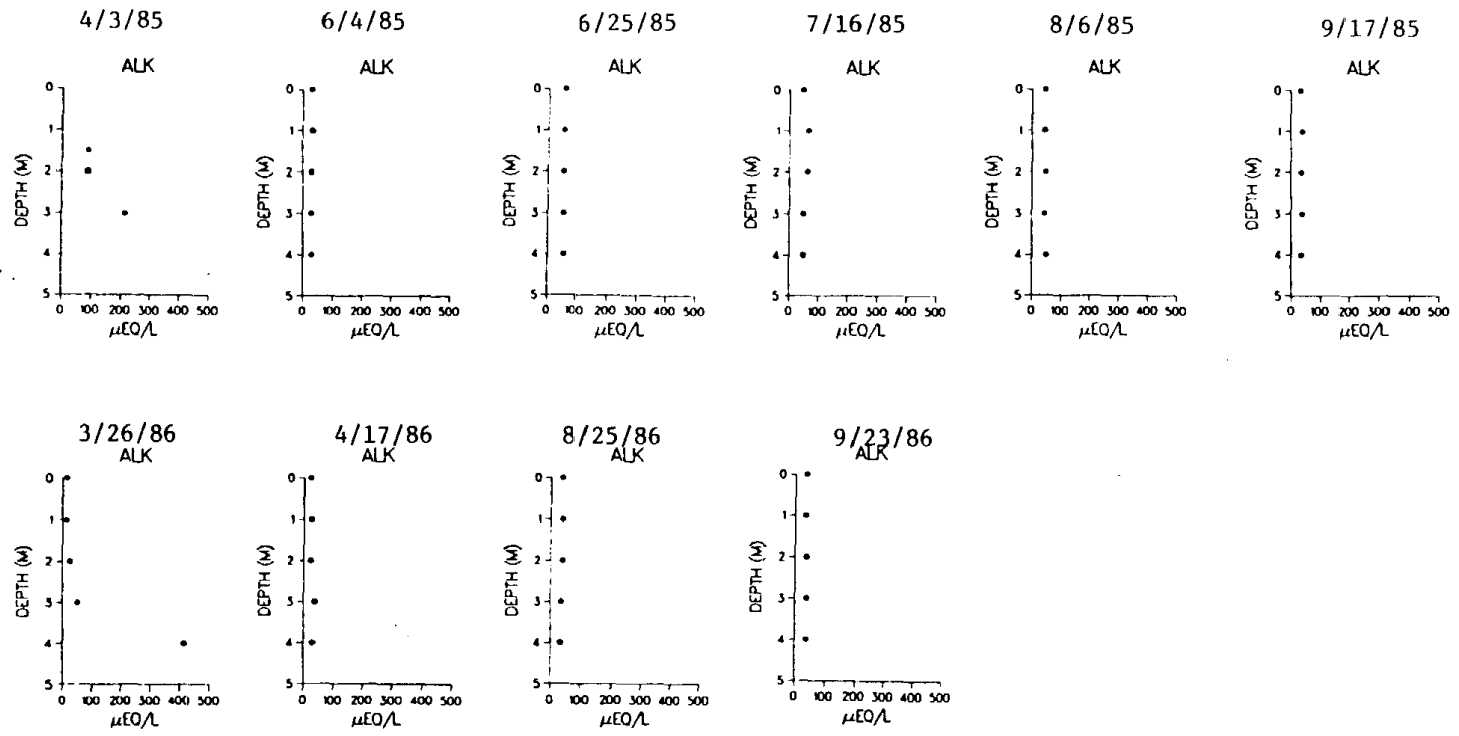


Figure 37. The alkalinity (Alk) of Mosquito lake water during the study.

Mosquito lake is much shallower than either Emerald or Eastern Brook lake, resulting in less pronounced stratification and increased vegetative growth in the lake compared to the two previously discussed. Mosquito lake becomes warmer in the summer because of its shallowness (Fig. 35). Dissolved oxygen ranges from 5 to 10 mg/L during most of the year (Fig. 36) with lower O<sub>2</sub> concentrations near the sediments on two occasions.

Alkalinity ranged from 25 to 70 ueq/L in summer (Fig. 37). In the winter, alkalinities up to 400 ueq/L were measured near the bottom.

Ammonium was measured on water columns from 5 sampling dates (Fig. 38). The April, under-ice, water column, with its relatively high NH<sub>4</sub> concentrations, indicates reduced O<sub>2</sub> levels. For other sampling periods, the NH<sub>4</sub> concentrations were near zero in the lake water.

Under ice (3/26 and 4/17/86), dissolved silica, although in low concentrations, showed a gradient from the sediments to the top of the water column (Fig. 39). This constituent is released from the sediments, probably by the dissolution of biogenic silica.

During the summer, water column CO<sub>2</sub> concentration is controlled by atmospheric equilibration (Fig. 40). Some diffusion from the sediments is probably occurring although the high standard deviation (45 ueq/L) makes this appear negligible. Winter water columns indicate strong diffusion of CO<sub>2</sub> from the sediments. Methane is not detectable in the lake water except in one winter measurement near the sediments, indicating anoxic conditions at the bottom at that time (Fig. 41).

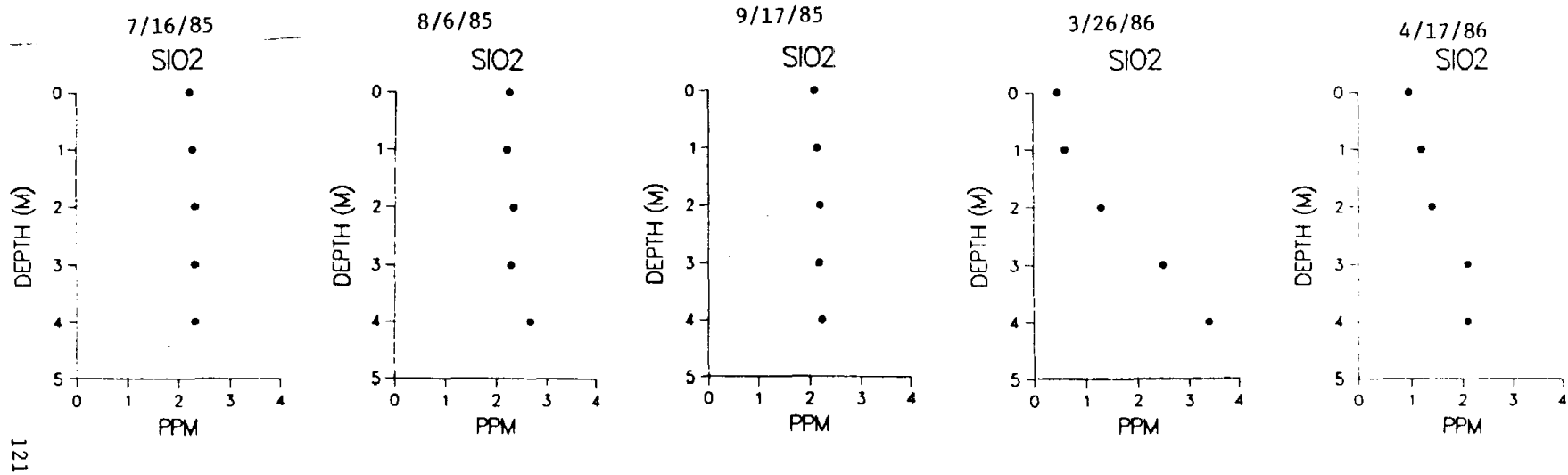


Figure 39. The silica ( $\text{SiO}_2$ ) concentration of Mosquito lake at selected times during the study.

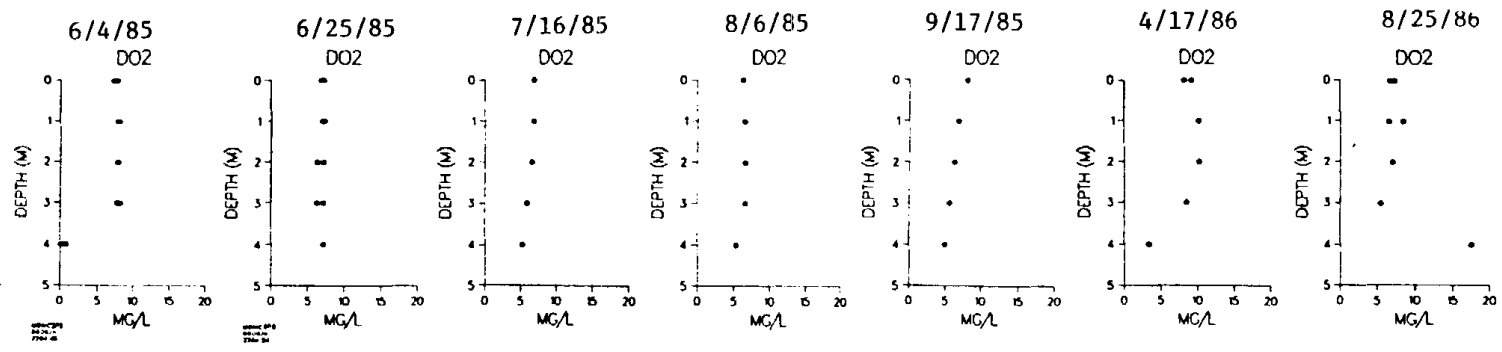


Figure 36. The dissolved oxygen (DO<sub>2</sub>) content of Mosquito lake at selected times during the study.

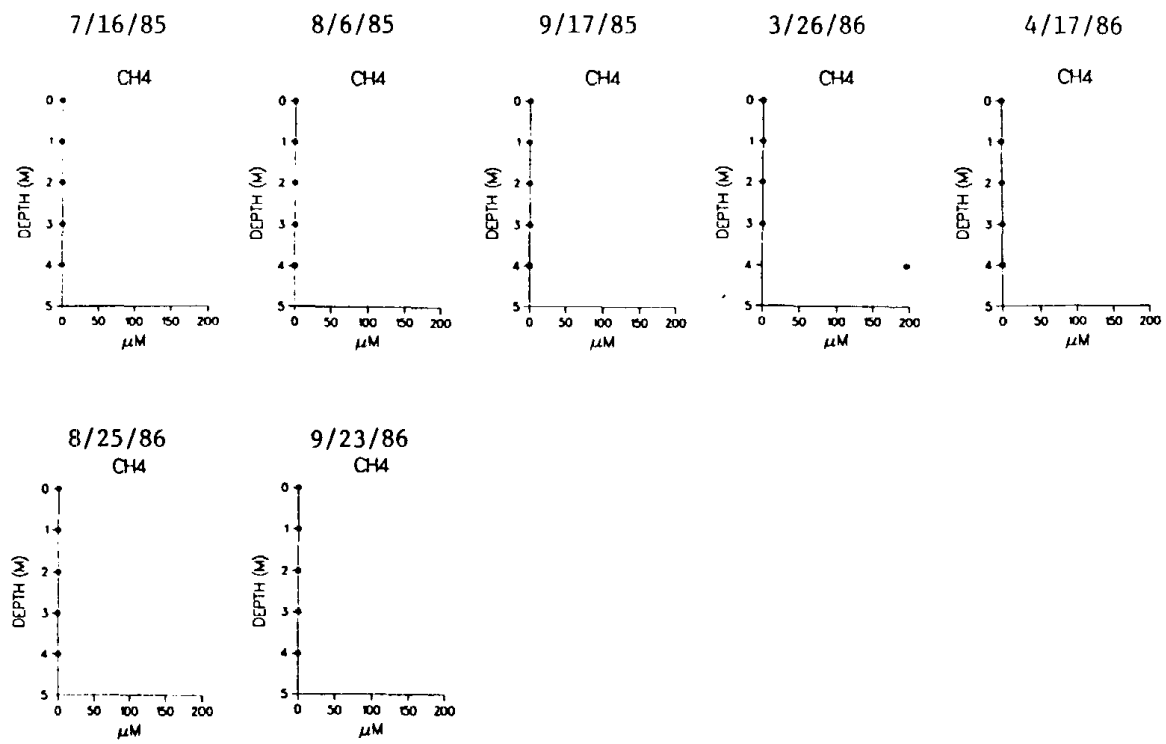


Figure 41. The methane (CH<sub>4</sub>) concentration of Mosquito lake water at selected times during the study.

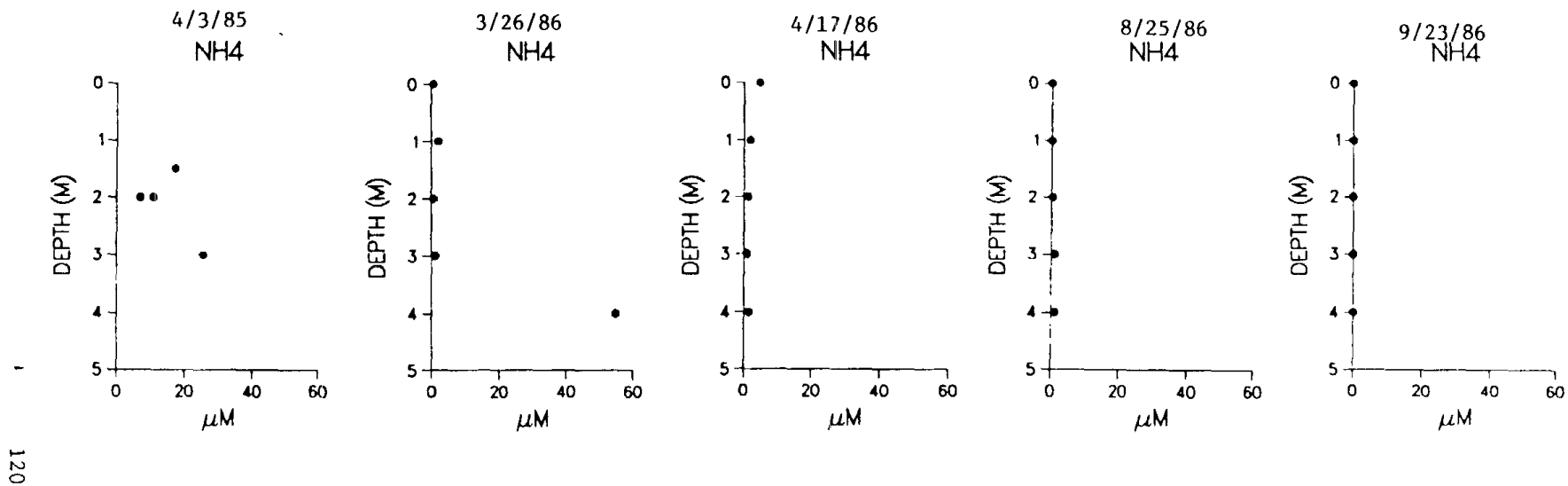


Figure 38. The ammonium ( $\text{NH}_4$ ) concentration in Mosquito lake at selected times during the study.

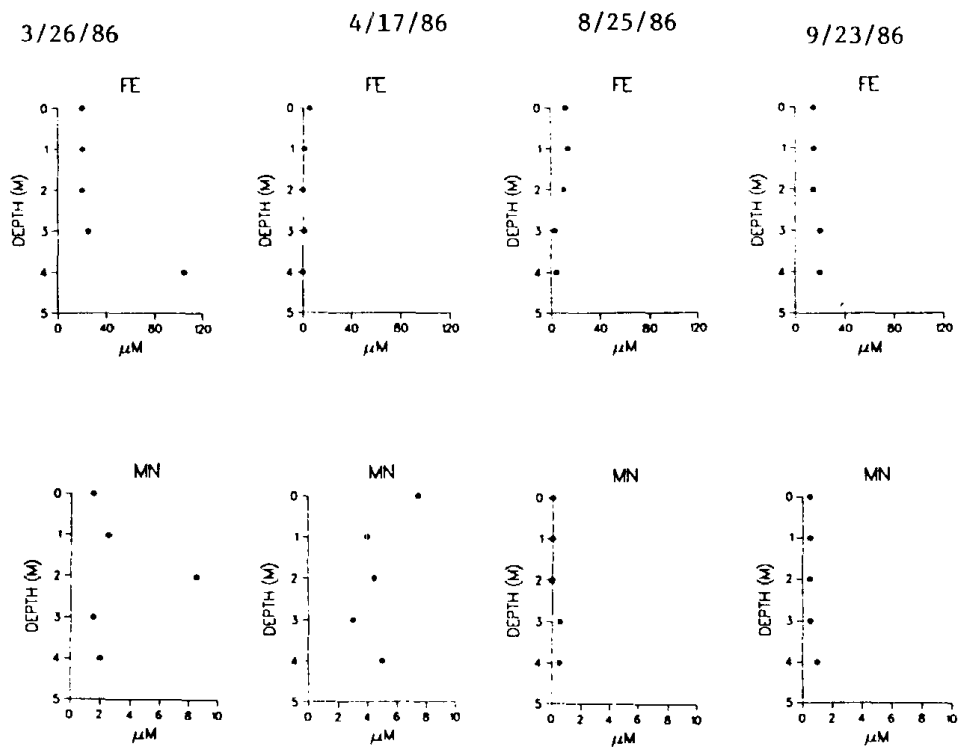


Figure 42 . The iron (Fe) and manganese (Mn) concentration in Mosquito lake during the study.

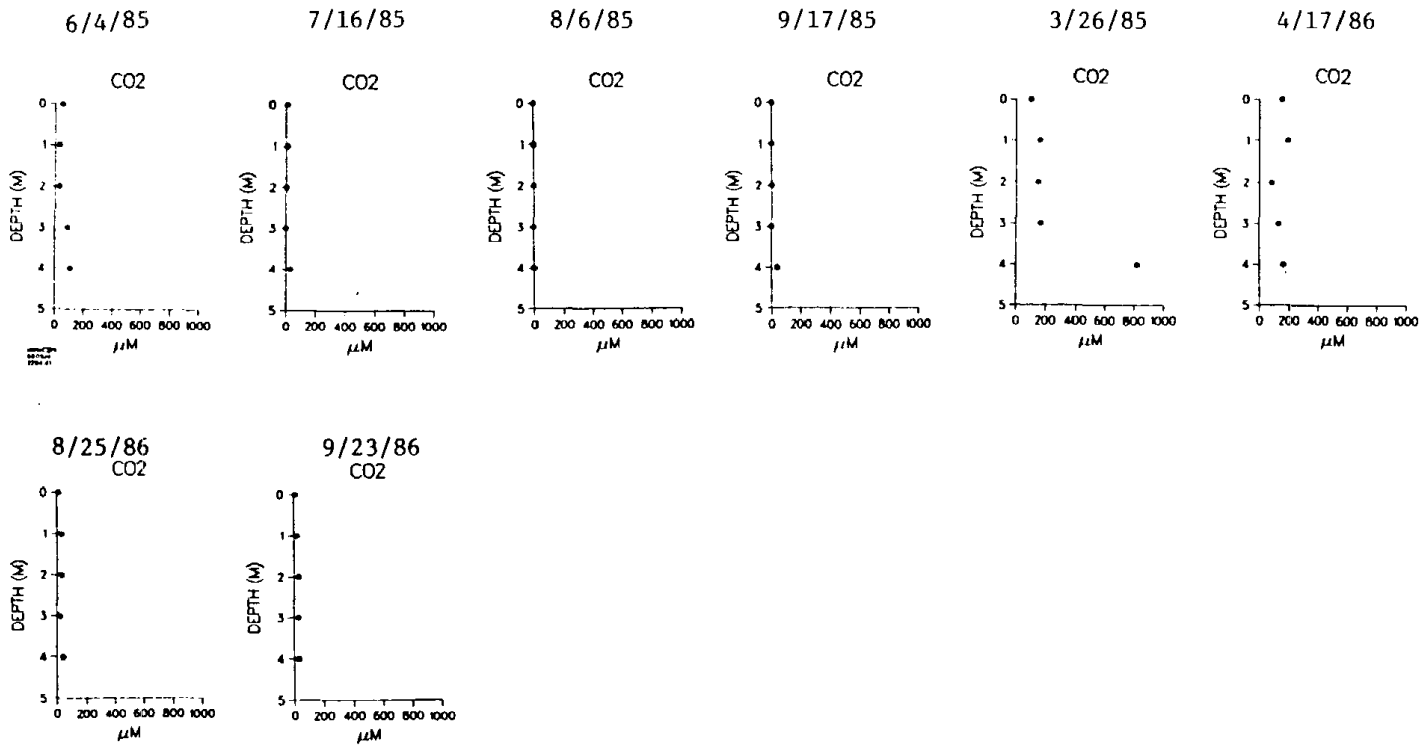


Figure 40. The carbon dioxide (CO<sub>2</sub>) concentration of Mosquito lake water at selected times during the study.

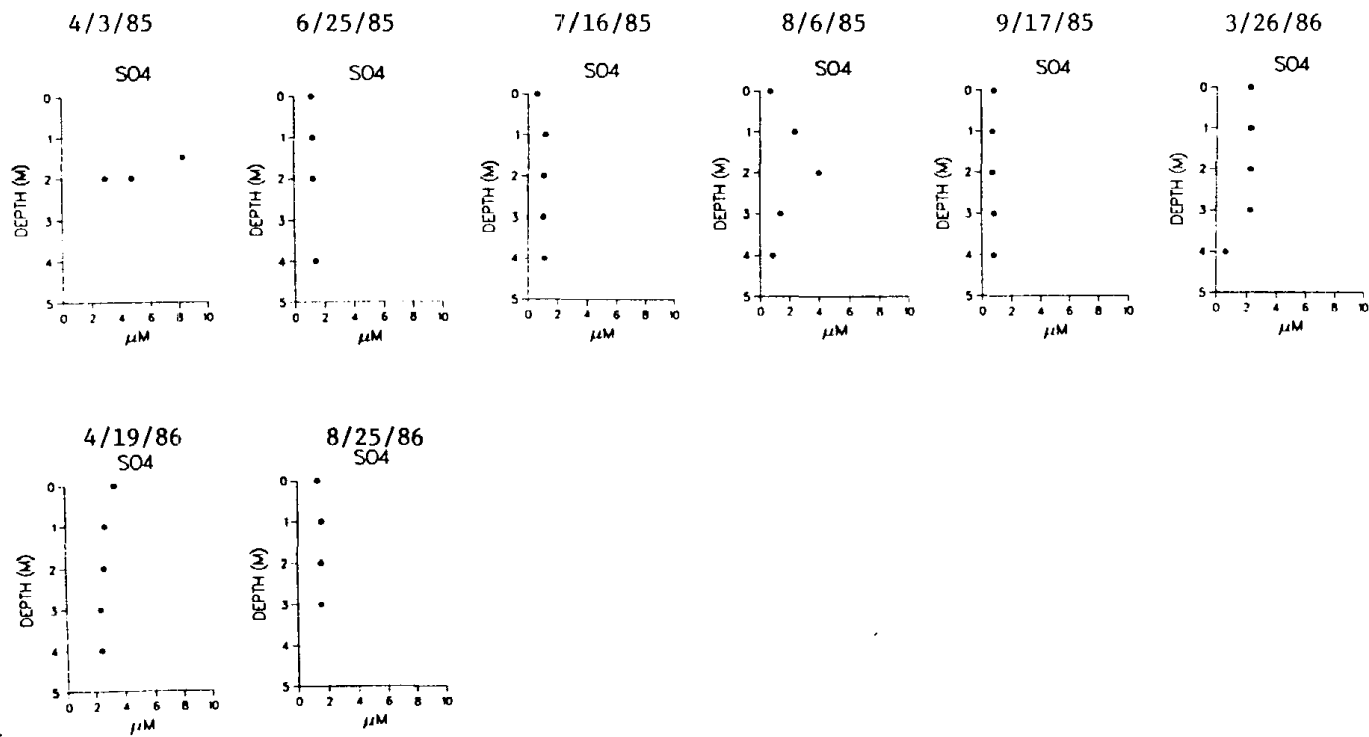


Figure 44. The sulfate ( $\text{SO}_4$ ) concentration in Mosquito Lake water at selected times during the study.

Dissolved iron was higher in Mosquito lake than in the other two lakes studied (Fig. 42). This could be due to mineralogical differences in the soils and rocks of the area. Near Mosquito lake are outcrops of ultramafic rock, such as the prominent Dardanelle's Cone. These iron-rich rocks have undoubtedly been transported into the watershed, thereby providing an abundant source of iron. A layer of flocculated iron-rich material was always present at the SWI in the summer while in the winter, the iron-rich material was found higher in the water column and usually coated the peepers above the SWI. Much of the iron measured in water column samples was probably in particulate form except for winter samples when  $\text{Fe}^{2+}$  generated by reduction could have also been present. Manganese concentrations were  $< 1 \text{ uN}$  in the summer and 2 to 8  $\text{uN}$  in the winter (Fig. 42).

In summer, nitrate concentrations were low, or below the detection limit (Fig. 43). Under ice, nitrate, possibly originating in the snow, was high near the surface and decreased toward the sediments, perhaps removed by denitrification. Sulfate was generally below  $4 \text{ uM}$  throughout the year (Fig. 44). Like nitrate, the under-ice sulfate showed a downwards decrease.

### 3.3.6. Mosquito Lake Interstitial Water

The sediment pore water of Mosquito lake, as in the other lakes, reflects a number of chemical processes and is presumed to be a factor controlling the chemistry of the overlying lake. The SWI is again defined as the zone where the silica gradients

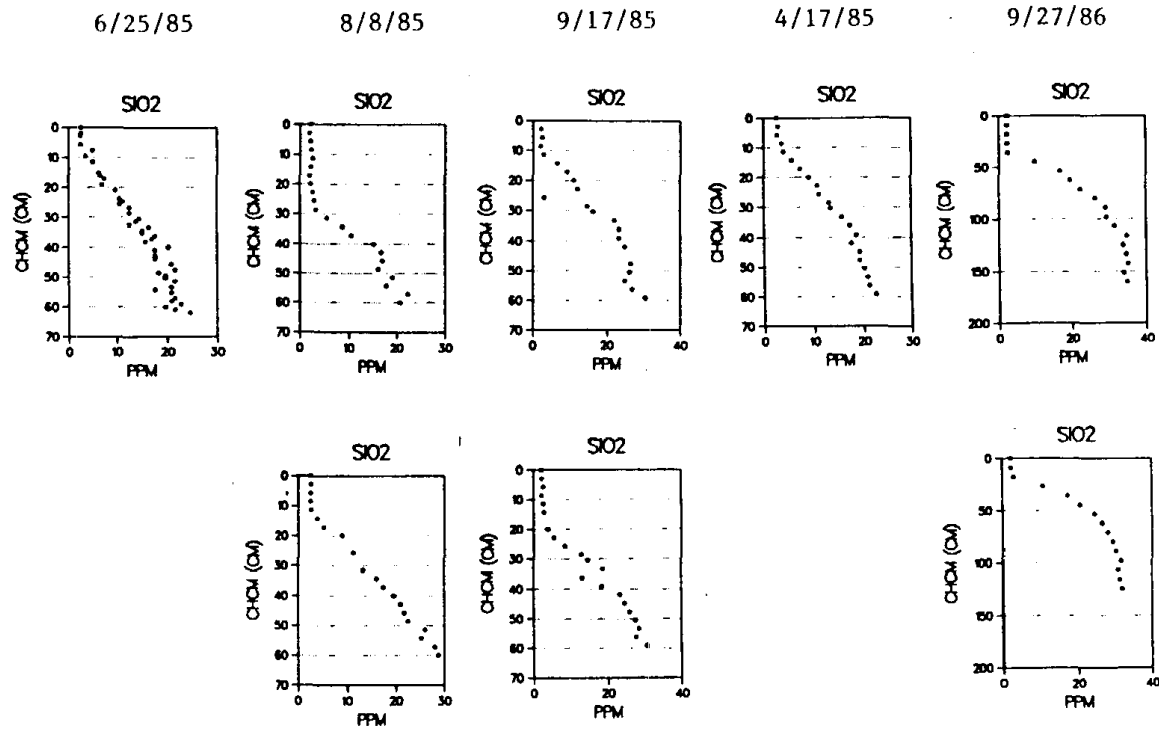


Figure 45. The silica concentration of the pore water and overlying lake water in Mosquito Lake.

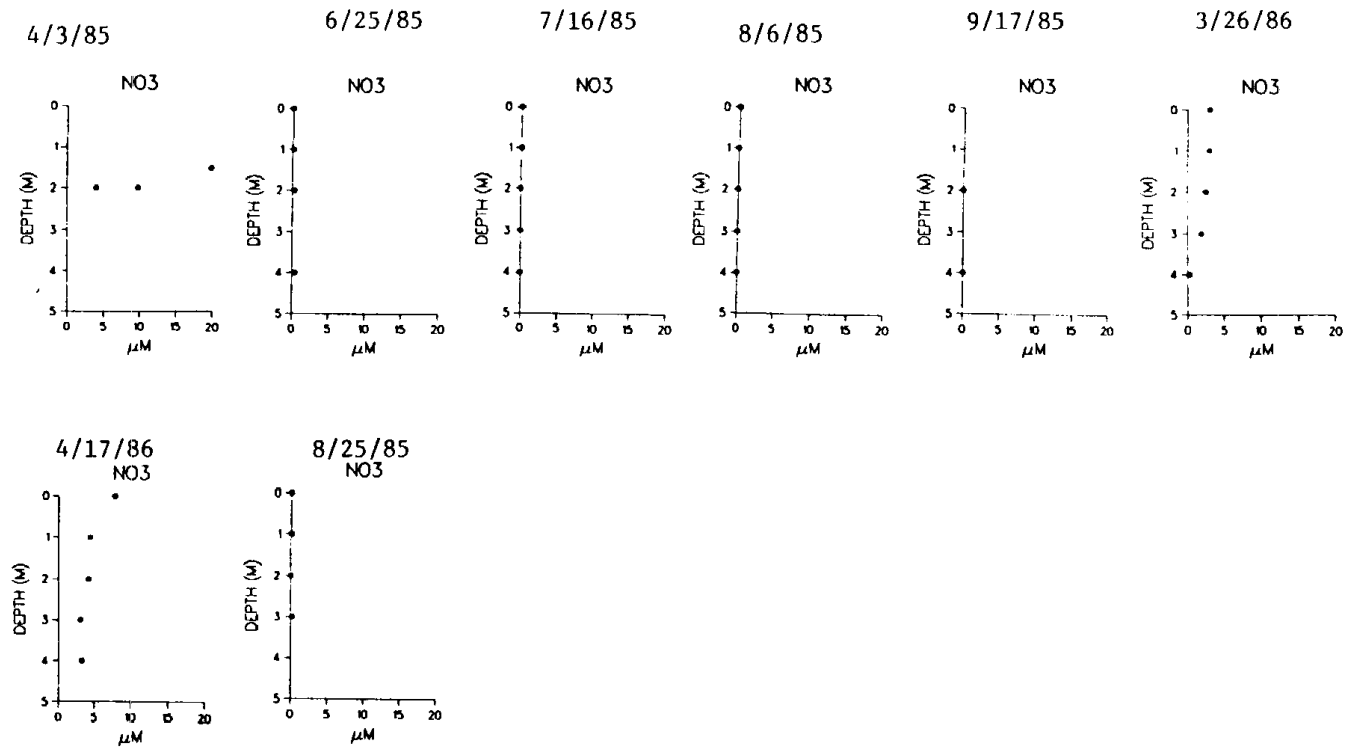


Figure 43. The nitrate ( $\text{NO}_3$ ) concentration in Mosquito lake water at selected times during the study.

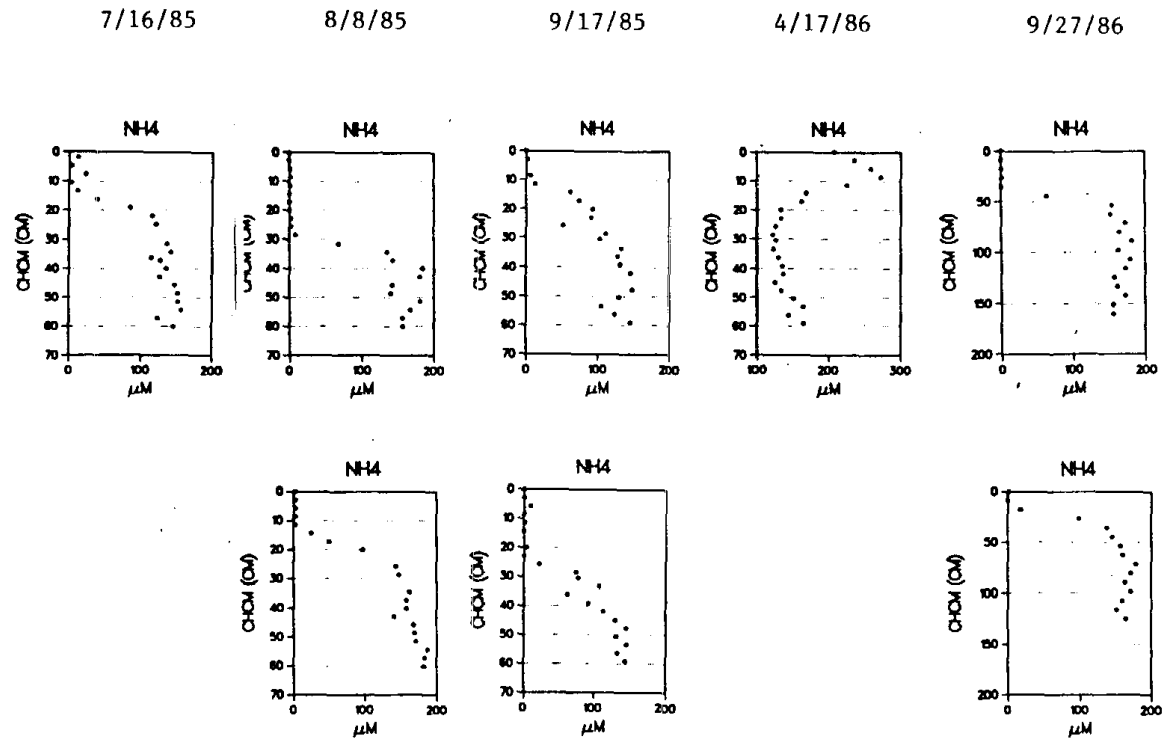


Figure 47. The concentration of ammonium in the pore water and overlying lake water of Mosquito Lake.

decreases sharply (Fig. 45). The peepers were usually inserted 30 to 50 cm in the sediments and at least 10 cm were always above the SWI based on the silica profiles. As with the other lakes, the silica concentration in the pore waters increased with increasing depth and reached a maximum value of 25 ppm. This indicates that dissolved  $\text{SiO}_2$  concentration was controlled by the same or similar minerals in all three lakes studied.

Concentration gradients indicate that alkalinity diffused from the sediments into the overlying lake for all sampling dates except the winter (4/17/86) (Fig. 46). The reversed gradient in the winter (i.e., apparent diffusion into the sediments) was most likely the result of bicarbonate production by the reduction of the iron hydroxide at the SWI and slow vertical transport in the overlying water. The measured alkalinities were only about 500  $\mu\text{eq/L}$  at the greatest depth in the Mosquito lake long peepers (9/27/86) compared to over 1000  $\mu\text{eq/L}$  in Emerald lake.

Except during the winter (4/17/86), the  $\text{NH}_4^+$  concentrations increased with increasing depth reaching a maximum of about 150 to 200  $\mu\text{M}$  (Fig. 47). In contrast,  $\text{NH}_4^+$  concentrations at similar depths in Emerald lake were much higher (800  $\mu\text{M}$ ) and also appeared to continue increasing with increasing depth. Under ice (4/17/86), the high concentrations above the SWI indicate anoxic conditions. The peak at the SWI probably resulted from a high rate of decomposition of the labile organic matter at that location and a low rate of transport into the overlying water.

Concentrations of  $\text{CH}_4$  and  $\text{CO}_2$ , like most constituents, increased with depth (Fig. 48 and 49). The highest  $\text{CH}_4$  and  $\text{CO}_2$

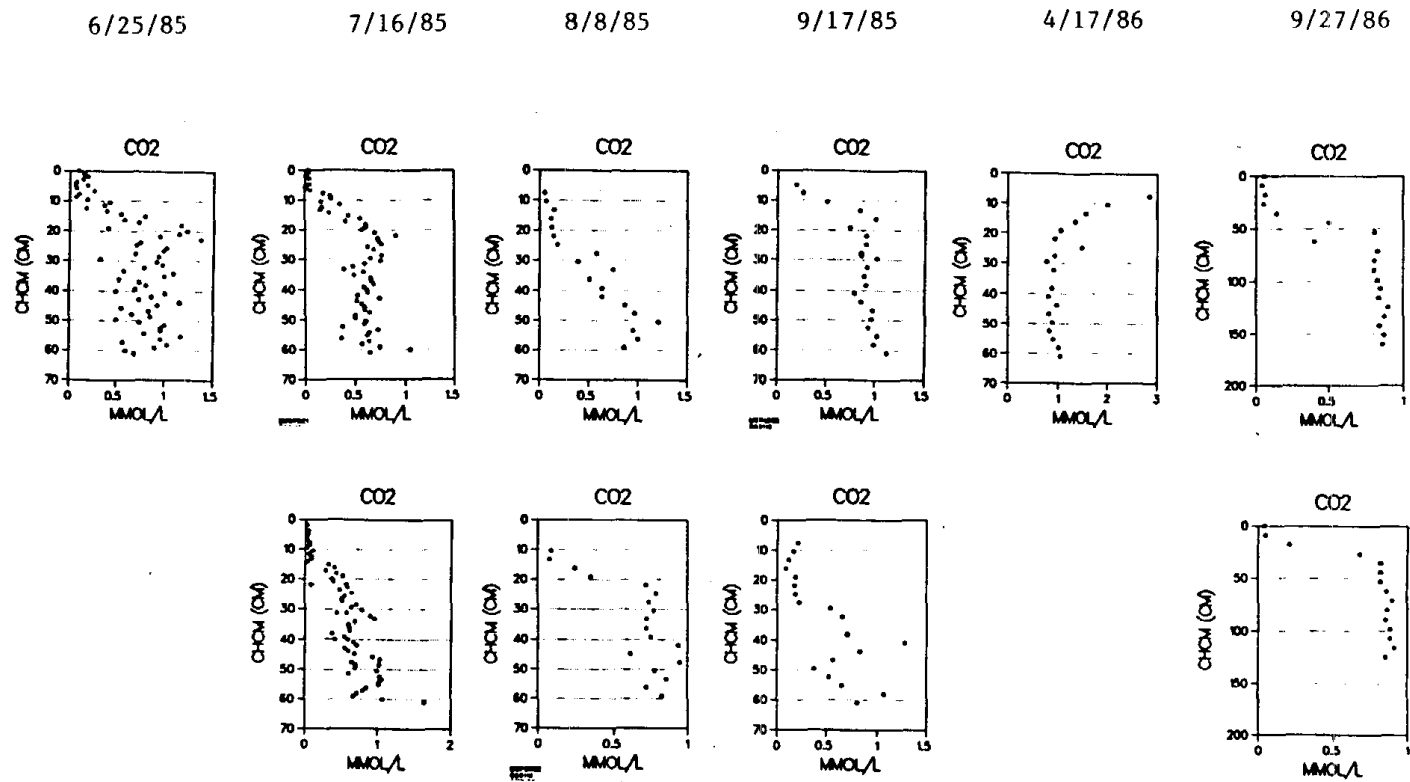


Figure 49. The concentration of carbon dioxide in the pore water and overlying lake water of Mosquito Lake.

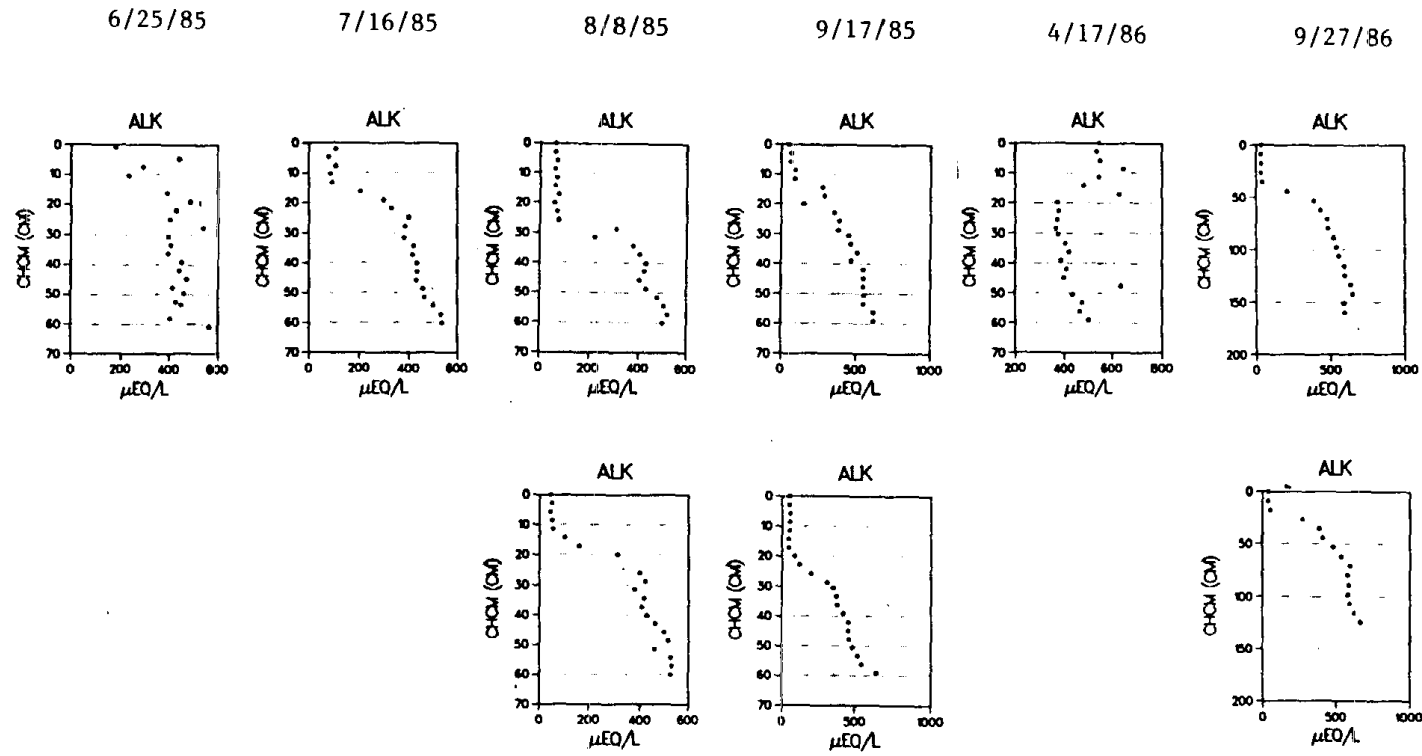


Figure 46. The alkalinity of the pore water and overlying lake water of Mosquito Lake.

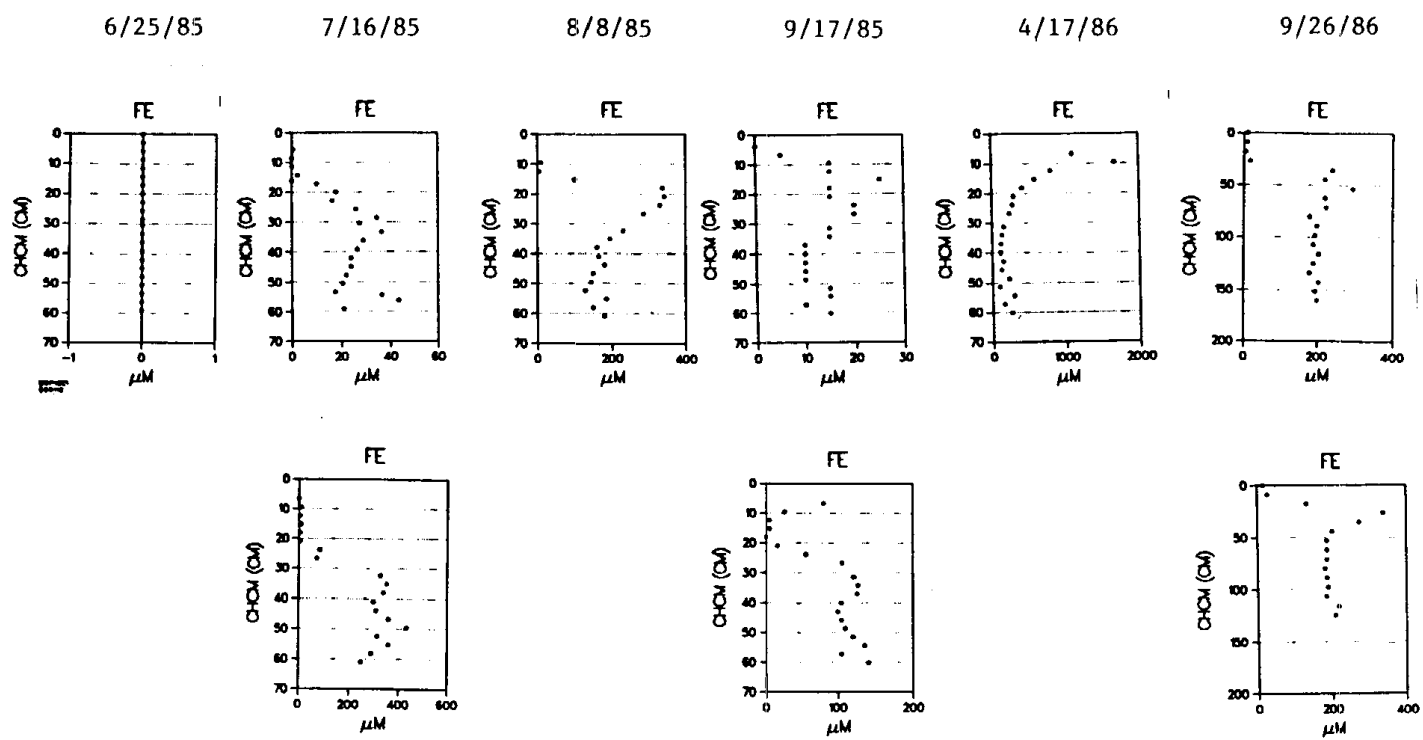


Figure 50. The concentration of iron in the pore water and overlying lake water of Mosquito Lake.

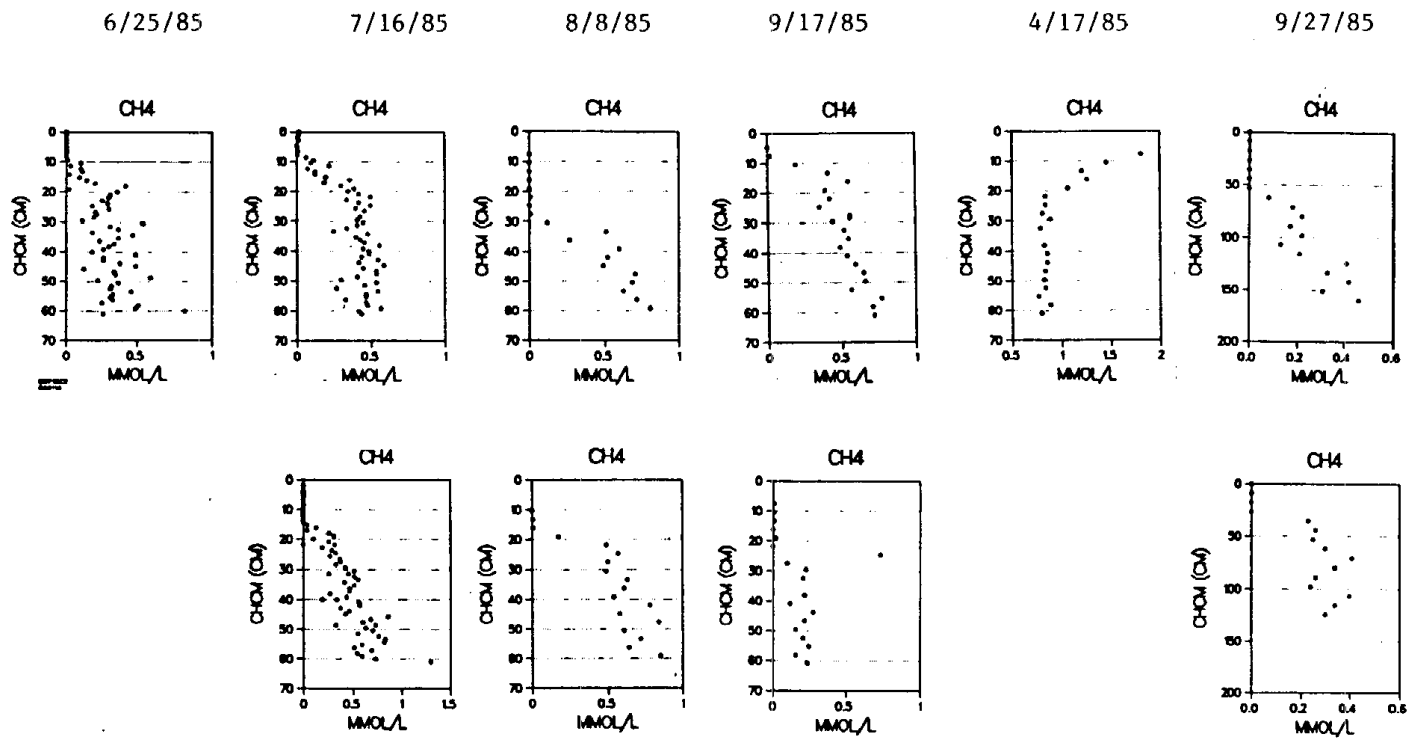


Figure 48. The concentration of methane in the pore water and overlying lake water of Mosquito Lake.

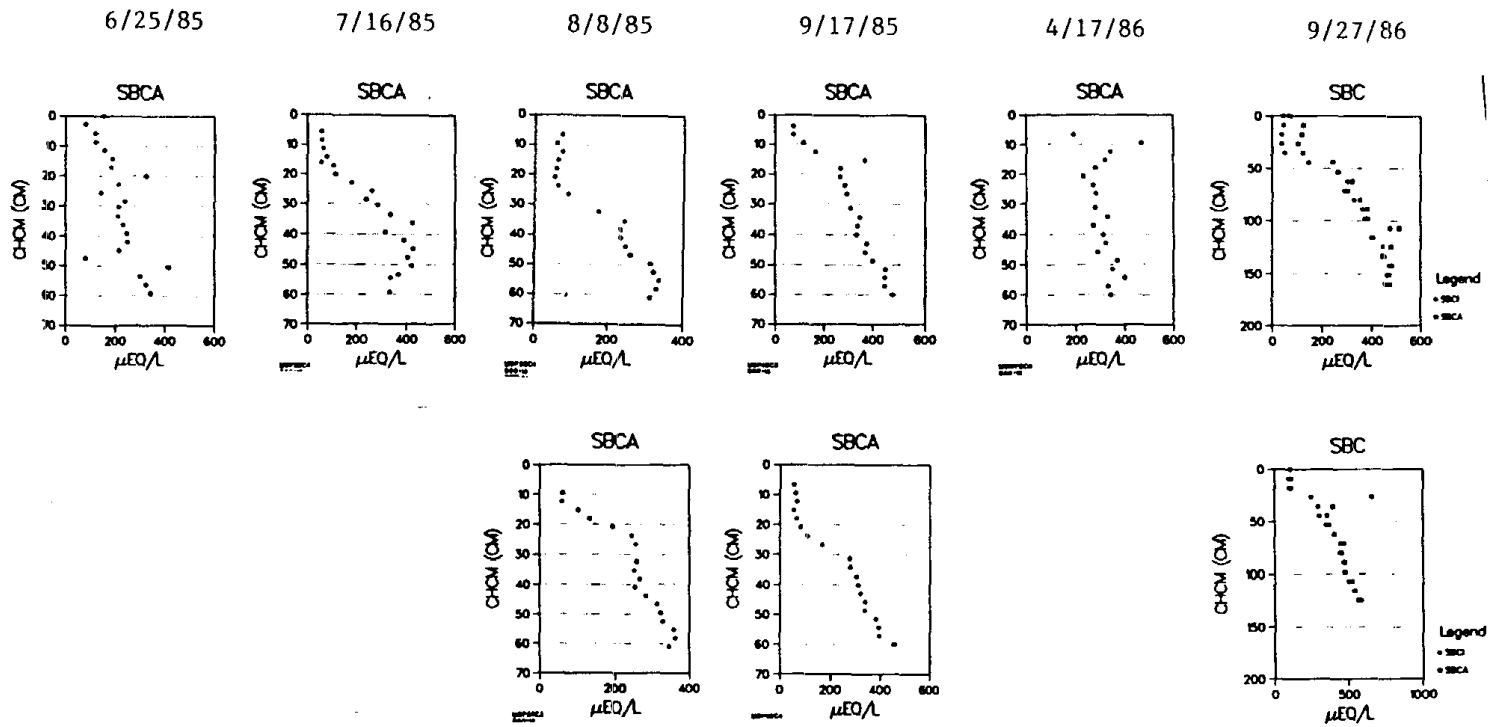


Figure 52. The sum of base cations (Ca, Mg, Na, K) in the pore water and overlying lake water of Mosquito Lake.

in concentrations in Mosquito lake were about one half those found in the sediments of Emerald. For both gases, but most notably for  $\text{CO}_2$ , a maximum concentration of 0.5 to 1.0 mmol/l commonly was reached only 10 to 20 cm below the SWI. In contrast, a maximum concentration of either gas was not measured in Emerald lake peepers.

The concentration of iron was quite variable with time and even between peepers sampled at the same time (Fig. 50). The iron concentration in 6/25/85 was zero because, as has already been discussed, the samples were not acidified. The reason for the variability among the other peepers is not known. It is somewhat surprising that the maximum iron concentration in the pore water (about 200  $\mu\text{M}$ ) is less than that in Emerald lake (600  $\mu\text{M}$ ). As mentioned, the presence of ultramafic rock in the Mosquito lake area, and the prominent red precipitate at the SWI, leads one to suspect that higher iron concentrations would have been present in the pore waters. The iron profile for 4/17/86 indicates that reduction of the iron minerals at the SWI was occurring and that diffusion of iron into the sediments occurred under anoxic conditions in the winter. Manganese concentrations were also quite variable, but lower than iron (Fig. 51).

The distribution and concentration of the SBC in Mosquito lake was similar to that of the other lakes (Fig. 52). SBC concentration usually increased with depth, reaching a measured maximum concentration of 500  $\mu\text{eq/l}$ . As with the other lakes, the significance of the low measured concentrations of  $\text{NO}_3^-$  and  $\text{SO}_4^{2-}$  is uncertain (Figs. 53 and 54).

In general, there was a good agreement between the sum of

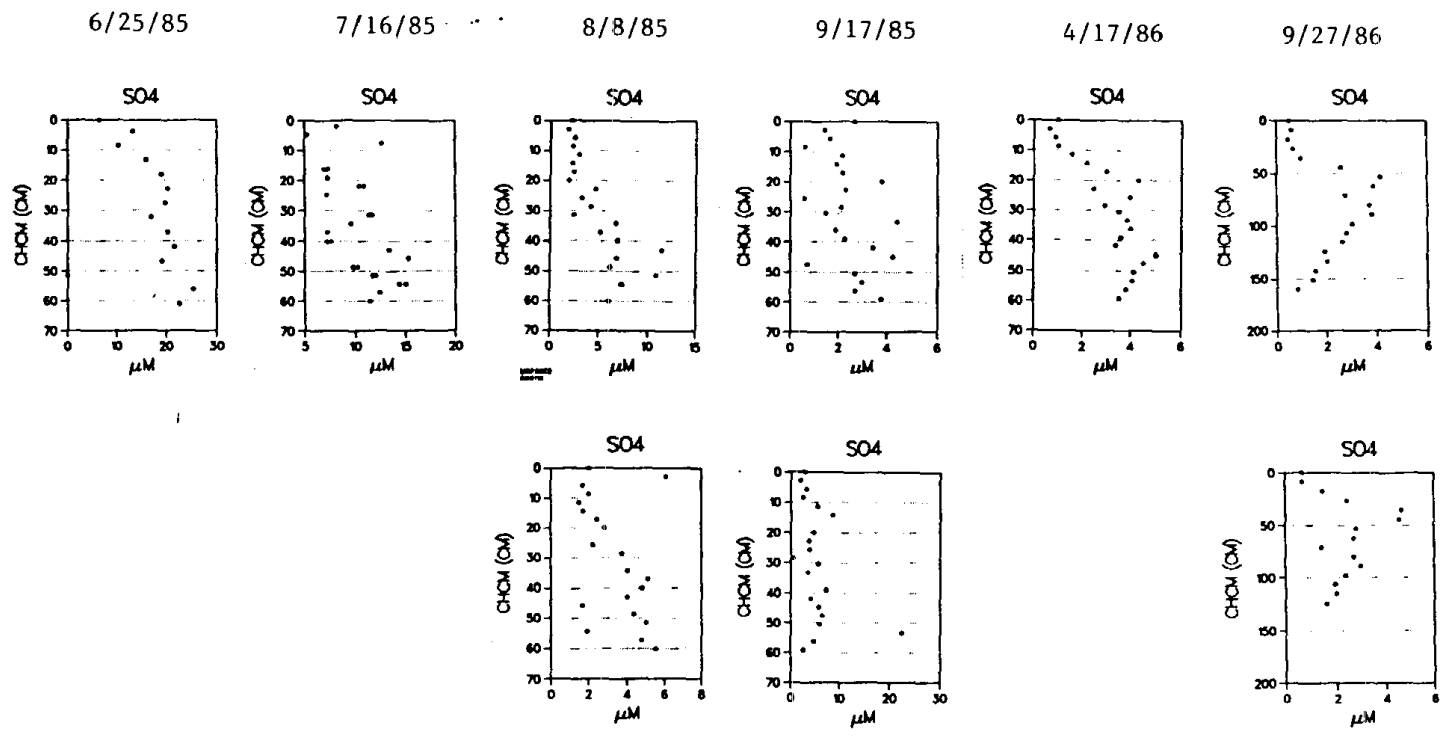


Figure 54. The concentration of sulfate in the pore water and overlying lake water of Mosquito Lake.

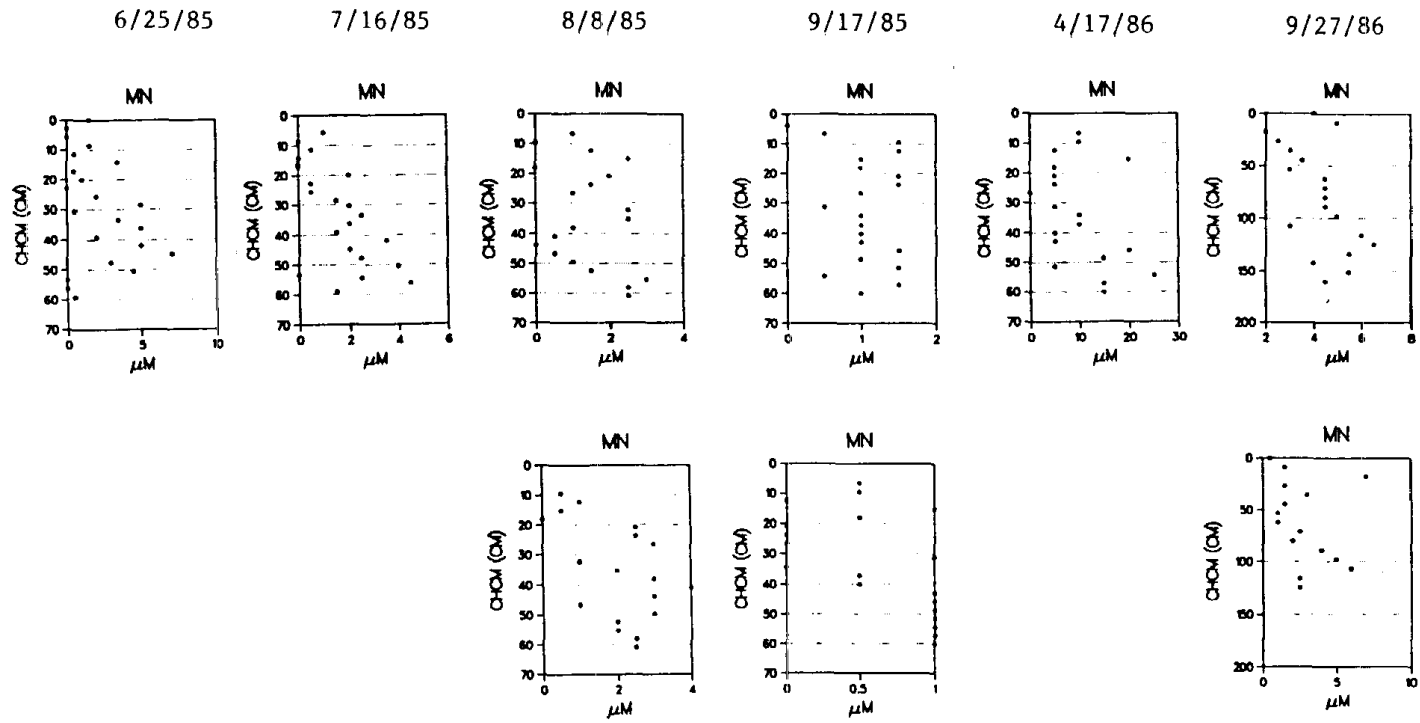


Figure 51. The concentration of manganese in the pore water and overlying lake water of Mosquito Lake.

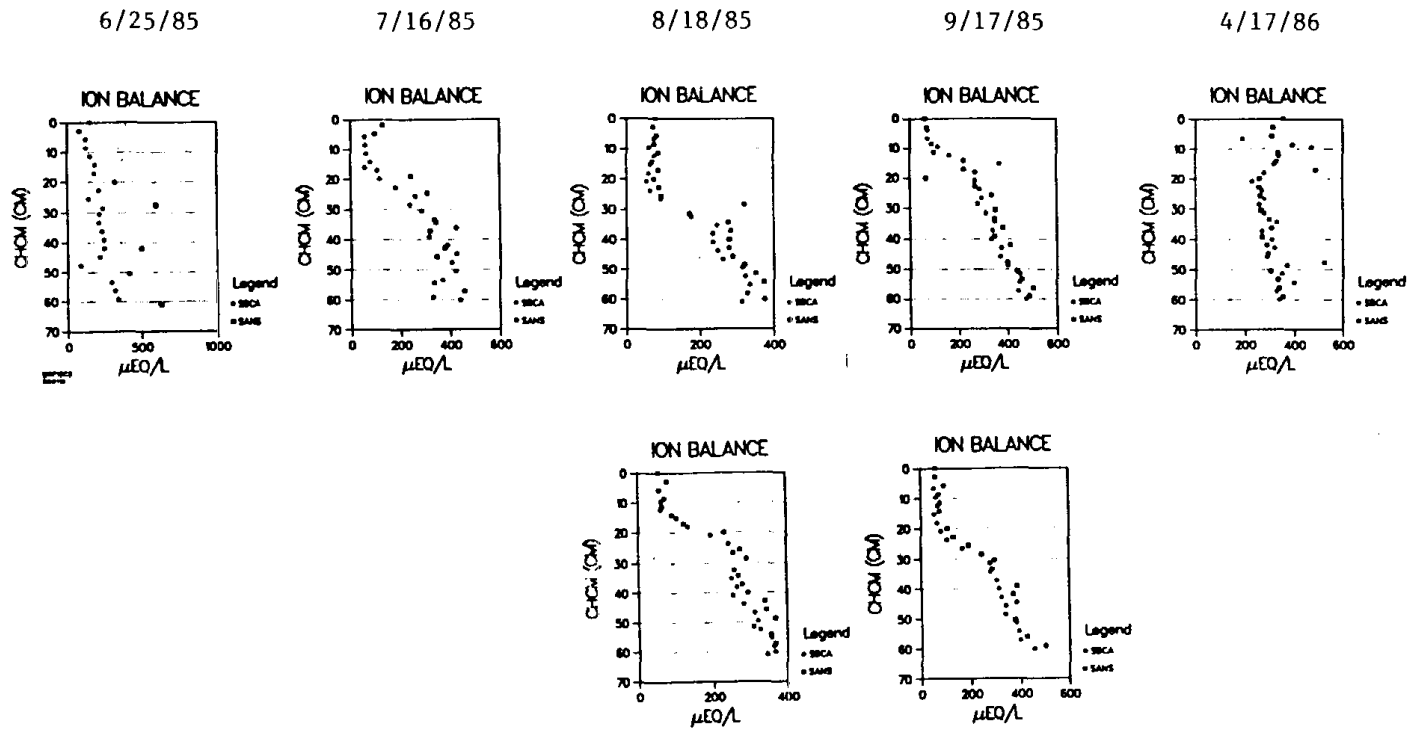


Figure 55. The balance of anions and cations in the pore water and overlying lake water of Mosquito Lake.

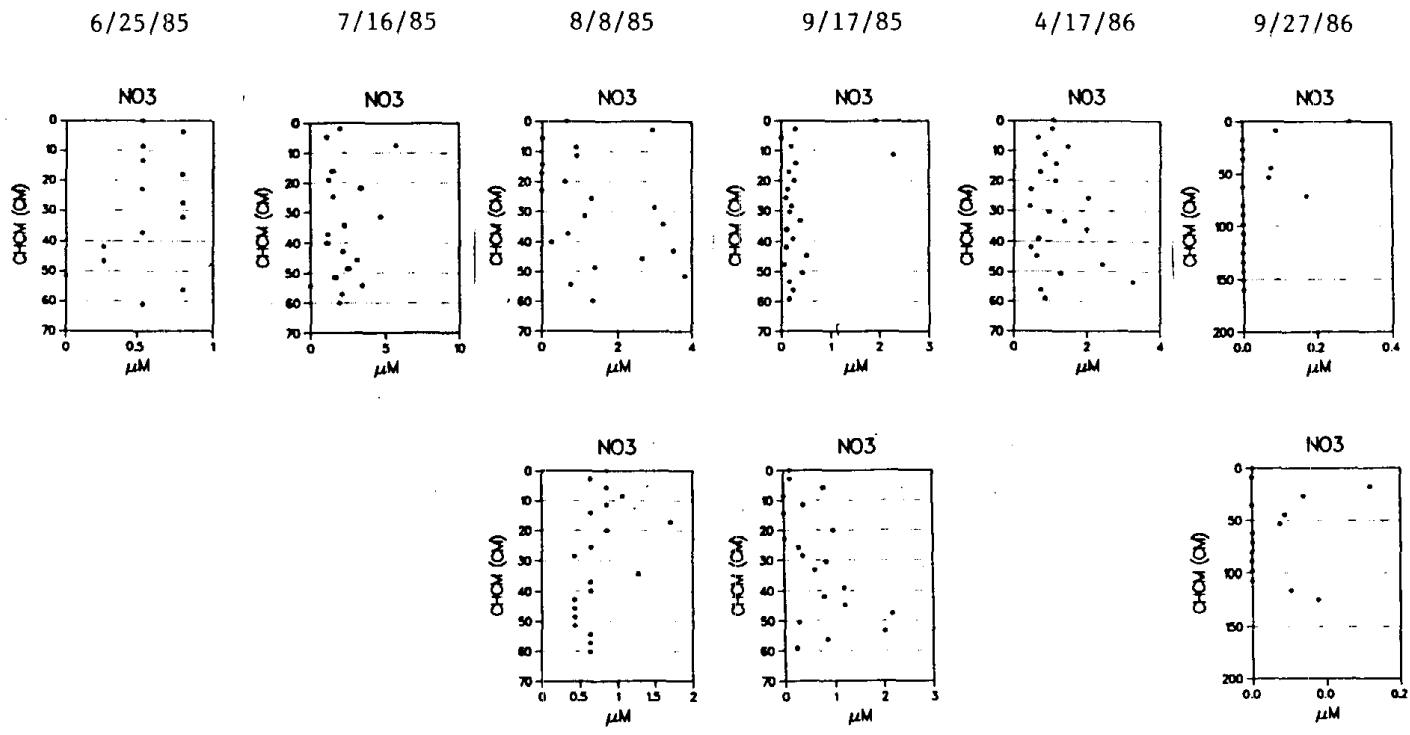
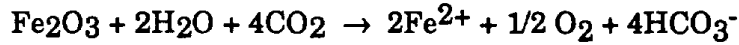


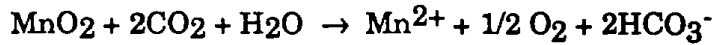
Figure 53. The concentration of nitrate in the pore water and overlying lake water of Mosquito Lake.

Table 6. The stoichiometric reactions for some alkalinity-producing processes in sediments and waters (Kuivila and Murray, 1984; Kelly et al., 1982).

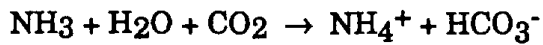
1. Iron reduction



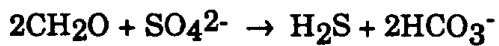
2. Manganese reduction



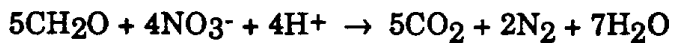
3. Ammonium production



4. Sulfate reduction



5. Nitrate reduction



6. Silicate mineral weathering

$\text{HCO}_3^-$  is produced in proportion to cations released.

measured cations and anions (Fig. 55). In instances where discrepancies existed, anions were measured in greater quantities than cations, possibly because of an underdilution of anion samples during the analysis procedure.

### 3.4. Discussion

#### 3.4.1. Organic Matter Diagenesis

The main processes controlling the chemistry of the interstitial waters of all three lakes are the result of the anaerobic decomposition of organic matter in the oxygen depleted sediments. The major products of the breakdown of organic components under anaerobic conditions are  $\text{CO}_2$ ,  $\text{CH}_4$ , and  $\text{NH}_4^+$  (Eq. 1, Table 5). The oxygen-depleted environment caused by microbial activity favors the reduction of Fe and Mn (Eqs. 1 and 2, Table 6), thereby elevating their concentrations in the pore waters many orders of magnitude above that found in the aerated waters of the overlying lake. The alkalinity associated with these reduced species is eliminated when they oxidize.

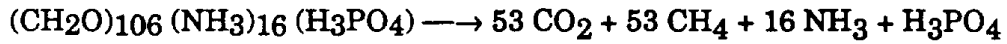
As the stoichiometry of Eq.1 in Table 5 indicates,  $\text{CO}_2$  and  $\text{CH}_4$  should be produced in 1:1 ratios during the anaerobic decomposition of organic matter. However, in all samples analyzed, the concentration of  $\text{CO}_2$  was greater than that of  $\text{CH}_4$ , usually by a factor of about 2. While a portion of the organic C is reduced to longer chain compounds than methane, we believe

illustrated in the various Figures discussed earlier, is actually a portion of the total alkalinity which existed in situ in the porewaters. Oxidation of iron and manganese consumes  $\text{HCO}_3^-$  and produces  $\text{CO}_2$  according to Eqs. 3 and 4, Table 5. Since the samples used for alkalinity were unacidified, most iron had precipitated prior to analysis. Manganese was not assumed to have precipitated because its oxidation is much slower (Stumm and Morgan, 1981 p. 466). The true in situ alkalinity can be calculated by adding the measured equivalents of  $\text{Fe}^{2+}$  to the alkalinities. Comparison with charge balance indicates that this is a good correction.

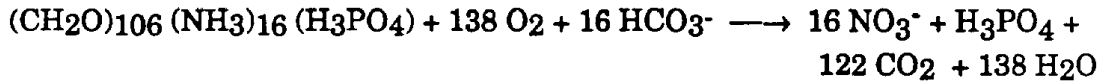
While the oxidation of  $\text{Fe}^{2+}$  causes the measured alkalinity to differ from that which occurs in situ, the measured alkalinity does represent the quantity of a more "permanent" form of alkalinity (i.e. less susceptible to oxidation upon diffusion into the oxygenated lake waters). However even this remaining alkalinity is subject to rapid alteration in the lakewater, particularly alkalinity associated with  $\text{NH}_4^+$  production (Eq. 3, Table 6). Ammonium can be either assimilated directly by organisms (resulting in a release of a proton and a loss of alkalinity) or through nitrification. Since  $\text{NO}_3^-$  does not accumulate in the water, it also must be lost, either through denitrification or assimilation. Therefore, the only permanent alkalinity addition to the overlying lake is associated with the diffusion of base cations ( $\text{Ca}^{2+}$ ,  $\text{Mg}^{2+}$ ,  $\text{Na}^+$ ,  $\text{K}^+$ ) released from organic matter decomposition or silicate mineral weathering (Eq. 6, Table 6). Quantitative fluxes will be presented in Chapter 4 and

Table 5. The stoichiometric reactions for some processes possibly important in CO<sub>2</sub> production in the sediments and waters. Equations derived from Kuivila and Murray (1984) and Kelly et al. (1982).

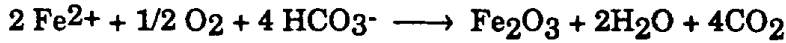
1. Anaerobic decomposition of organic matter



2. Aerobic decomposition with nitrification



3. Iron oxidation to lepidocrocite



4. Manganese oxidation



Ecol. Monogr. 11:21-60.

Kelly, C.A., J.W. Rudd, R.B. Cook, and D.W. Schindler. 1982. The potential importance of bacterial processes in regulating rate of lake acidification. *Limnol. Oceanogr.* 27:868-882.

Kuivila, K.M. and J.W. Murray. 1984. Organic matter diagenesis in freshwater sediments: The alkalinity and total CO<sub>2</sub> balance and methane production in the sediments of Lake Washington. *Limnol. Oceanogr.* 29:1218-1230.

Melack, J.M., S.D. Cooper, and R.W. Holmes. 1987. Chemical and Biological Survey of Lakes and Streams Located in the Emerald Lake Watershed, Sequoia National Park. Final Report, California Air Resources Board Contract A3-096-32.

Mortimer, C.H. 1941 and 1942. The exchange of dissolved substances between mud and water in lakes. *J. Ecol.* 29:280-329 and 30:147-201.

Seitzinger, S.P. 1988. Denitrification in freshwater and coastal marine ecosystems: ecological and geochemical significance. *Limnol. Oceanogr.* 33:702-724.

Stumm, W. and J.J. Morgan. 1981. *Aquatic Chemistry*. 2nd Edition. John Wiley and Sons. New York. 780 p.

Rudd, J.W.M., C.A. Kelly, V. St. Louis, R.H. Hesslein, A. Furutani, and M.H. Holoka. 1986. Microbial consumption of nitric and sulfuric acids in acidified north temperature lakes. *Limnol. Oceanogr.* 31:1267-1280.

compared with the magnitude of other alkalinity sources.

### 3.4.3. Significance of Pore Water Chemistry to Lake Water

In the preceding sections, we have alluded to the importance of diffusion-driven transport of dissolved chemical constituents between the sediments and the overlying lake waters. The data presented in this chapter will serve as constraints on the calculated diffusion rates and will provide the empirical data needed (such as concentration gradients) to make realistic estimates of the contribution of sediments to the chemistry of the three lakes which we have examined. The purpose of the following chapter is to present the mathematical approach which has been developed to calculate diffusion and to present some results of these calculations and compare them to other alkalinity-producing processes in the lakes.

### 3.5. References

Heslien, R.H. 1976. An in situ sampler for close interval pore water studies. *Limnol. Oceanogr.* 21:912-914.

Holmes, R.W. 1986. Calibration of diatom-pH-alkalinity methodology for the interpretation of the sedimentary record in Emerald Lake-Integrated watershed study. Final Report, California Air Resources Board Contract A4-118-32.

Hutchinson, G.E. 1941. *Limnological studies in Connecticut*. IV. The mechanism of intermediary metabolism in stratified lakes.

## Chapter 4

### FLUX CALCULATIONS

#### 4.1. Introduction

The sediments are one of the sources of alkalinity to the overlying lakewater. The rate at which sediments are contributing alkalinity must be known, along with the rate at which other watershed sources are contributing alkalinity to the lakewater, in order for the Air Resources Board to set a deposition standard which will protect sensitive Sierran Lakes. The solid phase data presented in Chapter 2 and the porewater profiles presented in the last chapter provide a means of calculating the fluxes between the sediments and the overlying water. This chapter is concerned with making these calculations and comparing the results with other methods of flux determination.

The rest of this introductory section presents a discussion of the theory of flux calculations and the methods we used to do these calculations. Considerable space is devoted to two phenomena that affect calculations of molecular diffusion: activity coefficient gradients and electrical forces. Some circumstances allow one to ignore these effects, and many workers have ignored one or both. We do the calculations with and without these refinements, so one of the results of this chapter is a determination of whether and when these effects are important.

Flux is the rate of transfer of material between two regions, in this study, the sediments and the overlying water, or,

Yoshimura, S. 1931. Contributions to the knowledge of the stratification of iron and manganese in lake water of Japan. Japanese Journal of Geology and Geography 9:61-69.

is less in a porous medium because the velocity moves the dissolved substance only through pore spaces, while the units of flux are mass per unit area of total sediment per unit time.<sup>2</sup>

#### 4.1.2. Turbulent diffusive flux: eddy diffusion and dispersion

Diffusion is transport down a concentration gradient due to random motion. Turbulent diffusion results from the "random" movement of parcels of water of larger than molecular scale. On a very small scale, turbulent diffusion appears advective, but viewed from a large enough scale, it can be modeled as a random process, and it results in a net flux only if there is a concentration gradient.

$$J_{td,i} = -\phi D_{td} \frac{\partial C_i}{\partial x}$$

where  $J_{td,i}$  is the turbulent diffusive flux of the  $i$ th species,  $D_{td}$  is the turbulent diffusion coefficient, and  $x$  is vertical distance increasing downwards. The negative sign indicates that the flux occurs in the in the direction of decreasing concentration. Turbulent diffusion in open water is usually caused by currents and is termed eddy diffusion.

Another process usually modeled with an equation of this form is porewater dispersion and results from the advective flux of water and solutes through porous media. This kind of mixing is

---

<sup>2</sup> Bear (1972, p. 22) has shown that areal porosity and volume porosity are identical, regardless of pore geometry and even for anisotropic porosity distributions. This fact is important because porosities are measured as volume porosities, while the porosity in the flux equation is an areal porosity.

caused by velocity gradients resulting from friction with the pore walls. Like eddy diffusion, dispersion does not look random on a microscopic scale, but on a larger scale it is well approximated as a diffusive process.

#### 4.1.3. Molecular diffusive fluxes

Molecular diffusion is caused by the random motion of molecules. Strictly speaking, molecular diffusion occurs down the chemical potential gradient, rather than the concentration gradient (Denbigh 1981, p. 86). The following one-dimensional development follows Lasaga (1979) and assumes that the diffusing species are ions. It applies equally well to neutral molecules, however, since the effect of the diffusion potential disappears when multiplied by the charge (zero) of a neutral molecule. This development is included to assist the interested reader in understanding where equation (16) comes from, but may also be skipped, except to pick up the definitions of some terms.

The force on the  $i$ th ion,  $F_i$ , can be thought of as having a thermodynamic component, the gradient in chemical potential ( $\nabla\mu_i$ ), and an electrical component, the charge on the ion ( $z_i$ ) times the gradient in electrical potential ( $\nabla E$ ).<sup>3</sup> The electrical potential, called the diffusion potential, results from the diffusion of ions with different diffusion coefficients. The effect of the electrical potential, indeed its essential mathematical

---

<sup>3</sup>  $\nabla$  is shorthand for gradient. Since we are considering gradients in the vertical ( $x$ ) direction only,  $\nabla C = \partial C / \partial x$ ,  $\nabla E = \partial E / \partial x$ , etc.

property, is the preservation of macroscopic electroneutrality.

The force on ion  $i$  is then

$$F_i = -\nabla\mu_i + z_i \nabla E$$

The molecular diffusive flux of ion  $i$  results from this force:

$$J_{md,i} = \phi C_i u_i F_i$$

where  $u_i$  is the limiting velocity due to a unit force on the  $i$ th species in the solvent environment. Substituting for  $F_i$ ,

$$J_{md,i} = -\phi u_i C_i \nabla\mu_i + \phi u_i z_i C_i \nabla E \quad (1)$$

For this equation to be useful,  $u_i$ ,  $\nabla\mu_i$ , and  $\nabla E$  must be converted into expressions involving terms available from my measurements or the literature: concentration gradients, activity coefficient gradients, and diffusion coefficients. To facilitate this conversion, we define two new variables:

$$A_i = -\phi u_i C_i \nabla\mu_i \quad (2)$$

and

$$B_i = \phi u_i z_i C_i \nabla E \quad (3)$$

so that

$$J_{md,i} = A_i + B_i \quad (4)$$

$A_i$  is the flux due to the chemical potential and  $B_i$  is the flux due to the diffusion potential. The chemical potential is expressed as follows (Stumm and Morgan 1981, p.42):

$$\mu_i = \mu_i^\circ + RT \ln(a_i) \quad (5)$$

where  $\mu_i^\circ$  is the chemical potential at some standard state,

R is the gas constant, T is the absolute temperature, and  $a_i$  is the activity, which is defined to be equal to concentration at infinite dilution. In a real solution, it is related to concentration by the activity coefficient,  $\gamma_i$ :<sup>4</sup>

$$a_i = \gamma_i C_i \quad (6)$$

Substituting for  $a_i$  and differentiating equation (5) with respect to depth (x) gives the following expression for the gradient of the chemical potential:

$$\frac{\partial \mu_i}{\partial x} = \frac{RT}{\gamma_i} \frac{\partial \gamma_i}{\partial x} + \frac{RT}{C_i} \frac{\partial C_i}{\partial x} \quad (7)$$

Substituting equation (7) into equation (2) gives

$$A_i = -\phi u_i C_i \frac{RT}{\gamma_i} \frac{\partial \gamma_i}{\partial x} - \phi u_i RT \frac{\partial C_i}{\partial x} \quad (8)$$

The Nernst-Einstein equation, which relates diffusion coefficients,  $D_i$ , to ionic mobilities,

$$D_i = RTu_i \quad (9)$$

allows the substitution in equation (8) of the diffusion coefficient,  $D_i$ , for  $RTu_i$ , giving

---

<sup>4</sup> Activity coefficients are approximated as a function of ionic strength,  $I$ , which is defined as  $I = 0.5 \sum_{i=1}^n z_i^2 C_i$  for a solution containing  $n$  species.

We are using the Guntelberg approximation for activity coefficients (Stumm and Morgan 1981, p. 135):  $\log \gamma_i = -0.5 z_i^2 \frac{\sqrt{I}}{1 + \sqrt{I}}$

$$A_i = -\phi D_i \left( \frac{C_i}{\gamma_i} \frac{\partial \gamma_i}{\partial x} + \frac{\partial C_i}{\partial x} \right) \quad (10)$$

This expression for the portion of the molecular diffusive flux due to the chemical potential includes both concentration and activity-coefficient gradients. If the activity-coefficient gradient is zero, this expression reduces to the familiar form of Fick's first law in which the flux is equal to a constant times the concentration gradient.

The next step is to obtain an expression for  $B_i$ , the molecular diffusive flux of ion  $i$  due to the diffusion potential. For a system containing  $n$  species, electrical neutrality requires that

$$\sum_{j=1}^n z_j J_{md, j} = 0 \quad (11)$$

Substituting for  $J_{md, j}$  from equation (4) gives

$$\sum_{j=1}^n z_j A_j + \sum_{j=1}^n z_j B_j = 0$$

Substituting for  $B_i$  from equation (3) gives

$$\sum_{j=1}^n z_j A_j + \sum_{j=1}^n \phi u_j z_j^2 C_j \nabla E = 0 \quad (12)$$

Solving for  $\nabla E$  gives

$$\nabla E = \frac{-\sum_{j=1}^n z_j A_j}{\phi \sum_{j=1}^n z_j^2 u_j C_j} \quad (13)$$

Substituting this expression for  $\nabla E$  into equation (3) gives

$$B_i = -\phi u_i z_i C_i \frac{\sum_{j=1}^n z_j A_j}{\phi \sum_{j=1}^n z_j^2 u_j C_j} \quad (14)$$

If the right side of this equation is multiplied by  $RT/RT$  and the Nernst-Einstein equation, (9), is used to substitute  $D_i$ 's for  $RTu_i$ 's, then

$$B_i = -\phi D_i z_i C_i \frac{\sum_{j=1}^n z_j A_j}{\phi \sum_{j=1}^n z_j^2 D_j C_j} \quad (15)$$

This expression for the molecular diffusive flux of ion  $i$  due to the diffusion potential can be understood as follows: The summation in the numerator is the charge imbalance that would result from diffusion of all species with no correction for the diffusion potential. The remainder of the expression apportions to the  $i$ th species a fraction of this total charge imbalance according to the charge, concentration, and diffusion coefficient of the  $i$ th species.

There is one remaining correction to be applied to the diffusive flux equation for an ion in a porous medium: the tortuosity factor,  $T$ . This is a factor between zero and one that reduces the diffusion coefficient for an ion or molecule in a non-porous medium,  $D_i$ , to account for the tortuous path it must take in a porous medium.<sup>5</sup>

---

<sup>5</sup> Tortuosity is discussed more fully below.

$$D_{i,s} = TD_i$$

where  $D_{i,s}$  is referred to as the whole-sediment diffusion coefficient for ion  $i$ .

After substituting equations (10) for  $A_i$  and (15) for  $B_i$  into equation (4) and including the tortuosity correction, the final expression for the flux due to molecular diffusion in a porous medium is

$$J_{md,i} = -\phi TD_i \left( \frac{C_i}{\gamma_i} \frac{\partial \gamma_i}{\partial x} + \frac{\partial C_i}{\partial x} \right) + \frac{\phi TD_i z_i C_i}{\sum_{j=1}^n z_j^2 C_j D_j} \sum_{j=1}^n z_j D_j \left( \frac{C_j}{\gamma_j} \frac{\partial \gamma_j}{\partial x} + \frac{\partial C_j}{\partial x} \right) \quad (16)$$

Note that the tortuosities and porosities associated with the summation terms cancelled each other out.

If there is a negligible gradient in ionic strength, then  $\nabla \gamma_i = 0$ , and equation (16) reduces to the following simpler form:

$$J_{md,i} = -\phi TD_i \frac{\partial C_i}{\partial x} + \frac{\phi TD_i z_i C_i}{\sum_{j=1}^n z_j^2 C_j D_j} \sum_{j=1}^n z_j D_j \frac{\partial C_j}{\partial x} \quad (17)$$

While Lasaga acknowledges that his method of handling the diffusion potential is an approximation, it can be shown by substituting either equation (16) or (17) into equation (11) that this method does result in macroscopic charge balance, as must be the case physically.

## Tortuosity

The tortuosity factor,  $T$ , decreases the diffusion coefficient because of the tortuous path a diffusing molecule must take in a porous medium as a result of its geometry. Different authors treat this factor differently, depending on their interpretation of its physical meaning. We follow Bear's (1972) usage in considering it a multiplicative coefficient:

$$D_{i,s} = TD_i$$

where  $D_{i,s}$  is the diffusion coefficient of ion  $i$  in the sediment,  $0 \leq T \leq 1$  is the tortuosity factor, and  $D_i$  is the diffusion coefficient in homogeneous aqueous solution. This equation can be converted into an operational definition of the tortuosity factor:

$$T = \frac{D_{i,s}}{D_i}$$

Unfortunately, to use this equation one must measure  $D_{i,s}$ . If  $D_{i,s}$  were measured, there would be no need to know  $T$ . Since  $D_{i,s}$  was not measured, some estimate of  $T$  is necessary.

Most authors have attempted to express the tortuosity factor as a function of porosity. This approach is intuitively appealing: In a nonporous solution, both the porosity and the tortuosity factor are equal to one. As the porosity decreases, more of the medium is taken up by solid particles, and the tortuosity factor should also decrease. Such a functional relationship is also useful, because porosity is a common and easy-to-make measurement. Most authors have chosen to use the relationship

$$T = \phi^n$$

Various authors have found such an empirical function for a given sediment, but, unfortunately, the function varies widely between sediments for reasons that are not clear.<sup>6</sup> There may be a large difference between the particle geometries of different sediments; there may also be a large component of measurement error. We use Lerman's (1979, p. 92) suggestion, that, in the absence of a better model,  $T = \phi^2$ . This function is close to what a number of authors have found for fine-grained sediments, but it remains a source of considerable uncertainty in flux calculations.

#### **Temperature corrections for molecular diffusion coefficients**

The diffusion coefficients used in equations (16) and (17) are infinite-dilution tracer or self-diffusion coefficients, which are measured by experimental setups that allow the measurement of ionic mobility in a way that decouples or subtracts the influence of other ions. The influence of ionic strength on  $D$  is relatively small (Lasaga 1979, Li and Gregory 1974, Krom and Berner 1980). The greatest influence on  $D$  is the viscosity of the solution, which results to a small degree from dissolved substances (the viscosity of seawater is about 8% greater than that of freshwater), but primarily from temperature: the viscosity of

---

<sup>6</sup> For examples, see Andrews and Bennett (1981), McDuff and Gieskes (1976), Kepkay et al. (1981), Hesslein (1980), Krom and Berner (1980), Li and Gregory (1974), Rudd et al. (1986), Berner (1980, p.37), Bear (1972, p. 112), Freeze and Cheery (1979, p.104), Thibodeaux (1979, p. 247).

Table 1. Molecular diffusion coefficients at 0°C and 25°C

Species	Diffusion coefficient (10 <sup>-6</sup> cm <sup>2</sup> sec <sup>-1</sup> )		References and notes
	0°C	25°C	
Cl <sup>-</sup>	10.1	20.3	a
NO <sub>2</sub> <sup>-</sup>	9.83	19.1	a
Br <sup>-</sup>	10.5	20.1	a
NO <sub>3</sub> <sup>-</sup>	9.78	19.0	a
SO <sub>4</sub> <sup>2-</sup>	5.00	10.7	a
Ca <sup>2+</sup>	3.73	7.93	a
Mg <sup>2+</sup>	3.56	7.05	a
Fe <sup>2+</sup>	3.41	7.19	a
Mn <sup>2+</sup>	3.05	6.88	a
Na <sup>+</sup>	6.27	13.3	a
NH <sub>4</sub> <sup>+</sup>	9.80	19.8	a
K <sup>+</sup>	9.86	19.6	a
CO <sub>2</sub>	8.42	19.2	b
CH <sub>4</sub>	7.55	17.3	b
H <sub>4</sub> SiO <sub>4</sub>	10.7	21.5	c
H <sup>+</sup>	56.1	93.1	a
OH <sup>-</sup>	25.6	52.7	a
HCO <sub>3</sub> <sup>-</sup>	5.62	11.8	d
FeHCO <sub>3</sub> <sup>+</sup>	4.23	8.50	e
FeCO <sub>3</sub> <sup>0</sup>	2.99	6.00	e
MnHCO <sub>3</sub> <sup>+</sup>	4.23	8.50	e

References and notes:  
a. Li and Gregory 1974  
b. Lerman 1979, p. 96. Reference supplied values at 5°C and 25°C.  
c. Applin 1987. Reference supplied value at 25.5°C.  
d. Li and Gregory 1974. Reference supplied value at 25°C.  
e. Values taken from similar ions in Applin and Lasaga 1984.

water doubles as the temperature falls from 25°C to 0°C. Between these two temperatures, diffusion coefficients are roughly linear. Therefore, my approach to adjusting diffusion coefficients for temperature has been to compile a table of values at 25°C and 0°C and to linearly interpolate between them. Where measured values were available at the two temperatures, we used those. If values were available at, say, 5°C and 25°C, we linearly extrapolated to 0°C to set up the table. Where values were only available for 25°C, we used the 25°C:0°C ratio of a similar ion to estimate a value for 0°C. Where the ratio for a similar species was not available, we used the ratio of the viscosity of water at the two temperatures, 2.01. The 0°C and 25°C values used to interpolate to the diffusion coefficients used in the flux calculations are presented in Table 1.

#### **4.1.4. The importance of dispersion and advection relative to molecular diffusion**

The importance of dispersion relative to molecular diffusion is estimated with the Peclet number,  $Pe=dv/TD$ , a dimensionless number, where  $d$  is particle diameter,  $v$  is water velocity,  $D$  is the molecular diffusion coefficient, and  $T$  is tortuosity. For Peclet numbers less than one, dispersion is considered negligible compared to molecular diffusion (Lerman 1979, p. 65). Using conservative estimates for the sediments of this study ( $d=2\mu\text{m}$ ,  $TD=3\times 10^{-6}\text{cm}^2\text{sec}^{-1}$ ),  $Pe<1$  implies that  $v<13\text{m/day}$ . Measurements in Emerald Lake (Steve Hamilton, personal communication) and porewater profiles in Eastern Brook and Mosquito Lake indicate that, in

these sediments,  $v < 1\text{mm/day}$ . Since velocities appear to be about four orders of magnitude less than the critical value of  $10\text{m/day}$ , dispersion coefficients are assumed to be zero.

The importance of advection relative to molecular diffusion has been examined in the sediment system by looking at porewater profiles for some steady-state solutions generated by a numerical model of advection, diffusion and reaction. Porewater profiles are unaffected by an advective velocity of  $0.01\text{mm/day}$ , but are noticeably affected by a velocity of  $0.1\text{mm/day}$ . This result is shown in Figure 1 for both positive (downward) and negative (upward) velocity cases.<sup>7</sup> Water velocities resulting from sedimentation in the sediments are less than  $1\text{mm/year} = 0.003\text{mm/day}$ , which are small enough to ignore. It is apparent, however, that what are usually considered very low velocities from a hydrologic-balance point of view could be important velocities in diagenetic modeling.

The effect of these low velocities on fluxes can be examined with some simple calculations. The total flux is the sum of the diffusive and advective fluxes, which, ignoring electrical effects and activity coefficient gradients, is

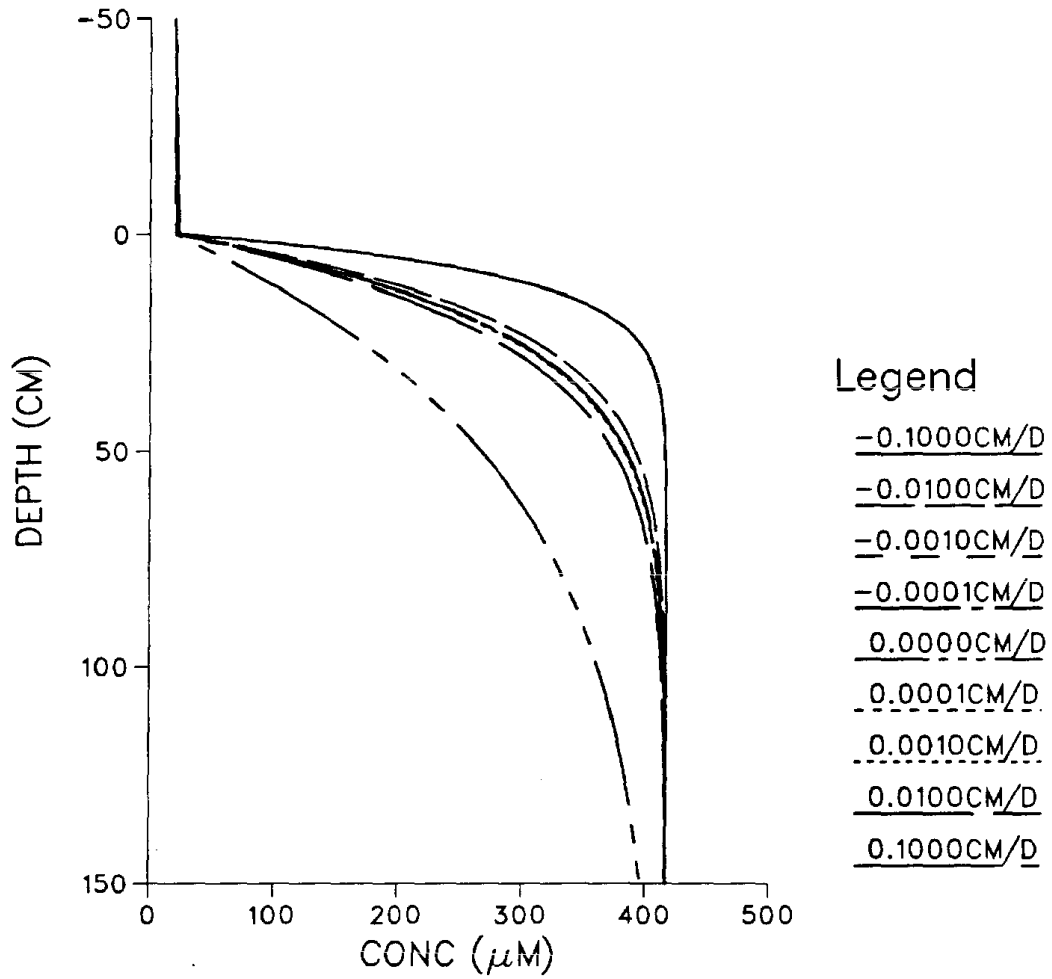
$$J = -\phi TD \nabla C + \phi Cv$$

The relative importance of the diffusive and advective terms may

---

<sup>7</sup> These model runs used  $D = 1.23\text{cm}^2\text{day}^{-1}$  and a simple mineral-dissolution expression:  $dC/dt = 0.0024(417 - C) \mu\text{M day}^{-1}$ . The upper boundary condition was  $20\mu\text{M}$ . Lower boundary condition for the positive velocity case was a rock seal. Lower boundary condition for the negative velocity case was  $417\mu\text{M}$ .

FIG. 1. EFFECT OF ADVECTION ON STEADY STATE SILICA PROFILES



be expressed as a ratio:

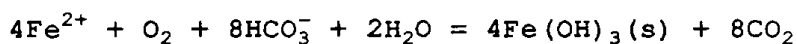
$$\frac{Cv}{TD \nabla C}$$

Near the sediment-water interface, gradients and  $TD$ 's tend to be high and concentration low, while at greater depths in the sediments the reverse is true. Therefore, diffusive flux will tend to be more important near the sediment-water interface than it is deeper in the sediments and the reverse will hold for advective flux. In Eastern Brook Lake near the sediment-water interface, representative concentration gradients for  $\text{HCO}_3^-$ ,  $\text{Ca}^{2+}$ , and  $\text{Na}^+$  are 20, 4.5 and 1.7  $\mu\text{M}/\text{cm}$ . Representative concentrations are 280, 115 and 40  $\mu\text{M}$ . Using  $TD=0.5\text{cm}^2\text{day}^{-1}$  and  $v=0.0003\text{ cm/day}$ , the three ratios are 0.008, 0.015, and 0.014. Thus, advective flux due to sedimentation represents 1%-2% of diffusive flux at the sediment-water interface. At the largest value at which  $v$  had no visible effect on the modeled profiles,  $v=0.001\text{cm/day}$ , the three ratios as percents are 3%-5%, which is surprisingly high considering that the profiles are not visibly affected. At  $v=0.01\text{cm/day}$ , the ratios increase to 30%-50%. If the advection is downward (i.e., the lake leaks out the bottom), then this effect decreases the flux of most species, because the advective flux is opposite to the diffusive flux. It also decreases the diffusive flux by decreasing the gradient at the sediment-water interface, although this change is a smaller effect. Upward advection would increase the flux of most species, because the advective flux is in the same direction as diffusive flux. If the upward advection were large enough, it would also increase

the diffusive flux by increasing the gradient at the sediment-water interface.

#### 4.1.5. Adjustments for in-situ concentration and complex formation

Samples for analysis by atomic absorption spectrophotometry were transferred into acidified bottles, which prevented the precipitation of  $\text{Fe}(\text{OH})_3(\text{s})$  after the oxidation of ferrous iron. Samples for alkalinity and gas measurements, however, were collected in unacidified containers, and the measurements were made after ferrous iron oxidized, forming a visible red precipitate. This reaction can be summarized as follows:



Hence, in-situ alkalinity should be greater and in-situ carbon dioxide should be less than measured, although the in-situ total of carbonate species should be the same as measured. The correctness of this scheme is reflected in the good charge balance we get by boosting in-situ alkalinity by ferrous charge equivalents. However, the symmetrical subtraction from carbon dioxide sometimes produces concentrations less than zero. This is probably because the gases were collected into evacuated containers, which limited the amount of oxygen available. Hence we have assumed that in-situ carbon dioxide is the same as measured.

The application of a similar scheme to manganese is more problematical, because its abiotic rate of oxidation is much slower than that of iron (Stumm and Morgan 1981, p. 466), and

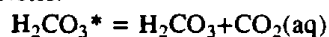
hence it is uncertain how complete the oxidation was at the time of alkalinity titration and gas analysis. Ignoring this adjustment for manganese is also justified by its relatively low concentration.

In addition to the gross effects of oxidation after sampling, the formation of soluble complexes also influences molecular diffusion. The results of metal analysis by atomic absorption spectrophotometry are elemental totals, with no discrimination between complexes. Soluble complexes have different diffusion coefficients and charges from the complexing species, thus affecting diffusion rates, coulomb forces, and activity coefficient gradients. GEOCHEM (Sposito and Mattigod 1979), an equilibrium model designed for soil solutions, which includes all the metals and ligands of importance in the system of this study, was applied to determine which inorganic complexes were important in the system. The only species whose complexes amounted to more than five percent of their totals were iron and manganese.

Based on the species determined to be important, a simple equilibrium model was constructed following the method of Morel and Morgan (1972) for incorporation into the flux calculation program. Table 2 shows the modeled reactions together with the equilibrium constants and molar enthalpy changes. The constants for bicarbonate, carbonic acid, and water were temperature-corrected by empirical expressions. Other constants were temperature corrected using molar enthalpy changes. The model converts thermodynamic equilibrium constants to conditional constants using activity coefficients calculated from the Guñtelberg

Table 2. Speciation: major reactions modeled in porewater			
Reaction	Equilibrium expression	Equilibrium constant (log K, 25°C) (ionic str.=0)	ΔH (kcal/mol)
$\text{Fe}^{2+} + \text{CO}_3^{2-} = \text{FeCO}_3^0$	$\frac{(\text{FeCO}_3^0)}{(\text{Fe}^{2+})(\text{CO}_3^{2-})}$	5.30 <sup>a</sup>	3. <sup>e</sup>
$\text{Fe}^{2+} + \text{H}^+ + \text{CO}_3^{2-} = \text{FeCO}_3^0$	$\frac{(\text{FeCO}_3^0)}{(\text{Fe}^{2+})(\text{H}^+)(\text{CO}_3^{2-})}$	13.00 <sup>a</sup>	-2.5 <sup>f</sup>
$\text{Mn}^{2+} + \text{CO}_3^{2-} = \text{MnCO}_3^0$	$\frac{(\text{MnCO}_3^0)}{(\text{Mn}^{2+})(\text{CO}_3^{2-})}$	4.50 <sup>a</sup>	3. <sup>e</sup>
$\text{Mn}^{2+} + \text{H}^+ + \text{CO}_3^{2-} = \text{MnCO}_3^0$	$\frac{(\text{MnCO}_3^0)}{(\text{Mn}^{2+})(\text{H}^+)(\text{CO}_3^{2-})}$	12.30 <sup>a</sup>	-2.5 <sup>g</sup>
$\text{H}^+ + \text{CO}_3^{2-} = \text{HCO}_3^-$	$\frac{(\text{HCO}_3^-)}{(\text{H}^+)(\text{CO}_3^{2-})}$	10.3 <sup>b</sup>	-3.5 <sup>h</sup>
$2\text{H}^+ + \text{CO}_3^{2-} = \text{H}_2\text{CO}_3^*$	$\frac{(\text{H}_2\text{CO}_3^*)}{(\text{H}^+)^2(\text{CO}_3^{2-})}$	16.7 <sup>c</sup>	-5.5 <sup>h</sup>
$\text{H}_2\text{O} = \text{H}^+ + \text{OH}^-$	$(\text{H}^+)(\text{OH}^-)$	-14.00 <sup>d</sup>	

Notes:



a. Sposito and Mattigod (1979)

b. Stumm and Morgan (1981), p. 206. Temperature corrections are based on an equation fitted to the empirical data in this reference:

$\log K = -6.529 + 2906./T + 0.02385 * T$ , where T is temperature in Kelvins

c. Stumm and Morgan (1981), pp. 205 and 206. Temperature corrections are based on an equation fitted to the empirical data in this reference:

$\log K = -21.35 + 6307./T + 0.0566 * T$ , where T is temperature in Kelvins

d. Stumm and Morgan (1981), p. 126. Temperature corrections are based on an equation fitted to the empirical data in this reference:

$\log K = 3.483 - 4077./T - 0.01276 * T$ , where T is temperature in Kelvins

e. Crude estimate based on  $\text{Ca}^{2+}$  and  $\text{Mg}^{2+}$ , Martell and Smith (1982), p. 403. The sign, at least, is probably correct.

f. Crude estimate, based on  $\text{Mn}^{2+}$ , Smith and Martell (1976), p. 403. The sign is probably correct.

g. Crude estimate, Martell and Smith (1982), p. 403. The sign is probably correct.

h. Smith and Martell (1976), p. 37.

approximation.<sup>8</sup> Inputs to the model were total iron, total manganese, total carbonate species, and in-situ alkalinity. Using the equilibrium expressions, all unknown species were written in terms of four unknowns:  $H^+$ ,  $Mn^{2+}$ ,  $Fe^{2+}$ , and  $CO_3^{2-}$ . These allowed four equations to be written: mass balances for manganese, iron, and carbonate species, and charge balance. These four non-linear algebraic equations were solved using a standard multi-dimensional Newton-Raphson algorithm (Press et al. 1986), which was then iterated until ionic strength converged.

#### 4.2. Calculations of fluxes from peeper data

##### 4.2.1. Introduction

To do these calculations, the following data are needed: temperature, concentrations, concentration gradients, velocities, diffusion coefficients, porosity, and tortuosity. Concentrations, gradients, porosity, temperature, and the velocity resulting from deposition have been measured. Molecular diffusion coefficients and tortuosity were estimated as described above. However, certain fluxes cannot be easily calculated by these methods. The most important of these is the eddy-diffusive flux resulting from a gradient too small for the precision of gradient measurements. This flux could be quite large if the eddy-diffusion coefficient is large. In the system of this study,

<sup>8</sup> The Güntelberg approximation for activity coefficients is (Stumm and Morgan 1981, p. 135):  $\log \gamma_i = -0.5z_i^2 \frac{\sqrt{I}}{1+\sqrt{I}}$

such a situation is likely to exist at the sediment-water interface. High rates of organic matter decomposition take place under aerobic conditions, but the transport of products into the overlying water is so rapid that concentration gradients large enough to measure do not develop. Of course, if these gradients were measurable, we would still have to find methods of measuring or estimating the eddy diffusion coefficients. Such methods are much more poorly developed for eddy diffusion than for molecular diffusion. Hence, the gradient-based calculations presented here are limited to species generated in regions where molecular diffusion dominates transport. Such regions are usually within the sediments, but may include the interface region and some overlying water during the under-ice periods when the bottom waters are very still.

If the location of the sediment-water interface is known exactly, from direct observation, a gradient can be estimated between the sediment-water interface and the first peeper chamber below the sediment-water interface by assuming that the concentration at the sediment-water interface is the same as in the overlying water. If there is a boundary layer, however, slow transport will result in a higher concentration at the sediment-water interface than in the overlying water, and therefore the use of a gradient that is too high. Nonetheless, this procedure is probably one of the best methods of calculating fluxes from observed gradients, but it is not one we can use, because we do not have direct observation of the sediment-water interface.<sup>9</sup>

---

<sup>9</sup> While the sediment-water interface is known approximately from sharp profile changes, the certainty is no better than the closest spacing of the peeper chambers: roughly 3cm for the short

The concentration in a peeper chamber centered at the sediment-water interface is not a good estimate of the concentration at the sediment-water interface, because of the vertical span of a single peeper chamber and because the gradient is especially variable at the sediment-water interface. At greater depths in the sediment, where the gradient may be approximated as constant over the vertical span of a peeper chamber, the concentration in the chamber is a good estimate of the porewater concentration at the center of the chamber.

The approach used here is to take a measured gradient at some point within the sediments, but close to the sediment-water interface. The concentrations in the peeper chambers are then reasonable estimates of the concentrations of porewater at the centers of the chambers, and the distance between the centers of the chambers is known precisely. The gradient calculated from these concentrations and this distance is then used to calculate the flux across some specified flux plane, somewhere between the two peeper chambers, by using the porosity, tortuosity, and concentration<sup>10</sup> at the flux plane. Since fluxes across the sediment-water interface are of interest, some calculations have

---

peepers and 10cm for the long peepers. Since the distance from the sediment-water interface to the first peeper below the sediment-water interface would be the denominator of a gradient estimation, this method would be highly uncertain.

<sup>10</sup> Concentration must be taken into account because the activity coefficient varies nonlinearly with ionic strength and because the electrical correction is apportioned among the diffusing ions according to their concentration. For the same concentration gradient,  $\nabla\gamma_i$  will be larger nearer the sediment-water interface where the ionic strength is low. This can be seen mathematically by starting from the Güntelberg approximation and observing that  $d\gamma/dI < 0$  and  $d^2\gamma/dI^2 > 0$ .

been made using the sediment-water interface as the flux plane, while using a gradient measured somewhat below the sediment-water interface. At the sediment-water interface, porosity is estimated by extrapolation, tortuosity is estimated from porosity, and concentration is taken to be that of the overlying water. The assumption inherent in this approach is that the gradient measured somewhat below the sediment-water interface is the same as the gradient at the sediment-water interface. The result is less defensible than using a flux plane between the peeper chambers used to calculate the gradient, but the exercise illustrates some important effects that concentrations at the flux plane have on fluxes.

#### **4.2.2. Methods**

In order to explore the effects of flux plane concentrations, activity coefficients, coulomb forces, and complex formation on fluxes, 24 methods were used to calculate the fluxes for each peeper. The methods were combinations generated by a  $2 \times 2 \times 2 \times 3$  tree. The first three levels ( $2 \times 2 \times 2$ ) generated 8 sets of concentrations at a flux plane and a "dummy plane" (0.01cm below the flux plane). The "dummy plane" is simply a plane chosen close to the flux plane for the purposes of gradient calculation. It needs to be close so that the activity coefficient gradients are accurate. The fourth level consisted of three methods of flux calculations for each set of flux and dummy plane concentrations.

*Level 1: Flux plane*

(1)

Specify a depth for the flux plane and interpolate between peeper chambers to generate concentrations at the flux and dummy planes.

(2)

Specify a concentration (such as the overlying water) for the flux plane, and then use the measured gradients to extrapolate to the dummy plane. The purpose of specifying a concentration for the flux plane was to explore the effects of concentration at the flux plane while keeping the gradients constant.

*Level 2: Charge balance*

(1)

Keep concentrations as generated in Level 1.

(2)

Adjust the concentrations generated in Level 1 to produce charge balance. This adjustment was done by increasing or decreasing the concentration of each species in proportion to its concentration and charge. The purpose of the charge balance adjustment was to be able to separate the effects of initial charge imbalance from charge imbalance caused by differential diffusion.

*Level 3: Speciation*

(1)

Keep concentrations as generated in Level 2

(2)

Calculate the concentrations of various complexes using the equilibrium program described previously.

At the conclusion of this level, there were then 8 sets of flux and dummy plane concentrations. For each of these, a concentration gradient was calculated between the flux and dummy planes. For each of these 8 sets of concentrations and gradients, fluxes were calculated in the following three ways:

*Level 4: Flux calculation method*

(1)

Fluxes were calculated using the concentration gradients:

$$J = -\phi TD_i \frac{\partial C_i}{\partial x}$$

(2)

Fluxes were calculated adjusting the concentration gradients for activity coefficients:

$$J = -\phi TD_i \left( \frac{C_i}{\gamma_i} \frac{\partial \gamma_i}{\partial x} + \frac{\partial C_i}{\partial x} \right)$$

(3)

Fluxes were calculated using the adjusted gradients in (2) with an electrical correction to assure a charge-balanced flux:

$$J = -\phi TD_i \left( \frac{C_i}{\gamma_i} \frac{\partial \gamma_i}{\partial x} + \frac{\partial C_i}{\partial x} \right) + \frac{\phi TD_i z_i C_i}{\sum_{j=1}^n z_j^2 C_j D_j} \sum_{k=1}^n z_k D_k \left( \frac{C_k}{\gamma_k} \frac{\partial \gamma_k}{\partial x} + \frac{\partial C_k}{\partial x} \right)$$

In each case, concentrations at the flux and dummy planes (0.01cm apart) were used to estimate the gradients, and

concentrations were those at the flux plane.

#### 4.2.3. Results: discussion of various factors

To examine the importance of the various factors affecting molecular diffusive fluxes (activity coefficient gradients, coulomb forces, and complex formation), the calcium fluxes resulting from the different combinations of flux plane, charge balance, speciation, and calculational method are presented for the six long peepers in Table 3.

The effect of activity coefficient gradients is to decrease the flux of species diffusing out of the sediments. The percentage change in flux resulting from applying the correction for activity coefficient,  $PC_{12}$ , is thus always negative, since the ionic-strength gradient has the same sign as the calcium concentration gradient, and therefore the activity coefficient gradient has the opposite sign from the calcium concentration gradient.

The activity correction produces a flux decrease of  $0.331 \text{ nmol cm}^{-2} \text{ day}^{-1}$  (-19%) in EBLPB and  $0.400 \text{ nmol cm}^{-2} \text{ day}^{-1}$  (-14%) in EBLPR. This correction is the product of three factors (see equation 16). The first is the activity coefficient gradient. The activity coefficient gradient for EBLPB is -0.0052, while that for EBLPR is -0.0076. The second factor is the concentration of calcium,  $135 \mu\text{M}$  for EBLPB and  $110 \mu\text{M}$  for EBLPR. The third factor is the inverse of the activity coefficient, which is  $1/0.82$  for EBLPB and  $1/0.86$  for EBLPR. The first factor is the dominant difference, thus resulting in the larger correction for EBLPR, although the second and third factors have the opposite

Table 3. Six long peepers: 24 calcium fluxes

Flux plane	Charge bal.	Peeper	Fluxes									
			Unspeciated					Speciated				
			FLX1	FLX2	PC12	FLX3	PC23	FLX1	FLX2	PC12	FLX3	PC23
I	NA	EBLPB	-1.747	-1.416	-18.9	-2.267	60.1	-1.747	-1.480	-15.3	-2.071	39.9
		EBLPR	-2.791	-2.391	-14.3	-3.331	39.3	-2.791	-2.442	-12.5	-3.092	26.6
		EMLPB	-0.947	-0.872	-8.0	-1.017	16.7	-0.947	-0.884	-6.6	-0.969	9.5
		EMLPR	-0.284	-0.252	-11.3	-0.303	20.0	-0.284	-0.256	-10.1	-0.284	11.2
		MOLPB	-1.965	-1.911	-2.8	-1.909	-0.1	-1.965	-1.915	-2.5	-1.873	-2.2
		MOLPR	-2.254	-2.095	-7.0	-2.563	22.3	-2.254	-2.113	-6.3	-2.477	17.2
	A	EBLPB	-1.780	-1.460	-17.9	-2.321	58.9	-1.780	-1.522	-14.5	-2.140	40.6
		EBLPR	-2.654	-2.279	-14.1	-3.594	57.7	-2.654	-2.327	-12.3	-3.402	46.2
		EMLPB	-0.921	-0.847	-8.1	-1.030	21.6	-0.921	-0.860	-6.7	-0.987	14.8
		EMLPR	-0.296	-0.263	-11.0	-0.292	10.9	-0.296	-0.267	-9.9	-0.272	1.8
		MOLPB	-1.897	-1.844	-2.8	-1.948	5.6	-1.897	-1.849	-2.6	-1.921	3.9
		MOLPR	-2.228	-2.076	-6.8	-2.567	23.6	-2.228	-2.093	-6.1	-2.489	18.9
S	NA	EBLPB	-1.979	-1.382	-30.2	-4.859	251.5	-1.979	-1.402	-29.2	-4.769	240.1
		EBLPR	-2.969	-2.605	-12.3	-4.135	58.7	-2.969	-2.617	-11.8	-4.058	55.0
		EMLPB	-1.322	-1.215	-8.1	-1.059	69.4	-1.322	-1.219	-7.8	-2.921	139.6
		EMLPR	-0.383	-0.342	-10.7	-0.593	73.3	-0.383	-0.343	-10.6	-0.658	92.1
		MOLPB	-2.296	-2.261	-1.5	-2.237	-1.1	-2.296	-2.262	-1.5	-2.221	-1.8
		MOLPR	-2.551	-2.297	-10.0	-4.023	75.2	-2.551	-2.302	-9.8	-3.905	69.7
	A	EBLPB	-3.997	-3.505	-12.3	-6.334	80.7	-3.997	-3.522	-11.9	-6.219	76.6
		EBLPR	-1.521	-1.130	-25.7	-3.869	242.4	-1.521	-1.143	-24.8	-3.797	232.1
		EMLPB	-1.692	-1.600	-5.4	-2.445	52.8	-1.692	-1.603	-5.3	-3.022	88.6
		EMLPR	-0.625	-0.587	-6.1	-0.733	24.9	-0.625	-0.587	-6.0	-0.765	30.1
		MOLPB	-2.141	-2.108	-1.5	-2.282	8.3	-2.141	-2.109	-1.5	-2.266	7.5
		MOLPR	-3.607	-3.409	-5.5	-4.828	41.6	-3.607	-3.412	-5.4	-4.718	38.3

Notes:  
 Flux plane: I = concentrations interpolated, S = concentrations specified  
 Charge balance: N = not adjusted, A = adjusted  
 FLX1,FLX2,FLX3: Flux calculation method as described under Level 4 in the text  
 Flux units are  $\text{nmol cm}^{-2}\text{day}^{-1}$   
 PC12: Percentage change between FLX1 and FLX2,  $=100(\text{FLX2}-\text{FLX1})/\text{FLX1}$   
 PC23: Percentage change between FLX2 and FLX3,  $=100(\text{FLX3}-\text{FLX2})/\text{FLX2}$

effect. The percent change in EBLPB is greater because the uncorrected flux is smaller.

In the Emerald Lake long peepers, the activity correction produces a flux decrease of  $0.075 \text{ nmol cm}^{-2} \text{ day}^{-1}$  (-8%) in EMLPB and  $0.032 \text{ nmol cm}^{-2} \text{ day}^{-1}$  (-11%) in EMLPR. The three factors for each peeper are  $-0.0066 \text{ cm}^{-1}$ ,  $33.00 \mu\text{M}$ , and  $1/.83$ ; and  $-0.0036 \text{ cm}^{-1}$ ,  $25.25 \mu\text{M}$ , and  $1/.87$ . In this case, all three factors are strongest for EMLPB, as is reflected in the greater absolute change in flux. The percent change in EMLPR is greater because the uncorrected flux is smaller.

The sign of the electrical correction (as a percentage, PC23 in Table 3) depends on whether iron or ammonium is the major positive diffusing species. Excess positive charge will tend to accumulate if ammonium is the major diffusing species (i.e., has the highest concentration gradient), because ammonium has a higher diffusion coefficient than bicarbonate, the major negative species. Excess negative charge will tend to accumulate if iron is the major diffusing species, because iron has a lower diffusion coefficient than bicarbonate. Three examples are shown in Table 4. Since the examples used are for concentrations that are not charge balanced, there is some question as to whether a flux charge imbalance is the result of differential diffusion or simply poor initial charge balance. Comparison of the "charge balance not adjusted" (NA) and "charge balance adjusted" (A) calculations in Table 3 indicates that the basic effect remains the same.

Table 4. Factors affecting electrical corrections: three examples (flux plane concentrations interpolated, charge balance not adjusted)			
Parameter	Peeper		
	EBLPB	MOLPB	MOLPR
Charge imbalance resulting from the flux ( $\text{neq cm}^{-2}\text{day}^{-1}$ )	14.	-0.66	8.7
% effect on Ca flux	60.%	-0.1%	22.%
$\nabla\text{Ca}^{2+}$ ( $\text{nmol cm}^{-4}$ )	3.6	4.9	5.2
$\nabla\text{Fe}^{2+}$ ( $\text{nmol cm}^{-4}$ )	34.	10.5	22.
$\nabla\text{NH}_4^+$ ( $\text{nmol cm}^{-4}$ )	9.	10.	9.
$[\text{Ca}^{2+}]$ ( $\mu\text{M}$ )	135.	30.	55.
$[\text{Fe}^{2+}]$ ( $\mu\text{M}$ )	500.	220.	234.
$[\text{NH}_4^+]$ ( $\mu\text{M}$ )	104.	63.	58.4

The size of the electrical correction to the calcium fluxes also depends on the concentration of positive species at the flux plane, as well as the size of the imbalance. If there is a lot of ammonium and iron at the flux plane, these species will carry the bulk of the correction. If they are of relatively low concentration compared with calcium, as they are likely to be at the sediment-water interface, then calcium will carry most of the correction. An example is EBLPB with specified (sediment-water interface) flux-plane concentrations (see Table 3). In this case, calcium flux is more than doubled by the electrical correction. Thus, while the charge imbalance is generated by species with high *gradients*, the correction affects species with high *concentrations*. In Table 3, the specified flux-plane concentration is an estimate of the sediment-water interface concentration. At this location, calcium tends to be the important positive ion, and it is apparent that the effect of the electrical correction on calcium flux is usually much greater than for the case where the flux-plane concentrations were interpolated.

One effect of complex formation is to decrease the activity correction. This occurs because complex formation reduces ionic strength to a larger extent where concentrations are higher. Hence, activity-coefficient gradients are reduced. The effect of complex formation on the electrical correction can go either way. In some cases, the charge imbalance is reduced because the gradients of charged species are reduced. In other cases, the effect of the correction on calcium is enhanced because the concentration of other positively charged species is reduced.

In conclusion, all three of the effects examined (activity coefficient gradients, coulomb forces, and complex formation) can have a significant effect on molecular-diffusive fluxes. The dramatic differences in electrical effects between the fluxes of the interpolated case (within sediment) and specified case (at the sediment-water interface) suggest that extrapolating measured gradients to the sediment-water interface is not a good idea. The use of charge-balanced concentrations at the flux and dummy planes was primarily a device for examining the electrical correction, and has no direct justification in doing actual flux calculations. Hence, the procedure followed in the following calculations uses gradients generated from interpolated, specified flux- and dummy-plane concentrations, with both activity and electrical corrections.

#### **4.2.4. Results: three lakes summer peepers**

Calculations were done for summer peepers for which the aluminum plate was above the sediment-water interface. If the plate was at or below the sediment-water interface, it acted as an impermeable barrier that distorted the natural fluxes. Because of the softness and depth of the Eastern Brook Lake sediments, all of the summer short peepers got buried, and only the winter peepers and long peepers provided acceptable data.

Flux calculations for the three lakes were done by selecting representative pairs of peeper chambers near, but not at or above, the sediment-water interface. The chambers representing the steepest gradient were chosen, but obvious outliers were

avoided. For the short peepers, because all species were not analyzed in all chambers, the pairs of chambers were different for different species. A flux plane roughly central to the groups of chambers was chosen. The dummy plane was always 0.01cm below the flux plane. The concentrations at the flux and dummy planes were calculated by interpolation and then speciated independently. The charge balance at the flux planes, an indicator of the quality of the analysis and the legitimacy of the interpolation procedure, is listed at the bottom of Tables 5, 6, and 7. Concentration gradients were calculated using the concentrations at the flux and dummy planes. Fluxes were then calculated using both activity and electrical corrections. The fluxes of individual species are presented in Tables 5, 6, and 7, in order of decreasing mean flux.

The fluxes of elemental and some other totals are presented in Tables 8, 9, and 10, in order of decreasing mean flux. The fluxes in all three lakes were dominated by carbon, followed by the trio of silica, nitrogen and iron (not necessarily in that order), followed by the base cations (calcium, magnesium, sodium and potassium). Standard deviations of fluxes for elemental totals based on replicate peepers are presented in Table 11.

#### 4.3. Discussion

Table 5. Eastern Brook Peeper Fluxes ( $\text{nmol cm}^{-2}\text{day}^{-1}$ ): Species  
(Flux-plane concentrations interpolated and speciated, charge balance not adjusted, activity and electrical corrections applied)

Species	Peeper (date: YYMMDD)				
	EBLPB (860729)	EBLPR (860729)	<i>n</i>	mean	sd
HCO3	-39.925	-43.930	2	-41.928	2.833
CO2	-36.040	-35.770	2	-35.905	0.193
CH4	-28.652	-16.737	2	-22.695	8.425
SIO2	-17.096	-11.107	2	-14.101	4.235
NH4	-9.717	-10.441	2	-10.079	0.512
FE	-8.289	-10.118	2	-9.204	1.294
FEHCO3	-6.564	-4.228	2	-5.396	1.652
CA	-2.088	-3.117	2	-2.602	0.728
NA	-1.298	-0.796	2	-1.047	0.354
K	-0.978	-0.986	2	-0.982	0.006
MG	-0.252	-0.467	2	-0.359	0.152
FECO3	-0.356	-0.237	2	-0.296	0.085
CL	-0.042	-0.073	2	-0.057	0.022
SO4	0.034	0.031	2	0.033	0.002
MN	-0.006	-0.045	2	-0.025	0.028
NO2	0.054	-0.018	2	0.018	0.051
MNHCO3	-0.012	-0.017	2	-0.015	0.003
NO3	0.005	0.023	2	0.014	0.012
BR	.	-0.013	1	-0.013	.
CO3	-0.005	-0.006	2	-0.006	0.001
H	-0.009	-0.001	2	-0.005	0.006
MNCO3	0.000	-0.001	2	-0.001	0.000
OH	0.000	0.000	2	0.000	0.000
Charge balance:					
COA	1.094	1.132	2	1.113	0.027
CMA	115.880	89.145	2	102.513	18.905
Notes:	A dot indicates a missing value COA= cations over anions for concentrations at the flux plane CMA= cations minus anions for concentrations at the flux plane				

Table 6. Emerald Lake Peeper Fluxes ( $\text{nmol cm}^{-2}\text{day}^{-1}$ ): Species  
(Flux-plane concentrations interpolated and speciated, charge balance not adjusted, activity and electrical corrections applied)

Species	Peeper (date: YYMMDD)								
	EMLPB (860819)	EMLPR (860819)	EMP3B (850905)	EMP3R (850905)	EMP4B (851002)	EMP4R (851002)	n	mean	sd
CO2	-42.329	-47.295	.	.	-119.974	-90.341	4	-74.985	36.937
CH4	-37.587	-24.773	.	.	-85.728	-61.264	4	-52.338	26.907
HCO3	-34.545	-18.136	-20.646	-15.230	-38.259	-76.958	6	-33.962	23.005
SIO2	-8.785	-10.306	-32.817	-22.456	-49.863	-29.589	6	-25.636	15.383
NH4	-10.962	-9.179	-16.837	-10.356	-16.091	-35.236	6	-16.444	9.729
FE	-6.890	-2.282	-0.025	-1.312	-6.167	-12.616	6	-4.882	4.660
FEHCO3	-5.054	-1.276	-0.140	-0.172	-1.497	-6.493	6	-2.439	2.681
NA	-1.568	-1.384	-2.005	-1.552	-2.007	-2.989	6	-1.917	0.584
CA	-0.973	-0.286	-0.647	-0.305	-2.089	-2.668	6	-1.161	0.993
K	-0.642	-0.462	-0.435	-0.247	-1.399	-0.814	6	-0.666	0.407
MG	-0.365	-0.169	0.004	-0.045	-0.226	-0.308	6	-0.185	0.145
FECO3	-0.172	-0.024	0.194	-0.202	-0.025	-0.162	6	-0.065	0.148
MN	-0.015	-0.121	-0.031	-0.002	-0.048	-0.132	6	-0.058	0.055
NO2	.	-0.016	-0.091	-0.043	0.015	.	4	-0.034	0.045
CL	-0.071	-0.009	-0.057	-0.075	.	0.056	5	-0.031	0.056
BR	-0.010	-0.001	.	-0.076	.	.	3	-0.029	0.041
NO3	-0.001	0.002	-0.091	-0.071	0.007	0.005	6	-0.025	0.044
H	0.008	-0.027	0.000	-0.001	-0.108	0.200	6	0.012	0.101
MNHCO3	-0.008	-0.009	-0.001	-0.001	-0.005	-0.011	6	-0.006	0.004
OH	0.000	0.000	0.002	0.024	0.000	-0.001	6	0.004	0.010
CO3	-0.003	-0.001	0.072	-0.038	-0.001	-0.006	6	0.004	0.036
SO4	-0.039	0.054	-0.037	-0.057	0.037	0.060	6	0.003	0.053
MNCO3	0.000	0.000	0.001	-0.001	0.000	0.000	6	0.000	0.001
Charge balance:									
COA	1.026	0.981	1.011	0.965	0.979	0.979	6	0.990	0.023
CMA	28.469	-13.480	3.261	-6.402	-7.328	-14.875	6	-1.726	16.130

Notes:

A dot indicates a missing value

COA= cations over anions for concentrations at the flux plane

CMA= cations minus anions for concentrations at the flux plane

Table 7. Mosquito Lake Peeper Fluxes ( $\text{nmol cm}^{-2}\text{day}^{-1}$ ): Species  
(Flux-plane concentrations interpolated and speciated, charge balance not adjusted, activity and electrical corrections applied)

Species	Peeper (date: YYMMDD)									
	MOLPB (860924)	MOLPR (860924)	MOP2R (850716)	MOP3B (850808)	MOP3R (850808)	MOP4B (850917)	MOP4R (850917)	n	mean	sd
CO2	-37.127	-50.183	-45.131	-20.793	-118.938	-119.610	-82.871	7	-67.808	39.794
HCO3	-22.697	-35.055	-22.632	-64.837	-92.024	-43.503	-111.686	7	-56.062	34.867
CH4	-7.394	-21.944	-26.714	-21.566	-89.141	-69.514	-57.881	7	-42.022	30.228
SiO2	-14.428	-16.145	.	-19.615	-23.764	-25.698	-28.035	6	-21.281	5.430
NH4	-9.854	-9.922	-16.370	-24.078	-18.383	-19.334	-20.805	7	-16.964	5.377
FE	-2.294	-6.833	-0.807	-10.893	-24.293	-1.260	-28.029	7	-10.630	11.237
FEHCO3	-1.448	-3.024	-0.152	-6.959	-12.090	-0.293	-5.972	7	-4.277	4.351
CA	-1.877	-2.486	-1.338	-2.315	-3.430	-7.174	-5.817	7	-3.491	2.184
FECO3	-0.042	-0.104	-0.003	-0.514	-0.226	-0.003	20.657	7	2.823	7.866
NA	-1.206	-1.630	-1.618	-2.737	-2.205	-1.113	-2.838	7	-1.907	0.698
MG	-0.811	-0.672	-0.110	-1.346	-0.905	-2.874	-1.060	7	-1.111	0.865
K	-0.672	-0.649	0.025	-1.746	-1.272	-0.716	-1.337	7	-0.909	0.584
CO3	-0.002	-0.003	-0.001	-0.016	0.022	-0.001	3.579	7	0.511	1.353
OH	0.000	0.000	0.000	-0.002	0.016	0.000	2.689	7	0.386	1.016
NO2	0.048	.	.	0.028	0.113	.	.	3	0.063	0.044
SO4	-0.091	-0.033	0.021	0.053	0.036	0.052	0.287	7	0.046	0.118
H	-0.021	-0.023	0.056	0.059	-0.158	0.691	-0.316	7	0.041	0.316
CL	-0.350	-0.107	0.025	0.147	0.315	0.004	0.126	7	0.023	0.211
NO3	0.001	0.011	0.002	0.014	0.037	0.004	0.060	7	0.019	0.022
BR	.	-0.018	.	.	.	.	.	1	-0.018	.
MN	-0.007	-0.005	0.002	-0.002	-0.028	-0.006	.	6	-0.007	0.010
MNHCO3	-0.004	-0.003	-0.001	-0.003	-0.009	-0.002	.	6	-0.004	0.003
MNCO3	0.000	0.000	0.000	0.000	0.000	0.000	.	6	0.000	0.000
Charge balance:										
COA	0.998	1.108	0.721	0.984	0.995	0.980	0.906	7	0.956	0.119
CMA	-1.331	64.374	-92.685	-14.145	-4.331	-5.034	-37.012	7	-12.881	46.885

Notes:

A dot indicates a missing value

COA= cations over anions for concentrations at the flux plane

CMA= cations minus anions for concentrations at the flux plane

Table 8. Eastern Brook Peeper Fluxes ( $\text{nmol cm}^{-2}\text{day}^{-1}$ ): Elemental Totals (Flux-plane concentrations interpolated and speciated, charge balance not adjusted, activity and electrical corrections applied)					
Species	Peeper (date: YYMMDD)				
	EBLPB (860729)	EBLPR (860729)	<i>n</i>	mean	sd
CCT	-111.555	-100.926	2	-106.240	7.516
FET	-15.209	-14.583	2	-14.896	0.443
SIO2	-17.096	-11.107	2	-14.101	4.235
NT	-9.657	-10.437	2	-10.047	0.551
CA	-2.088	-3.117	2	-2.602	0.728
NA	-1.298	-0.796	2	-1.047	0.354
K	-0.978	-0.986	2	-0.982	0.006
MG	-0.252	-0.467	2	-0.359	0.152
CL	-0.042	-0.073	2	-0.057	0.022
MNT	-0.018	-0.063	2	-0.041	0.032
SO4	0.034	0.031	2	0.033	0.002
BR	.	-0.013	1	-0.013	.
Other totals:					
CO3T	-46.863	-48.419	2	-47.641	1.100
CT	-82.902	-84.189	2	-83.546	0.908
SBC	-6.956	-8.949	2	-7.953	1.410

Notes:  
A dot indicates a missing value  
FET=FE+FEHCO3+FECO3  
MNT=MN+MNHCO3+MNCO3  
NT=NH4+NO3+NO2  
CO3T=HCO3+CO3+FEHCO3+FECO3+MNHCO3+MNCO3  
CT=CO3T+CO2  
CCT=CT+CH4 (total carbon)  
SBC=2\*CA+2\*MG+NA+K (sum of base cations) ( $\text{neq cm}^{-2}\text{day}^{-1}$ )

Table 9. Emerald Lake Peeper Fluxes ( $\text{nmol cm}^{-2}\text{day}^{-1}$ ): Elemental Totals  
(Flux-plane concentrations interpolated and speciated, charge balance not adjusted, activity and electrical corrections applied)

Species	Peeper (date: YYMMDD)								
	EMLPB (860819)	EMLPR (860819)	EMP3B (850905)	EMP3R (850905)	EMP4B (851002)	EMP4R (851002)	n	mean	sd
CCT	-119.698	-91.514	.	.	-245.490	-235.235	4	-172.984	78.759
SIO2	-8.785	-10.306	-32.817	-22.456	-49.863	-29.589	6	-25.636	15.383
NT	-10.963	-9.194	-17.019	-10.470	-16.069	-35.231	6	-16.491	9.713
FET	-12.116	-3.583	0.030	-1.686	-7.688	-19.271	6	-7.386	7.289
NA	-1.568	-1.384	-2.005	-1.552	-2.007	-2.989	6	-1.917	0.584
CA	-0.973	-0.286	-0.647	-0.305	-2.089	-2.668	6	-1.161	0.993
K	-0.642	-0.462	-0.435	-0.247	-1.399	-0.814	6	-0.666	0.407
MG	-0.365	-0.169	0.004	-0.045	-0.226	-0.308	6	-0.185	0.145
MNT	-0.023	-0.130	-0.031	-0.004	-0.053	-0.143	6	-0.064	0.058
CL	-0.071	-0.009	-0.057	-0.075	.	0.056	5	-0.031	0.056
BR	-0.010	-0.001	.	-0.076	.	.	3	-0.029	0.041
SO4	-0.039	0.054	-0.037	-0.057	0.037	0.060	6	0.003	0.053
Other totals:									
CO3T	-39.783	-19.446	.	.	-39.787	-83.630	4	-45.661	27.067
CT	-82.111	-66.740	.	.	-159.762	-173.971	4	-120.646	54.050
SBC	-4.886	-2.757	-3.725	-2.500	-8.036	-9.754	6	-5.276	2.976

Notes:

A dot indicates a missing value

FET=FE+FEHCO3+FECO3

MNT=MN+MNHCO3+MNCO3

NT=NH4+NO3+NO2

CO3T=HCO3+CO3+FEHCO3+FECO3+MNHCO3+MNCO3

CT=CO3T+CO2

CCT=CT+CH4 (total carbon)

SBC=2\*CA+2\*MG+NA+K (sum of base cations) ( $\text{neq cm}^{-2}\text{day}^{-1}$ )

Table 10. Mosquito Lake Peeper Fluxes ( $\text{nmol cm}^{-2}\text{day}^{-1}$ ): Elemental Totals  
(Flux-plane concentrations interpolated and speciated, charge balance not adjusted, activity and electrical corrections applied)

Species	Peeper (date: YYMMDD)								n	mean	sd
	MOLPB (860924)	MOLPR (860924)	MOP2R (850716)	MOP3B (850808)	MOP3R (850808)	MOP4B (850917)	MOP4R (850917)				
CCT	-68.713	-110.317	-94.635	-114.688	-312.406	-232.927	-234.175	7	-166.837	92.058	
SIO2	-14.428	-16.145	.	-19.615	-23.764	-25.698	-28.035	6	-21.281	5.430	
NT	-9.805	-9.911	-16.368	-24.036	-18.233	-19.330	-20.745	7	-16.918	5.367	
FET	-3.785	-9.961	-0.962	-18.366	-36.609	-1.556	-13.344	7	-12.083	12.586	
CA	-1.877	-2.486	-1.338	-2.315	-3.430	-7.174	-5.817	7	-3.491	2.184	
NA	-1.206	-1.630	-1.618	-2.737	-2.205	-1.113	-2.838	7	-1.907	0.698	
MG	-0.811	-0.672	-0.110	-1.346	-0.905	-2.874	-1.060	7	-1.111	0.865	
K	-0.672	-0.649	0.025	-1.746	-1.272	-0.716	-1.337	7	-0.909	0.584	
SO4	-0.091	-0.033	0.021	0.053	0.036	0.052	0.287	7	0.046	0.118	
CL	-0.350	-0.107	0.025	0.147	0.315	0.004	0.126	7	0.023	0.211	
BR	.	-0.018	.	.	.	.	.	1	-0.018	.	
MNT	-0.011	-0.008	0.001	-0.005	-0.037	-0.008	.	6	-0.011	0.013	
Other totals:											
CO3T	-24.192	-38.189	-22.789	-72.329	-104.327	-43.803	-93.423	7	-57.007	33.107	
CT	-61.319	-88.373	-67.920	-93.122	-223.265	-163.414	-176.294	7	-124.815	62.495	
SBC	-7.254	-8.594	-4.490	-11.805	-12.147	-21.924	-17.929	7	-12.020	6.113	

Notes:

A dot indicates a missing value

FET=FE+FEHCO3+FECO3

MNT=MN+MNHCO3+MNCO3

NT=NH4+NO3+NO2

CO3T=HCO3+CO3+FEHCO3+FECO3+MNHCO3+MNCO3

CT=CO3T+CO2

CCT=CT+CH4 (total carbon)

SBC=2\*CA+2\*MG+NA+K (sum of base cations) ( $\text{neq cm}^{-2}\text{day}^{-1}$ )

Table 11. Standard deviations of calculated elemental total fluxes based on pooled variances from replicate peepers from three lakes (nmol cm<sup>-2</sup>day<sup>-1</sup>, except SBC, which is neq cm<sup>-2</sup>day<sup>-1</sup>)

Species	Degrees of freedom	Standard deviation
BR	1	0.0064
CA	7	0.6233
CCT	6	59.0461
CL	6	0.0946
CO3T	6	22.3982
CT	6	39.0244
FET	7	7.1725
K	7	0.2700
MG	7	0.5070
MNT	6	0.0441
NA	7	0.5912
NT	7	5.6663
SBC	7	1.4839
SIO2	7	6.4486
SO4	7	0.0699
Other totals:		
CO3T	6	22.3982
CT	6	39.0244
SBC	7	1.4839
Notes:		
A dot indicates a missing value		
FET=FE+FEHCO3+FECO3		
MNT=MN+MNHCO3+MNCO3		
NT=NH4+NO3+NO2		
CO3T=HCO3+CO3+FEHCO3+FECO3+MNHCO3+MNCO3		
CT=CO3T+CO2		
CCT=CT+CH4 (total carbon)		
SBC=2*CA+2*MG+NA+K (sum of base cations) (neq cm <sup>-2</sup> day <sup>-1</sup> )		

#### 4.3.1. Origins of fluxes

Table 12 compares the gradient-calculated fluxes as mole percents of carbon with those assembled by Vallentyne (1974) as averages for freshwater flora. While Vallentyne's values can be considered only rough approximations to the elemental composition of the biota which form the sediments in the lakes of this study, the numbers are consistent with organic-matter decomposition being a source of the major species except iron. However, Vallentyne's analyses are of living plants, and, if many of the base cations are contained in the cytoplasm, cell lysis, which is likely to occur when the plants die, would release these base cations. Since the plants die before they are buried in the sediments, the sedimentary organic matter is likely to contain fewer base cations than Vallentyne's analysis would indicate. Nonetheless, some base cations are likely to be released from the decomposition of organic matter. An elemental analysis of the sedimentary organic matter in our lakes could resolve this question. The remaining base cations must be originating from mineral dissolution.

In an effort to examine the relationship of the fluxes to mineral weathering, we have used the mean water column concentrations of base cations as estimates of average mineral weathering in the watershed, including the minerals in the sediments. Table 13 compares the gradient-calculated fluxes as mole percents of calcium with both mean water column values and with those assembled by Vallentyne as averages for freshwater flora. This table suggests that sodium is likely to be primarily a product of

Table 12. Elemental fluxes for three lakes and the elemental composition freshwater flora (Vallentyne 1974) normalized as mole percents of carbon				
Element	Mole-percent of carbon			
	Vallentyne (1974)	Eastern Brook	Emerald	Mosquito
Carbon	100.	100.	100.	100.
Silica	8.6	13.	21.	13.
Nitrogen	9.2	9.4	14.	10.
Calcium	1.8	2.4	0.96	2.1
Potassium	1.4	0.92	0.55	0.54
Magnesium	0.53	0.34	0.15	0.67
Sodium	0.32	1.0	1.6	1.1
Iron	0.07	14.	6.1	7.2

Table 13. Base cation fluxes for three lakes, the base cation composition freshwater flora (Vallentyne 1974), and the mean water column concentrations of base cations normalized as mole percents of calcium							
Cation	Mole-percent of calcium						
	Vallentyne (1974)	Eastern Brook		Emerald		Mosquito	
		Flux	WC	Flux	WC	Flux	WC
Calcium	100	100	100	100	100	100	100
Magnesium	14	14	15	16	21	32	53
Sodium	9	40	68	165	146	55	130
Potassium	38	38	25	57	25	26	23

WC=water column

mineral weather rather than decomposition of organic matter. Magnesium and potassium could be either. A firm resolution of the origin of base cations will have to await further work. An analysis of the base cations in the sedimentary organic matter would be a good start.

#### **4.3.2. Comparison of gradient-calculated fluxes with other measurements**

Melack et al. (1987) measured fluxes using benthic chambers, mesocosm bags, and in-lake measurement. Table 14 compares individual-ion benthic-chamber measurements with the gradient-calculated fluxes.

The most obvious feature of the comparison is that the benthic chambers measured a flux of calcium and sodium 80 times greater, a flux of potassium and magnesium 120 times greater, and a flux of ammonium 20 times greater than the gradient-calculated fluxes. Note, however, that the order of the sizes of the fluxes of the individual ions is the same in the benthic chambers and in the gradient-calculated fluxes, suggesting that the same processes operating at different rates are generating the fluxes in both cases. An explanation for why the ratio of benthic-chamber ammonium flux to gradient-calculated ammonium flux is so much less than the same ratios for base cations is that the ammonium is being nitrified and denitrified in the benthic chamber, just as is likely to be occurring in the lake after the ammonium leaves the sediments.

Table 14. Cation flux (neq cm <sup>-2</sup> day <sup>-1</sup> ) comparisons for Emerald Lake			
Ion	Our results <sup>a</sup>	Benthic chambers <sup>b</sup>	Ratio
NH <sub>4</sub> <sup>+</sup>	16.	370.	23.
Ca <sup>2+</sup>	2.3	190.	83.
Na <sup>+</sup>	1.9	160.	84.
K <sup>+</sup>	0.67	80.	120.
Mg <sup>2+</sup>	0.37	40.	110.
SBC	5.3	470.	89.

Notes:  
**SBC = sum of base cations**  
a. Emerald Lake means. See Table 6.  
b. Melack et al. (1987), Table II-7, p. 87. Mean of all experiments at the 9m depth, n=8.

If the base cations were coming principally from organic matter, a hypothesis which could explain the enhanced benthic chamber fluxes is that rapid stirring in the benthic chambers resulted in the oxygenation of the sediment surface, which in turn caused rapid aerobic decomposition of organic matter, which is generally thought to be much more rapid than anaerobic decomposition (Nedwell 1984, Skopintsev 1981). If, on the other hand, the base cations are coming principally from mineral dissolution, then perhaps the benthic chambers are causing enhanced mixing in the pore waters.

The gradient-calculated fluxes must be a lower limit, since they capture only what goes on below the flux plane, which is somewhat below the sediment-water interface. It is reasonable that a large proportion of organic-matter breakdown occurs naturally at or above the sediment-water interface, since that is the locus of both the most labile organic matter and the highest oxygen levels. The benthic-chamber fluxes are likely to be an upper limit, since oxygenation of the sediment-water interface and mixing in the pore waters are probably enhanced by stirring.

Melack et al. measured the shear velocity at the sediment-water interface in the benthic chambers and on the lake bottom and from these numbers calculated boundary layer thicknesses. The shear velocities in the benthic chambers were from 6 to 14 times higher than on the lake bottom, depending on the benthic-chamber pump setting, corresponding to boundary layers that were 5 to 19 times smaller. The measured boundary layer thicknesses were roughly 1 mm in the lake and 0.1 mm in the benthic chambers.

For the products of organic matter decomposition, it is appropriate to reduce the fluxes measured in the benthic chambers by the shear-velocity ratios, as Melack et al. do for specific chamber experiments, assuming that the transport of oxygen to the sediment-water interface is the rate-limiting step in aerobic organic-matter decomposition.<sup>12</sup> This correction brings the gradient-calculated numbers into closer agreement by about a factor of ten. If mineral dissolution is the primary source of base cations it seems unlikely than a smaller boundary layer alone would cause such greatly enhanced fluxes. Also, if mineral dissolution is the primary source of base cations, surface effects would tend to be less important, because freshly deposited minerals would not be that much more labile than deeper minerals, at least not to the same degree as organic matter.

A back-of-the-envelope calculation can provide some insight as to the reasonableness of the various flux values. If the mean gradient-calculated carbon flux,  $120\text{nmol cm}^{-2}\text{day}^{-1}$ , is multiplied by 100 (the degree of enhancement of the benthic-chamber fluxes

---

<sup>12</sup> Melack et al. state (p. 85), "Since flux is proportional to shear velocity and inversely proportional to boundary layer thickness, flux values from the benthic chamber can be corrected for artificial circulation by dividing by the appropriate factor for a pump setting (for example: 6 for 80% or 14 for 90%)." Actually, flux is proportional to the gradient at the flux plane, which, for species diffusing out of the deep sediments, will be changed only slightly by the roughly 1mm difference in boundary layer thickness that is considered here. The gradient that is changed dramatically by boundary layer thickness is that of oxygen and other electron acceptors, such as nitrate and sulfate, that are diffusing from the overlying water into the sediments. This process is appropriately modeled by a well mixed reservoir of dissolved oxygen (the overlying water) separated from the reactive substrate (the sediment) by a resistive boundary layer.

over the gradient-calculated fluxes), the result is about  $100\text{mg cm}^{-2}\text{yr}^{-1}$  of organic matter, assuming that organic carbon is 50% of organic matter. The burial rate of organic matter in Emerald Lake is about  $9\text{mg cm}^{-2}\text{yr}^{-1}$ , so this scenario implies that roughly 90% of the sedimenting organic matter is mineralized before burial. This mineralization rate seems high, based on some comparisons with a variety of freshwater and marine sediments (Adams and Fendinger 1986, Nedwell 1984, Aller and Mackin 1984, Skopintsev 1981). If the factor-of-ten correction for enhanced benthic-chamber shear velocity is correct, then the numbers imply a more reasonable remineralization rate before burial of about  $10\text{mg cm}^{-2}\text{yr}^{-1}$ , or 50%.

Another back-of-the-envelope check on these fluxes is how they relate to total lake volume. The various hydrologic balances that have been attempted are sufficiently uncertain that the sediment contribution to lake chemistry is not statistically distinguishable from zero. A casual look at the inflow graphs and lake chemistry graphs in Melack et al. (1987) leads to a similar conclusion: The sediments must be contributing less than 10% to total lake alkalinity. The gradient-calculated base cation flux of  $5\text{neq cm}^{-2}\text{day}^{-1}$  equates to  $18.\text{meq m}^{-2}\text{ yr}^{-1}$  or  $200\text{eq yr}^{-1}$  for the entire lake if the sediment area is about  $11,000\text{m}^2$ . Given a lake volume of  $160,000\text{m}^3$ , the calculated flux of base cations amounts to  $1.2\mu\text{eq L}^{-1}$  of lake water each year. Of course, since the hydraulic residence time is much less than a year, the actual contribution to an average liter of lake water

would never be this high. On the other hand, the sediment contribution to bottom water under stratified conditions would be very significant. The corrected benthic-chamber estimate of ten times the gradient-calculated flux ( $12\mu\text{eq L}^{-1}$ ) is still reasonable: Following fall overturn after three months of stratification, the sediment contribution to lakewater base cations might be about  $4\mu\text{eq L}^{-1}$ . The uncorrected benthic-chamber flux, however, does not seem reasonable: it could result in an increase of  $40\mu\text{eq L}^{-1}$  after fall overturn, producing an average total alkalinity of  $75\mu\text{eq L}^{-1}$ , a figure far in excess of any actual measurements.

#### 4.3.3. Denitrification and sulfate reduction

Kelly et al. (1987) estimated denitrification rates and sulfate reduction rates as a function of the lakewater concentrations of these species, based on five lakes for nitrate and 8 lakes for sulfate. They found that the denitrification rate in  $\text{neq cm}^{-2}\text{day}^{-1}$  was  $2.5\pm 0.7$  times the water column concentration of nitrate in  $\mu\text{eq L}^{-1}$ , and the sulfate reduction rate in  $\text{neq cm}^{-2}\text{day}^{-1}$  was  $0.15\pm 0.04$  times the water column concentration of sulfate in  $\mu\text{eq L}^{-1}$ . While these rates are generalizations, they do provide order-of-magnitude estimates of these processes in the lakes of this study, as shown in Table 15.

Based on these numbers for Emerald Lake, which has an unusually high nitrate concentration, denitrification could be contributing twice the alkalinity that the gradient-calculated flux of

Table 15. Denitrification and sulfate reduction estimates, compared with mean gradient-calculated base-cation fluxes

Lake	Nitrate		Sulfate		Grad-calc'd base cation fluxes ( $\text{neq cm}^{-2}\text{day}^{-1}$ )
	Water col. conc. ( $\mu\text{M}$ )	Red'n rate ( $\text{neq cm}^{-2}\text{day}^{-1}$ )	Water col. conc. ( $\mu\text{M}$ )	Red'n rate ( $\text{neq cm}^{-2}\text{day}^{-1}$ )	
Eastern Brook	0.6 <sup>a</sup>	1.5	4. <sup>a</sup>	0.6	8.
Emerald	4. <sup>b</sup>	10.	6. <sup>c</sup>	0.9	5.
Mosquito	2. <sup>a</sup>	5.	2. <sup>a</sup>	0.3	10.

Notes:  
a. Mean of all of water column measurements in this study  
b. Melack et al. (1987), Figure II-6, p. 25.  
c. Melack et al. (1987), Figure II-7, p. 25.

base cations does. Denitrification would represent 20% of the sediment-related base-cation flux if the corrected benthic-chamber numbers are correct.

These numbers also suggest that, in watersheds like that of Emerald Lake that are limited by a nutrient other than nitrogen, increases in atmospheric nitrate loading would result in increases in in-lake alkalinity generation via denitrification. Additional nitrate loading would not cause an increase in sediment denitrification in Eastern Brook Lake and Mosquito Lake, which have very low nitrate levels. In these watersheds, nitrate would first be consumed by primary producers. Sulfate concentrations would have to increase to levels at which the lakes were acidified before sulfate reduction would produce even the small amount of alkalinity currently produced by deep fluxes of base cations.

#### **4.3.4. Winter peepers and annual averages**

The gradient-calculated fluxes have only been done for "summer", or open water, peepers, whose concentration profiles indicate relatively rapid transport in the bottom water. The "winter", or under-ice, peepers are characterized by relatively slow transport in the bottom water. The main reason for the transport difference is the presence of wind-generated seiches in the open-water lakes and their absence in the under-ice lakes. In the under-ice peepers, the slowness of transport in the overlying water enables us to see what is invisible in the summer peepers: the high rate of organic-matter mineralization at the

sediment-water interface. This slow transport causes reaction products to accumulate at the site of the reaction, producing the peaks visible at the sediment-water interface in the winter peepers. The slowness of transport also means that oxygen becomes depleted faster than it can be replenished by diffusion. Hence the accumulation of reduced products, such as ammonium, ferrous iron, and methane. After the depletion of oxygen, nitrate, and manganic, ferric iron becomes the preferred electron acceptor (Berner 1980, p. 82). The presence of a reservoir of oxidized iron and labile organic matter at the sediment-water interface sustains a relatively rapid rate of mineralization even after oxygen depletion.

The development of a concentration peak at the sediment-water interface causes the diffusion of alkalinity and base cations into the sediments as well as into the water column. A similar, but weaker effect occurs during summer stratification. The concentrations of base cations in the porewater near the sediment-water interface become higher than during periods when the lake is well mixed, and the exchange sites become loaded as well. After overturn, the bottom water, which has an accumulation of nutrients and alkalinity, mixes quickly into the lake, while the sediments release their buildup of nutrients and alkalinity more slowly, probably contributing alkalinity at an accelerated rate for a few weeks after overturn. Peepers EMP4B, EMP4R, MOP4B, and MOP4R, which were sampled in mid-September and early October, had base cation fluxes more than double those of the July and August peepers (see Tables 8 to 10). So, while fluxes of base cations

decrease during stratification, after overturn the gradient across the sediment-water interface becomes abnormally high, which results in an enhanced flux into the water column until the gradients stabilize. Since these surface effects probably do not change mineralization rates in the bulk of the sediments, which are permanently anoxic, the flux swings at the sediment-water interface can be viewed as oscillations in an otherwise constant flux from the deep sediments.

#### **4.3.5. Whole-lake flux estimates**

In addition to the actual fluxes out of the sediments, two factors are of importance in determining how much influence the sediments have on lakewater chemistry. The first is the ratio of the lake volume to the sediment area. Mosquito Lake is shallow with 50% of its area covered with sediments; Emerald Lake is deep with only 40% of its area in sediments. The volume to sediment-area ratio is almost four times greater in Emerald Lake. The second factor is the hydraulic residence time. During periods of rapid flow, the sediments will have little effect on lakewater chemistry; during stagnant periods they will have a much greater effect. This factor will vary drastically over the course of a single year and also from year to year. All three of the study lakes receive most of their precipitation as snowfall, and most of their flow occurs during spring melt. During maximum melt, hydraulic residence time may be only a few days; at the end of a dry summer or in mid-winter, when inflows have ceased, it is infinite. Of course, the short annual average residence time

guarantees that the sediments of these lakes will never have longer than a few months to influence a given batch of lake water.

Whole lake estimates of sediment-related alkalinity generation are presented in Table 17. These estimates are based on the lake parameters described in Table 16. It is very difficult to estimate the uncertainty of the average annual gradient-calculated fluxes, for two reasons. The first is that seasonal sampling was limited. We took enough samples to know that seasonal variation is very high (ranging even to reversed fluxes in some under-ice conditions) but not enough samples to generate precise annual averages. The numbers we have used for our estimates are averages of fluxes calculated for open-lake conditions. Simply using the standard deviation for all the peepers is not a valid technique, because they do not represent a full sample of the annual cycle and because they lead to a contradiction: negative fluxes fall within the confidence interval generated by such a procedure, and the porewater profiles indicate unequivocally that the annual net flux into the water must be positive. The second difficulty is that spatial sampling was limited. Replicate pairs of peepers were placed 5-10 m apart in the soft sediments in the deep part of the lakes. We have assumed that our calculated fluxes apply to the whole of the region of organic sediments. We estimate a "confidence interval" of our gradient calculated fluxes as annual averages to be between half and double their stated values.

Table 16. Assumptions used to make whole-lake estimates of sediment-related alkalinity generation			
Parameter	Lake		
	Eastern Brook	Emerald	Mosquito
Area (ha)	4.4	2.7	2.
Sediment area (ha)	2.2	1.1	1.
Volume (m <sup>3</sup> )	180,000.	160,000.	40,000.
Average depth (m)	4.1	5.9	2.
Ratio of vol. to sed. area (m)	8.2	15.	4.
Average SBC in lakewater ( $\mu\text{eq L}^{-1}$ )	160.	50.	60.

Table 17. Sediment-related alkalinity generation: whole-lake estimates									
Source	Lake								
	Eastern Brook			Emerald			Mosquito		
	Abs.	Norm.	%	Abs.	Norm.	%	Abs.	Norm.	%
Deep fluxes of base cations	638.	3.54	2.2	212.	1.3	2.6	439.	11.	18
Surface reactions? <sup>a</sup>									
Denitrification	120.	0.7	0.4	400.	2.5	5.	180.	4.6	8
Sulfate reduction	48.	0.3	0.2	36.	0.2	0.5	11.	0.3	0.5

Notes:

Abs. = absolute amount ( $\text{eq}\cdot\text{yr}^{-1}$ )

Norm. = normalized to lake volume ( $\mu\text{eq L}^{-1}\cdot\text{yr}^{-1}$ )

% =  $100(\text{Norm.})/(\text{average sum of base cations in lakewater})$

a. While decomposition of organic matter at the sediment-water interface may be the most important source of sediment-related alkalinity, we have no good estimate. See Melack et al. (1987).

#### 4.4. Summary and conclusions

The major deep sediment fluxes, which this study measured, are dominated by organic-matter decomposition, resulting in fluxes of carbon dioxide, methane, and ammonium. Calculations based on measured gradients indicate that diffusive transport in freshwater sediments is significantly affected by activity coefficient gradients, coulomb forces, and complex formation.

Annual average base cation fluxes from deep sediments are roughly 8, 5, and 12 neq cm<sup>-2</sup>day<sup>-1</sup> for Eastern Brook Lake, Emerald Lake, and Mosquito Lake. Calculated for the entire sediment area, these fluxes are 600, 200 and 400 eq yr<sup>-1</sup>. Normalizing to lake volume, they are 4, 1, and 10 µeq L<sup>-1</sup>yr<sup>-1</sup>. (See Table 17.) These estimates are necessarily very rough, because of large temporal variability and limited sampling. We estimate that the "confidence interval" for these numbers ranges from one half to double the stated values. They are probably less than 10% of other watershed sources of alkalinity, except for Mosquito Lake, which is very shallow. Assuming the hydrologic residence times are roughly equal, the sediments in Mosquito Lake, the shallowest lake, have the most influence on lakewater chemistry, and the sediments in Emerald Lake, the deepest lake, have the least influence.

During periods when the hydrologic residence time is short, the sediments have very little influence. During times when the hydrologic residence time is long, they have a greater influence. During periods of summer and winter stratification, the alkalinity and nutrients released from the sediments are trapped below

the thermocline. After turnover, they mix into the rest of the lake. During stratification, the elevated concentrations in the bottom water cause elevated concentrations to develop in the porewater of the upper sediments. After turnover, the higher porewater concentrations result in higher gradients and enhanced fluxes out of the sediments, possibly for several weeks, until the porewater profiles re-equilibrate with lower concentrations in the overlying water. During winter stratification, vertical transport near the bottom is very slow, due to the absence of wind-generated seiches, and oxygen depletion results in the accumulation in the bottom water of the reduced species ammonium, methane, and ferrous iron.

#### 4.5. References

- Adams, D. D. and N. J. Fendinger, 'Early diagenesis of organic matter in the recent sediments of Lake Erie and Hamilton Harbor,' in: *Sediments and Water Interactions*, P. G. Sly, ed., p. 305-318, Springer-Verlag, New York, 1986.
- Aller, R. C. and J. E. Mackin, 'Preservation of reactive organic matter in marine sediments,' *Earth and Planetary Science Letters*, 70: 260-266, 1984.
- Andrews, D. and A. Bennett, 'Measurements of diffusivity near the sediment-water interface with a fine-scale probe,' *Geochimica et Cosmochimica Acta*, 45: 2169-2175, 1981.
- Applin, K. R. and A. C. Lasaga, 'The determination of SO<sub>4</sub><sup>2-</sup>, NaSO<sub>4</sub><sup>-</sup>, and MgSO<sub>4</sub> tracer diffusion coefficients and their application to diagenetic flux calculations,' *Geochimica et Cosmochimica Acta*, 48: 2151-2162, 1984.
- Applin, K. R., 'The diffusion of dissolved silica in dilute aqueous solution,' *Geochimica et Cosmochimica Acta*, 51: 2147-2151, 1987.
- Bear, J., *Dynamics of Fluids in Porous Media*, American Elsevier, New York, 1972. 764 pages.
- Berner, R. A., *Early Diagenesis, A Theoretical Approach*, Princeton University Press, Princeton, New Jersey, 1980, 241 pp.
- Denbigh, K., *The Principles of Chemical Equilibrium*, Fourth Edition, Cambridge University Press, New York, 1981. 494 pages.
- Freeze, R. A. and J. A. Cherry, *Groundwater*, Prentice-Hall, Inc., Englewood Cliffs, N.F., 1979. 604 pages.
- Hesslein, R. H., 'In situ measurements of porewater diffusion coefficients using tritiated water,' *Canadian Journal of Fisheries and Aquatic Science*, 37: 545-551, 1980.
- Kelly, C. A., J. W. M. Rudd, R. H. Hesslein, D. W. Schindler, P. J. Dillon, C. T. Driscoll, S. A. Gherini, and R. E. Hecky, 'Prediction of biological acid neutralization in acid-sensitive lakes,' *Biogeochemistry*, 3: 129-140, 1987.
- Kepkay, P. E., R. C. Cooke, and A. J. Bowen, 'Molecular diffusion and the sedimentary environment: results from in situ determination of whole sediment diffusion coefficients,' *Geochimica et Cosmochimica Acta*, 45: 1401-1409, 1981.
- Krom, M. D. and R. A. Berner, 'The diffusion coefficients of sulfate, ammonium, and phosphate ions in anoxic marine sediments,' *Limnology and Oceanography*, 25(2): 327-337, 1980.
- Lasaga, A. C., 'The treatment of multi-component diffusion and ion pairs in diagenetic fluxes,' *American Journal of Science*, 279: 324-346, 1979.
- Lerman, A., *Geochemical Processes: Water and Sediment Environments*, John Wiley and Sons, New York, 1979. 481 pages.

- Li, Y. H. and S. Gregory, ``Diffusion of ions in sea water and in deep-sea sediments,`` *Geochimica et Cosmochimica Acta*, 38: 703-704, 1974.
- Martell, A. E. and R. M. Smith, *Critical Stability Constants*, Vol. 5: *First Supplement*, Plenum Press, New York, 1982. 604 pages.
- McDuff, R. E. and J. M. Gieskes, ``Calcium and magnesium profiles in DSDP interstitial waters: diffusion or reaction?,`` *Earth and Planetary Science Letters*, 33: 1-10, 1976.
- Melack, J. M., S. D. Cooper, R. W. Holmes, J. O. Sickman, K. Kratz, P. Hopkins, H. Hardenbergh, M. Thieme, and L. Meeker, *Chemical and Biological Survey of Lakes and Streams Located in the Emerald Lake Watershed, Sequoia National Park*, Marine Science Institute and Department of Biological Sciences, University of California, Santa Barbara, California, 93106, February 18, 1987. Prepared for the California Air Resources Board, Contract A3-096-32.
- Morel, F. and J. Morgan, ``A numerical method for computing equilibria in aqueous chemical systems,`` *Environmental Science and Technology*, 6(1): 58-67, January 1972.
- Nedwell, D. B., ``The input and mineralization of organic carbon in anaerobic aquatic sediments,`` *Advances in Microbial Ecology*, 7: 93-131, 1984.
- Press, W. H., B. P. Flannery, S. A. Teukolsky, and W. T. Vetterling, *Numerical Recipes, The Art of Scientific Computing*, Cambridge University Press, New York, 1986. 818 pages.
- Rudd, J. W. M., C. A. Kelly, V. S. Louis, R. H. Hesslein, A. Furutani, and M. H. Holoka, ``Microbial consumption of nitric and sulfuric acids in acidified north temperate lakes,`` *Limnology and Oceanography*, 31(6): 1267-1280, 1986.
- Skopintsev, B. A., ``Decomposition of organic matter of plankton, humification and hydrolysis,`` in: *Marine Organic Chemistry: Evolution, Composition, Interactions and Chemistry of Organic Matter in Seawater*, E. K. Duursma and R. Dawson, eds., Elsevier Scientific Publishing Company, New York, 1981. 521 pages. (Elsevier Oceanography Series; vol. 31.)
- Smith, R. M. and A. E. Martell, *Critical Stability Constants*, Vol. 4: *Inorganic Complexes*, Plenum Press, New York, 1976. 257 pages.
- Sposito, G. and S. V. Mattigod, *Geochem: A Computer Program for the Calculation of Chemical Equilibria in Soil Solutions and Other Natural Water Systems*, The Kearney Foundation of Soil Science, University of California, 1979. Department of Soil and Environmental Sciences, University of California, Riverside, California 92521.
- Stumm, W. and J. J. Morgan, *Aquatic Chemistry: An Introduction Emphasizing Chemical Equilibria in Natural Waters*, 2nd. ed., John Wiley & Sons, New York, 1981.
- Thibodeaux, L. J., *Chemodynamics*, John Wiley and Sons, New York, 1979. 501 pages.
- Vallentyne, J. R., *The Algal Bowl, Lakes and Man*, Department of the Environment, Canadian Fisheries and Marine Service,

Ottawa, 1974. 186 pages.